UNIVERSITÀ
DEGLI STUDI
DI PADOVA

Head Office: Università degli Studi di Padova

Department of Women's and Children's Health

Ph.D. COURSE IN: Developmental Medicine and Health Planning Sciences

CURRICULUM: haemato-oncology, genetic, rare diseases, and predictive medicine

SERIES XXXIV cycle

Understanding the molecular mechanisms of Mucopolysaccharidosis type I pathogenesis in a newly generated model of *Drosophila melanogaster*

Thesis written with the financial contribution of Istituto di Ricerca Pediatrica Città della Speranza

Coordinator: Prof. Gianni Bisogno

Supervisor: Prof. Maurizio Scarpa

Co-Supervisor: Dr. Rosella Tomanin

Ph.D. student: Concetta De Filippis

SUMMARY

ABSTRACT

Mucopolysaccharidosis type I (MPS I) is an autosomal recessive disease, belonging to the group of the inborn errors of metabolism. It is caused by mutations in the gene encoding for the lysosomal enzyme α-L-iduronidase (IDUA), which lead to a deficit in the enzymatic activity. IDUA is the second enzyme of the glycosaminoglycans (GAGs) heparan- and dermatan-sulfate degradative chains. Therefore, MPS I is characterized by accumulation of these undegraded GAGs in different tissues and organs, leading to a progressive multi-organ impairment.

The syndrome presents a spectrum of phenotypes, from the attenuated forms, known as Scheie and Hurler-Scheie syndromes, to the severe form, known as Hurler syndrome.

Clinical manifestations of the disease are: typical coarse facial features, hepatosplenomegaly, heart valve disease, joint stiffness, skeletal abnormalities, recurrent respiratory upper way infections, and, in the severe form, a progressive neurological involvement leading to neuro-developmental delays.

To date, together with symptomatic therapies, the enzyme replacement therapy (ERT) and the hematopoietic stem cells transplantation (HSCT) are available. ERT, consisting in the weekly infusion of the recombinant enzyme, although quite efficient in treating the peripheral tissues pathology, is inefficient in treating the CNS disease, due to the inability of the enzyme to cross the blood-brain barrier, as well as in treating some difficult districts, as the bones and the heart valves. On the other hand, HSCT is efficient in treating the CNS compartment and greatly increases patient's quality of life by significantly reducing the hospitalization rate and slowing down the progression of the disease. However, it is effective only if carried out very early in patients' life (usually during the first year) and it is unable to revert the altered phenotypes, already established before the start of treatment.

Although clinically well characterized, the disease remains poorly understood from the pathogenic point of view, and the molecular mechanisms underlying the pathology are not enough clarified. The animal model mainly used for the study of MPS I is the mouse, firstly developed in the 90s. Albeit being a very good model, well resembling the human pathology, the MPS I mouse was mainly used for therapeutic efficacy studies, while deepened pathogenic investigations have not been conducted to date. This is due to the extended experimental time required, the high costs associated to the maintenance of the mice colonies and the increasing ethical issues involved in the use of mammals in research.

Understanding the pathological mechanisms underlying MPS I could be of great interest to find out altered pathways involved in the pathogenesis, possibly addressable as new therapeutic targets of innovative therapies supporting the existing ones.

To this aim, in this project a *Drosophila melanogaster* model for MPS I was developed and characterized.

D. melanogaster offers several advantages as an animal model, since it has a short life cycle, which permits to perform rapid developmental studies conducted in a high number of flies, also thanks to the elevated progeny that can be obtained from a single crossing. In addition, *Drosophila* is easy to handle, and it has relatively contained costs of maintenance. Furthermore, the availability of transgenic fluorescent lines allows to conduct simplified and accurate *in vivo* studies. Lastly, in *D. melanogaster* it is possible to conduct rapid pharmacological screenings.

The MPS I *Drosophila* model was developed using the RNA interference (RNAi) approach, taking advantage of the UAS/Gal4 system available for the fly.

The ubiquitous downregulation of the *Drosophila Idua* homologous (*D-idua*) led to a decrease of the enzymatic activity, up to one-third, in the third instar larvae and to a complete lethality at pupal stage. The selective downregulation of *D-idua* in neurons and glial cells led to a mild, progressive locomotor impairment and, on the other hand, to an increased lifespan.

The *D-idua Drosophila* model showed some cellular and molecular features similar to those observed *in vitro* in human fibroblasts and in the mouse model, as the increased number and size of lysosomes, both in the brain and in the muscle tissue, together with a decreased percentage of acidified lysosomes. In addition, autophagy impairment, as well as metabolic pathways alterations are present in this model, both of which ameliorated in starvation conditions. Furthermore, alterations of the mitochondrial network, together with impaired mitochondria polarization were observed. Lastly, the increased volume of the brain and the abnormal morphology of motor axon terminations represent signs of nervous system structural alterations.

Overall, the MPS I *Drosophila* model appears to mimic some aspects associated to the human MPS I pathology, and shows strong alterations in some pathways, which were still poorly characterized in the disease. Therefore, the MPS I fly model shows great potential for deepening the mechanisms involved in the pathogenesis of the disease. Starting from the involvement of different metabolic pathways, which in this project were shown to be drastically affected, the MPS I fly model offers the possibility to conduct in the future pharmacological screenings specifically

targeted to these altered pathways, as well as to expand the knowledge on other mechanisms possibly involved in the onset of the pathology.

RIASSUNTO

La mucopolisaccaridosi di tipo I (MPS I) è una malattia genetica rara, a trasmissione autosomica recessiva, appartenente al vasto gruppo delle malattie metaboliche pediatriche. È causata da mutazioni nel gene codificante per l'enzima lisosomiale α-L-iduronidasi (IDUA), che portano a un deficit di attività enzimatica. IDUA è il secondo enzima delle catene degradative dei glicosaminoglicani (GAG) eparan- e dermatan-solfato. Di conseguenza, la MPS I è caratterizzata dall'accumulo di questi GAG non degradati in diversi tessuti e organi, accumulo che porta a un progressivo danneggiamento degli stessi organi.

MPS I si presenta con uno spettro di fenotipi, dalle forme attenuate, conosciute come sindrome di Scheie e sindrome di Hurler-Scheie, alla forma severa, conosciuta come sindrome di Hurler.

Le manifestazioni cliniche della malattia sono principalmente rappresentate da facies caratteristica, epatosplenomegalia, valvulopatie, rigidità articolare, deformità ossee, infezioni ricorrenti delle alte vie respiratorie, e, nelle forme severe, da un progressivo coinvolgimento neurologico che porta a ritardi nello sviluppo cognitivo.

Ad oggi, insieme alle terapie sintomatiche, sono disponibili per i pazienti la terapia enzimatica sostitutiva (ERT) e il trapianto di cellule staminali ematopoietiche (HSCT). ERT consiste nell'infusione settimanale dell'enzima ricombinante e, sebbene si sia dimostrata parzialmente efficace nel trattare la malattia a livello periferico, è inefficiente sia per il trattamento del sistema nervoso centrale, a causa dell'incapacità dell'enzima di attraversare la barriera emato-encefalica, che per il trattamento di alcuni distretti periferici, quali ossa e valvole cardiache. D'altra parte, il trapianto di cellule staminali ematopoietiche è efficace nel trattamento del sistema nervoso centrale e migliora notevolmente la qualità di vita dei pazienti, riducendo in maniera significativa la necessità di ospedalizzazione. Tuttavia, il trapianto di cellule staminali ematopoietiche è efficace solo se effettuato molto precocemente nella vita del paziente (solitamente entro il primo anno di età) e non è in grado di revertire aspetti fenotipici alterati, già eventualmente instauratisi nelle fasi precedenti il trapianto.

Sebbene ben caratterizzata dal punto di vista clinico, la malattia rimane ancora poco conosciuta dal punto di vista della patogenesi e i meccanismi molecolari coinvolti non sono stati ancora sufficientemente chiariti.

L'animale modello tipicamente utilizzato per lo studio della MPS I è il topo, sviluppato durante gli anni '90. Pur essendo un buon modello animale, che riproduce sotto diversi aspetti la patologia

umana, il topo è utilizzato principalmente per studi di efficacia terapeutica, mentre è stato più raramente impiegato per condurre più approfondite indagini sulla patogenesi, a causa dei lunghi tempi di sperimentazione richiesti, degli elevati costi associati al mantenimento delle colonie murine e dei crescenti problemi etici coinvolti nell'uso dei mammiferi in ricerca.
La comprensione dei meccanismi patologici che stanno alla base della MPS I può essere di grande interesse per identificare pathways alterati coinvolti nella sua patogenesi, che possano potenzialmente rappresentare nuovi target terapeutici, cui indirizzare anche nuove terapie, a supporto di quelle esistenti.
A questo scopo, nel progetto qui presentato è stato sviluppato un modello di MPS I basato su *Drosophila melanogaster*, meglio conosciuta come moscerino della frutta.
D. melanogaster offre diversi vantaggi come animale modello, poiché ha un ciclo vitale molto breve, che permette di effettuare studi rapidi sullo sviluppo, condotti su un numero elevato di animali, poiché da un singolo incrocio è possibile ottenere una numerosa progenie. Inoltre, *Drosophila* è semplice da maneggiare e ha dei costi di mantenimento relativamente contenuti. In aggiunta, la disponibilità di linee transgeniche fluorescenti permette di condurre semplici e accurati studi *in vivo*. Infine, in *D. melanogaster* è possibile condurre rapidi screening farmacologici.
Il modello di MPS I di *Drosophila* è stato sviluppato utilizzando l'approccio dell'RNA interference (RNAi), grazie alla disponibilità del sistema UAS/Gal4 nel moscerino.
La riduzione ubiquitaria dell'omologo del gene umano *Idua* in *Drosophila* (*D-idua*) porta ad una diminuzione dell'attività enzimatica fino a circa un terzo del livello normale, nel terzo stadio larvale, mentre causa una completa letalità allo stadio di pupa. La selettiva diminuzione di *D-idua* nei neuroni e nelle cellule della glia causa una lieve, ma progressiva disfunzione motoria e, allo stesso tempo, un aumento dell'aspettativa di vita. Il modello di *Drosophila* mostra alcune caratteristiche simili a quelle osservate *in vitro* nei fibroblasti umani e nel topo, quali l'aumento del numero e della dimensione dei lisosomi nel cervello e nel tessuto muscolare, insieme a una riduzione della percentuale di lisosomi acidificati. Inoltre, sono state osservate disfunzioni autofagiche e alterazioni di alcuni pathway metabolici, entrambe migliorate in condizioni di deprivazione di nutrienti. Il modello presenta anche alterazioni della rete mitocondriale, insieme ad un'alterata polarizzazione dei mitocondri. Infine, l'aumento del volume cerebrale e la morfologia alterata delle terminazioni degli assoni motori riflettono alcune alterazioni strutturali del sistema nervoso.

Nel complesso il modello di *Drosophila* della MPS I sembra mimare alcuni aspetti associati alla patologia umana, e mostra forti alterazioni in alcuni pathway che rimangono poco caratterizzati in questa malattia. Pertanto, il modello di MPS I generato nel moscerino della frutta mostra un grande potenziale per approfondire i meccanismi coinvolti nella patogenesi della malattia. A partire dalle alterazioni osservate nei diversi pathways analizzati nel modello, la *Drosophila* MPS I offre la possibilità di svolgere in futuro degli screening farmacologici indirizzati specificatamente a questi pathways alterati, e di ampliare la conoscenza su altri meccanismi che sono potenzialmente coinvolti nell'esordio della patologia.

INTRODUCTION

1. Lysosomal storage disorders and Mucopolysaccharidoses

Lysosomal storage disorders (LSDs) are a group of over 70 inborn errors of metabolism characterized by lysosomal dysfunctions, with an estimated incidence of 1 in 5,000 to 1 in 5,500 live births for those involving enzymes or defects of membrane proteins. Most of them are autosomal recessive, while three are X-linked diseases (Hunter syndrome, Fabry disease and Danon disease) (Platt et al., 2018). LSDs are monogenic diseases caused by mutations in genes encoding for different lysosomal proteins involved in several functions, such as hydrolases, transporters, membrane proteins, and enzyme modifiers or activators. The mutated proteins lead to progressive accumulation of different species and to the subsequent dysfunction of lysosomes. LSDs are commonly classified based on these accumulated species (as for example sphingolipidoses, mucopolysaccharidoses and glycoproteinoses) and are genetically and clinically very heterogenous, although many of these patients present with a progressive neurological impairment.

Mucopolysaccharidoses (MPSs) are a group of eleven LSDs caused by mutations in the genes encoding for the lysosomal enzymes responsible for the degradation of mucopolysaccharides or glycosaminoglycans (GAGs). Mutations in these genes cause a deficit in the lysosomal enzymes activity that leads to the progressive accumulation of undegraded GAGs in several tissues and organs. They are all inherited as autosomal recessive traits, except MPS II, which is an X-linked inherited disease. Depending on the gene involved, accumulation of different GAG species and different clinical phenotypes are registered, each disease usually presenting with a continuum of phenotypes. Some MPSs are characterized by severe forms, often presenting with neurological involvement.

Although individually very rare, the prevalence of all forms of mucopolysaccharidosis is estimated to be one in 25,000 births (“Mucopolysaccharidoses,” n.d.) and it highly varies among different populations, based on the genetic and cultural background (Zhou et al., 2020; Celik et al., 2021). The accumulation of undegraded GAGs leads to a progressive multi-organ impairment and common symptoms among most MPSs are hepatosplenomegaly, bone deformities, joints stiffness, characteristic facies, and cardiac valves impairment. Moreover, patients usually present recurrent high respiratory tract infections, and corneal clouding is a diffused sign.

The onset of symptoms varies among different MPSs and among different patients with the same disease, and usually, we distinguish mild forms characterized by a late onset and a slower progression, and severe forms characterized by an early onset, during the first two-three years of age, and often presenting with or developing a neurological involvement.

2. Mucopolysaccharidosis type I

Mucopolysaccharidosis type I (MPS I) is caused by mutations in the gene encoding for the lysosomal enzyme α-L-iduronidase (IDUA), hydrolyzing the terminal alpha-L-iduronic acid residues of heparan-sulftate (HS) and dermatan-sulfate (DS); mutations lead to a deficit of the enzymatic activity. IDUA is the second enzyme of the degradative chains of HS and DS, which accumulate undegraded in different organs and tissues. Prevalence of MPS I varies from 0.19 to 1.85 per 100,000 live births depending on the country, and it is the most common disease among MPSs (Celik et al., 2021).

Clinically, MPS I is characterized by a continuum spectrum of phenotypes, although typically it is distinguished in Scheie and Hurler-Scheie syndrome, representing the attenuated forms, and Hurler syndrome, which represents the severe form. The latter usually has a very early onset of symptoms (during the first months of life) and presents with a progressive neurological impairment. Without treatment, children with severe MPS I usually die within the first decade of life, as a result of cardiorespiratory failure and progressive neurologic disease (Clarke, 1993; Muenzer et al., 2009).

2.1. Diagnosis

Starting from a clinical suspicion, the first biomarker commonly used for the diagnosis of MPS I is the measurement of GAG levels in urine through the DMB assay and the gel electrophoresis. More recently, the availability of new sophisticated techniques, as the tandem mass spectrometry, permits to evaluate in a rapid and precise way different GAG species in different types of samples (urine, serum/plasma, dried blood spots, amniotic fluid, cerebrospinal fluid, cultured cells, and tissues) (Filocamo et al., 2018).

Another assay commonly carried out for the diagnosis of MPS I is the enzyme activity measurement, usually performed in skin fibroblasts. The assay is based on the measurement of the fluorescence emission of the product of degradation of the substrate by the IDUA enzyme. In fact, the assay uses IDUA-specific substrates with a fluorogenic radical (4-methylumbelliferyl) to

generate a fluorophore product that will absorb energy at a specific wavelength and then emit it at a longer wavelength, enabling to determine the quantity of product generated (Ou et al., 2014). In case of positive results from GAGs measurement and enzyme activity, a molecular diagnosis test is suggested to confirm the diagnosis of MPS I. The aim of the molecular diagnosis is to identify the mutations associated to the gene. Moreover, sometimes GAG levels and enzyme activity measurement alone are not sufficient for the diagnosis, since there are some patients presenting normal enzyme activity and elevated GAG levels and, on the other side, patients presenting absence of enzyme activity and normal GAG levels in urine. These conditions are known as pseudo-deficits and need to be further investigated at a molecular level (Kubaski et al., 2020). Since 2016, MPS I has been included in the new-born screening program in the United States of America (Elliott et al., 2016) as well as in other countries (Taiwan, Italy, Austria, Belgium, Brazil, and Mexico) (Metz et al., 2011; Navarrete-Martínez et al., 2017; Bravo et al., 2017; Burlina et al., 2018; Eyskens and Devos, 2019; Chan et al., 2019).

2.2. Treatments

The first treatment successfully applied to MPS I was the bone marrow transplantation (Hobbs et al., 1981). Nowadays, the hematopoietic stem cells transplantation (HSCT) has become the gold standard for the treatment of the severe forms of MPS I in patients diagnosed and treated before 2-2.5 years of age (de Ru et al., 2011). HSCT is also more efficient if carried out very early, usually before 12 months of age (Poe et al., 2014; Aldenhoven et al., 2015). It alters the natural history of MPS I and stops the progression of the disease also at a neurological level, allowing affected individuals to achieve long-term survival (Poe et al., 2014). However, HSCT still presents some issues, since its successfulness strictly depends on the age of the patients at the time of transplantation, and, although it can stop the disease progression, it remains inefficient for the treatment of some districts, which may be already damaged before the transplantation, as bones and brain (Parini et al., 2017).

As for other MPSs, enzyme replacement therapy (ERT) is available also for MPS I patients, specifically authorized for this disease in USA and Europe starting 2003 (Wraith et al., 2004). ERT consists of weekly infusion of the recombinant enzyme Laronidase (Aldurazyme^{R}, BioMarin, Novato, CA), which reaches the lysosomes through the Mannose 6-phosphate receptor (Gary-Bobo et al., 2007). When HSCT is planned, the therapy is administered starting from the diagnosis up to the engraftment of the transplantation, to stabilize the clinical conditions of pre-

transplantation patients and, in patients where the transplantation is not possible, for the entire life (Parini and Deodato, 2020). ERT can reduce urine GAG levels and liver size and can improve joints mobility. However, it is inefficient in treating the Central Nervous System (CNS) signs, being the enzyme unable to cross the blood brain barrier; it is also inefficient in other districts, such as bones and heart valves, and it does not ameliorate the corneal clouding (Cox-Brinkman et al., 2007; Kakkis et al., 2009; Clarke et al., 2009; Tylki-Szymanska et al., 2010). Furthermore, a long-term study conducted in patients treated with ERT showed that albeit total GAGs in urine were significantly decreased, heparan- and dermatan-sulfate were still significantly elevated (de Ru et al., 2013).

Finally, although in general well tolerated, ERT often results in the production of anti-drug and neutralizing antibodies, which can impair the biological activity of the enzyme. Therefore, antibodies may be responsible for the further reduction of the efficacy of ERT, although a progressive decline of autoantibodies over time was also observed, suggesting the development of a natural immune tolerance (Kakavanos et al., 2003; Laraway et al., 2016; Xue et al., 2016).

2.3. Available *in vitro* and *in vivo* models of MPS I

Different *in vitro* and *in vivo* models of MPS I have become available since the 70s, and they were mainly used for therapeutic efficacy studies. However, the characterization of these models brought us additional knowledge on some typical features of the pathology. These models will be hereafter described.

2.3.1. *In vitro* models

For *in vitro* studies, human fibroblasts are commonly used, as well as cells derived from the animal models.

Beside the absence of enzyme activity and the consequent GAGs accumulation, a common feature of MPS I human fibroblasts is the presence of enlarged vacuoles in the cytoplasm (Conrad et al., 1972; Keeling et al., 2001).

It has been widely shown that MPS I cells are more sensitive to apoptosis compared to normal cells and present reduced proliferation (Pan et al., 2005; Pereira et al., 2010; Viana et al., 2016).

Pan and colleagues showed that heparan-sulfate is defective in binding the Fibroblast Growth Factor (FGF) receptor, and that some other factors interfere with FGF mitogenic signalling, leading

to impairment of both mitogenic and survival-promoting activities, and therefore reduced proliferation and survival (Pan et al., 2005).

Different mechanisms have been suggested to be involved in the induction of apoptosis in MPS I cells. For example, the oxidative stress, that leads to increased toxic products from lipid peroxidation, could induce the premature cell death via apoptosis (Pereira et al., 2008). Together with the oxidative stress, it was noticed an imbalance of the calcium homeostasis, with multi-organellar calcium storage and decrease of calcium concentration in cell cytoplasm, which therefore leads to altered intracellular and lysosomal pH and to altered mitochondria potential (Pereira et al., 2010; Viana et al., 2016, 2017). Alterations of calcium homeostasis and pH cause lysosomal permeability and leakage, which can consequently activate apoptotic cell death (Pereira et al., 2010). Another recent interesting finding about MPS I cells is their impaired phagocytosis ability; however, the pathway is not well characterized so far (Viana et al., 2016).

2.3.2. The mouse model

The first mouse model for MPS I was generated in 1997 by the disruption of the *Idua* gene (Clarke et al., 1997). Since then, other mouse models were generated using different approaches, and nowadays five different mouse models are available, among which three were generated through a knock-out approach and two were generated through a knock-in approach (**Table I**). All these models share common phenotypes, but are characterized by different degrees of disease severity, as well as different ages of symptoms onset (**Figure I**).

Table I. Mouse models of MPS I.

Mouse model	Year of publication	References
Knock-out (targeted disruption of *Idua* gene)	1997	(Clarke et al., 1997; Russell et al., 1998; Braunlin et al., 2006; Garcia-Rivera et al., 2007; Pan et al., 2008; Wilkinson et al., 2012; Derrick-Roberts et al., 2017)
Knock-out (targeted disruption of *Idua* gene)	2002	(Ohmi et al., 2003; Jordan et al., 2005; Reolon et al., 2006, 2009; Baldo et al., 2012, 2017)

Knock-out (targeted disruption of *Idua* gene)	2015	(Kim et al., 2015)
Knock-in (point non-sense mutation)	2010	(Wang et al., 2010; Oestreich et al., 2015)
Knock-in (point non-sense mutation CRISPR-mediated)	2015	(Mendez et al., 2015)

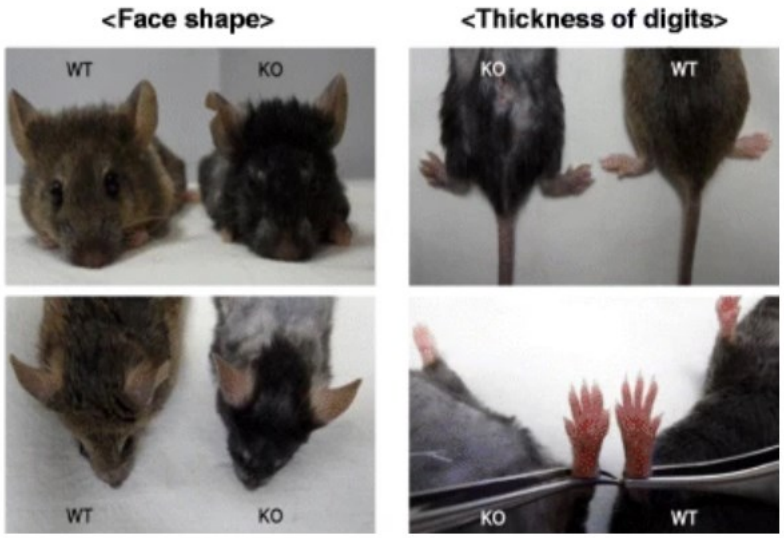

Figure I. The mouse model of MPS I. Adapted from (Kim et al., 2015).

The MPS I mouse presents altered facial features, similar to those observed in patients, with a broader head (Clarke et al., 1997; Garcia-Rivera et al., 2007; Wang et al., 2010; Mendez et al., 2015), dysostosis multiplex and a severe skeletal disease. This is characterized by the thickening and deformity of the bones, which leads to progressive decline of movement and motor dysfunction, together with the loss of contractile capacity (Russell et al., 1998; Wang et al., 2010; Baldo et al., 2012; Mendez et al., 2015; Oestreich et al., 2015; Kim et al., 2015; Baldo et al., 2017). Other typical features of the MPS I mouse model are the broadened paws and the coarse, rough fur (Clarke et al., 1997; Garcia-Rivera et al., 2007; Mendez et al., 2015). Moreover, the MPS I model presents a decreased average lifespan and an increased body weight compared to wild-type littermates (Russell et al., 1998; Pan et al., 2008; Wang et al., 2010; Oestreich et al., 2015; Derrick-Roberts et al., 2017).

As in the human pathology, typical biomarker of the MPS I mouse model is the increased GAG levels in urine and organs. Progressive accumulation of GAGs was observed in urine, liver, spleen, heart and cardiac valves, lung, kidney, skeletal muscle, trachea and brain (Clarke et al., 1997;

Russell et al., 1998; Jordan et al., 2005; Braunlin et al., 2006; Garcia-Rivera et al., 2007; Pan et al., 2008; Wang et al., 2010; Kim et al., 2015; Mendez et al., 2015; Derrick-Roberts et al., 2017; Baldo et al., 2017). Such progressive accumulation of GAGs leads to typical cell phenotypes, where vacuolation and enlargement of lysosomes can be observed, in particular in splenocytes, glial cells, neurons, Purkinje cells, and kidney cells (Clarke et al., 1997; Wang et al., 2010; Baldo et al., 2012; Kim et al., 2015).

Another trait of the MPS I mouse model, in common with the human pathology, is the heart disease: heart of MPS I mouse is enlarged and presents with thickened valves, which lead to cardiac dysfunction (Jordan et al., 2005; Braunlin et al., 2006; Baldo et al., 2017). At a microscopic level, loss of collagen together with disarrangement of elastin fibres, both in the cardiac muscle and in the aorta, were noticed, the latter presenting with thickened walls (Braunlin et al., 2006; Baldo et al., 2017).

The neurological involvement is a very clear sign of the MPS I mouse model. A secondary storage of the gangliosides GM2 and GM3 was observed in the brain, together with a remarkable neuroinflammation, as both the astroglia and the microglia are activated (increase of GFAP and CD68 markers) and many inflammatory markers are upregulated (isolectin-B4, monocyte chemoattractant protein-1, macrophage inflammatory protein-1α, interleukin-1α) (Russell et al., 1998; Ohmi et al., 2003; Wilkinson et al., 2012; Baldo et al., 2012; Mendez et al., 2015; Derrick-Roberts et al., 2017). Moreover, different structural and molecular alterations in the brain cells were observed, such as a reduced thickness of myelination in axons and alterations in the synaptic proteins VAMP2 and Homer1, which are responsible for the rearrangement of the pre-synaptic compartment and for the altered signalling at the post-synaptic density respectively (Wilkinson et al., 2012). Other alterations observed in neural cells are the progressive loss of the Purkinje cells of the cerebellum and the presence of multiple vesicular organelles which resemble autophagosomes in neurons (Russell et al., 1998; Wilkinson et al., 2012).

The MPS I mouse model displays different behavioural deficits, presenting with hypoactivity and learning and memory deficit (Reolon et al., 2006; Garcia-Rivera et al., 2007; Pan et al., 2008; Mendez et al., 2015; Derrick-Roberts et al., 2017), which may reflect both the skeletal and the CNS diseases.

Finally, different signs of oxidative stress were noticed in the mouse model, as the increase of the SOD (SuperOxide Dismutase) activity, of the catalase activity and of the carbonyl groups, but these mechanisms are still poorly characterized (Reolon et al., 2009).

2.3.3. The dog model

The spontaneous dog mutant for the gene *Idua* was first identified in 1982 (Shull et al., 1982). Since then, some studies were conducted to characterize the pathology of the MPS I dog. As already seen in the human and in the MPS I mouse model, the MPS I dog presents elevated GAG levels in urine, cornea, kidney, liver and spleen (Shull et al., 1982, 1984; Constantopoulos et al., 1989; Newkirk et al., 2011; Simonaro et al., 2016). The dog presents with impaired mobility and reduced flexibility of joints, with corneal clouding and with enlarged heart, reflecting similar aspects of the human pathology (Shull et al., 1982, 1984; Constantopoulos et al., 1989; Newkirk et al., 2011). In particular, the characterization of cardiac disease observed that, together with the enlarged heart, the MPS I dog model presents vascular lesions of aorta, with extensive elastin fragmentation, occlusion of the vascular lumen with atherosclerotic-line plaques and loss of smooth muscle cells (Lyons et al., 2011; Simonaro et al., 2016). Moreover, an increased expression of the clusterin was observed, which is involved in the morphological transformation of vascular smooth muscle, and can be used as a biomarker of the cardiac disease (Khalid et al., 2016; Simonaro et al., 2016).

The most evident sign at a microscopical level is the vacuolation of neurons, astrocytes, Kupffer cells and mesenchymal cells of the cornea, which may be a consequence of GAGs accumulation (Shull et al., 1982, 1984; Constantopoulos et al., 1989; Newkirk et al., 2011).

The brain pathology of the MPS I dog model is still uncharacterized; however, as already seen in the MPS I mouse model, a secondary storage of the gangliosides GM2 and GM3 in the brain was identified (Shull et al., 1982, 1984).

Finally, some evidences of inflammation were found in the dog model, where increased levels of TNF-α and IL-8 were measured in serum and in the cerebrospinal fluid (Simonaro et al., 2016).

2.3.4. The cat model

The spontaneous cat mutant for the gene *Idua* was identified in 1979 and displays some common features with the human pathology and the other MPS I animal models (Haskins et al., 1979). The MPS I cat presents with short, broad face, corneal clouding and skeletal disease (Haskins et al., 1979, 1983). As already seen in the other MPS I models, the cat also presents elevated GAG levels in urine, cornea, spleen, liver, kidney, lung and heart (Haskins et al., 1979, 1983; Hinderer et al., 2014). The thickening of the heart valves reflects the human pathology as well (Haskins et al., 1979, 1983; Sleeper et al., 2008). A common trait of the pathology observed at a microscopical

level is the presence of vacuoles in the cytoplasm of different cells, as neurons and hepatocytes (Haskins et al., 1979, 1983). Also in this case, the brain pathology is not well characterized yet; however, neuronal loss and astrocytosis were observed, as well as secondary storage of the ganglioside GM3 (Haskins et al., 1983; Hinderer et al., 2014).

3. *Drosophila melanogaster* as a model of LSDs

The MPS I animal models so far described are very useful to characterize the pathology and to conduct therapeutic efficacy studies. However, the analysis of the mechanisms involved in the onset and progression of the disease can be more difficult, because of the complexity of these animals, the long experimentation timing needed, the elevated maintenance costs, and the ethical issues involved in their handling; all these aspects contribute to the reduction of the sample size available for testing (De Filippis et al., 2022). Therefore, studying the disease in a less complex animal model can be advantageous to understand its pathogenesis and to identify new biomarkers of the pathology as well as new therapeutic targets.

Drosophila melanogaster was one of the first animal models historically used to conduct studies on genetic diseases, and it still is, since approximately 75% of the disease-causing genes in humans are conserved in *D. melanogaster* and, in the last few years, many LSDs have been successfully modelled in the fruit fly (Rigon et al., 2021).

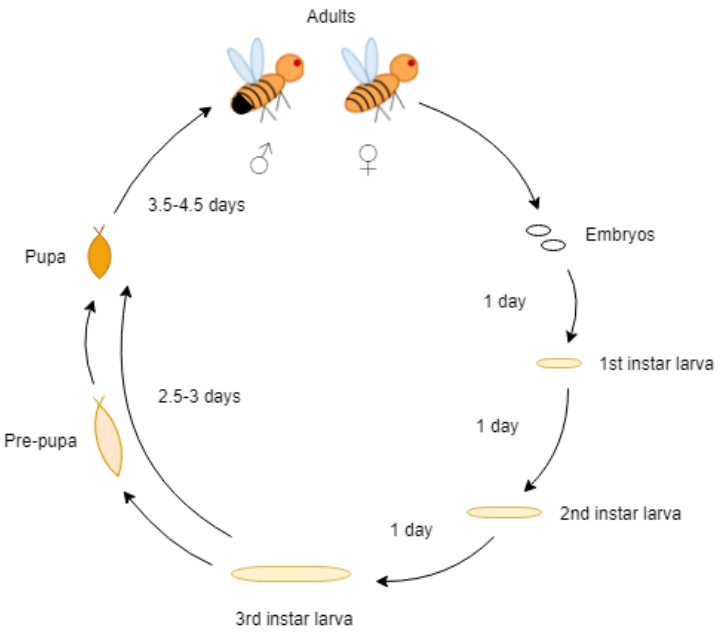

Figure II. *Drosophila melanogaster* life cycle at 25°C.

Many tools are available in *Drosophila* for the easy and rapid genetic manipulation of the organism and for the conduction of *in vivo* studies, including numerous fluorescent transgenic lines, allowing the direct visualization of fluorescent proteins of interest, and the accessibility to vital dyes, directly usable on the alive organism. In addition, there is an increasing availability of antibodies specific for *D. melanogaster* testing.

Different approaches are used for the genetic manipulation of *D. melanogaster*:

- the UAS/GAL4 system, which permits to selectively downregulate the gene of interest ubiquitously, or in a tissue-specific manner (Duffy, 2002);
- the use of transposable elements, which allows to generate knock-out models through chromosomal deletions, homologous recombination or gene replacement; they can be used for gene tagging and chromosome engineering, which allow to generate molecularly marked mitotic clones for mosaic analysis, as well as fluorescent tagged genes for the *in vivo* studies of some protein patterns; lastly, they can be used for targeted misexpression, through RNA interference (RNAi) delivery (Ryder and Russell, 2003);
- the CRISPR/Cas9 technology, a recent and innovative approach which permits to generate a variety of engineered modifications, including genomic deletions and replacements, precise sequence edits, incorporation of protein tags, and tissue-specific knock-out models (Gratz et al., 2015).

In the last ten years, many *Drosophila* models have been generated for LSDs, well reflecting the human pathologies. On the metabolic side, the main finding in these models is the involvement of the endolysosomal and autophagic pathways, which were found altered in most LSD flies. In some models, imbalances in the lipid pathway were also detected. These models revealed to be particularly useful for the study of the neurological pathology, presenting with abnormalities such as dysfunctional motility, abnormal axonal trajectory, decreased number of neuromuscular junction (NMJ) boutons, loss of dopaminergic neurons, as well as apoptosis and increased autophagy at neuronal and glial cells level.

Drosophila LSD models to date available are reported in **Table II**.

Table II. *Drosophila* LSDs models. Adapted from (Rigon et al., 2021).

Disease	Human Gene	*Drosophila* Gene	Protein Alignment Data	Model Generation Method
Neuronal ceroid-lipofuscinosis (CLN) or Batten disease				
CLN1	CLN1/PPT1	*CG12108/Ppt1*	72% similarity, 55% identity	RNAi
CLN3	CLN3	*CG5582/Cln3*	Data not available	Minos transposable element imprecise excision; RNAi
CLN4	CLN4/DNAJC5	*CG6395/Csp*	Data not available	P-element insertion
CLN10	CLN10/CTSD	*CG1548/cathD*	65% similarity, 50% identity	P-element imprecision excision
Mucolipidosis (ML) and Mucopolysaccharidoses (MPSs)				
MLIV	MCOLN1	*CG8743/Trpml*	40% identity	P-element insertion
MPS II, Hunter Syndrome	IDS	*CG12014/Ids*	47% identity	RNAi
MPS IIIA, San Filippo Syndrome type A	SGSH	*CG14291/Sgsh*	53% identity	RNAi
MPS IIIB, San Filippo Syndrome type B	NAGLU	*CG13397*	41% identity	none
MPS VII, Sly Syndrome	GUSB	*CG2135/βGlu*	40% identity, 60% similarity	Homologous recombination
Sphingolipidosis				
Gaucher disease (GD) or glucocerebrosidase deficiency	GBA	*CG31148/GBA1a* *CG31414/GBA1b*	31% identity, 49% similarity	Minos transposable element insertion; Homologous recombination; Transposon insertion and precise excision; RNAi
Niemann Pick disease type 1C (NPC1)	NPC1	*CG5722/Npc1a* *CG12092/Npc1b*	Npc1a: 44% similarity, 63% identity;	RNAi

			Npc1b: 55% similarity, 38% identity	
Niemann Pick disease type 2C (NPC2)	NPC2	*CG7291, CG3153, CG3934, CG12813, CG31410, CG6164, CG11314, CG11315 (Npc2a-h)*	Npc2a: 53% similarity, 36% identity	P-element insertion and imprecise excision
Metachromatic leukodystrophy	ARSA	*CG32191*	Data not-available	PhiC31 integrase system
Fabry disease	GLA	*CG5731*	Data not available	
Saposin deficiency sphingolipidoses	PSAP	*CG12010 (Saposin-related)*	Data not available	P-element insertion and imprecise excision; FLP-FRT based deletion
LSD-like				
Spinster/Benchwarmer	-	*CG8428 (spin* or *bnch)*	Data not available	P-element insertion and imprecise excision; P-element insertion

Most fruit fly models generated to study lysosomal disorders, although not completely characterized in terms of molecular pathways and pathological mechanisms, share similar phenotypes, such as a reduced lifespan, locomotor deficits, and neuronal cell death, highlighting the potential of these invertebrate models to study the neurological mechanisms often associated with LSDs. However, some *Drosophila* models have been deeply analyzed. At cellular level, alterations of vesicular trafficking, inhibition of autophagosome-lysosome fusion, and defects of autophagosome formation/accumulation seem to be common mechanisms, as it was observed in the *Drosophila* models of mucolipidosis type IV, mucopolysaccharidosis type IIIA, and Gaucher disease (Venkatachalam et al., 2008; Kinghorn et al., 2016; Webber et al., 2018). The *Drosophila* model of mucolipidosis type IV showed an increased number of lysosomes and an increased storage of lipofuscin, the latter being a sign of disrupted autophagy (Venkatachalam et al., 2008). The fly model of mucopolysaccharidosis IIIA showed a disruption of vesicular trafficking, with impaired autophagic activity (Webber et al., 2018). The *Drosophila* model of Gaucher disease showed a block of the autophagic flux, together with an altered acidification of lysosomes (Kinghorn et al., 2016). Alterations of the autophagic pathway can cause an accumulation of damaged mitochondria, which leads to oxidative stress and, consequently, to apoptosis, as it was observed in mucolipidosis type IV, in mucopolysaccharidosis type VII and in Gaucher disease *Drosophila* models (Venkatachalam et al., 2008; Kinghorn et al., 2016; Bar et al., 2018). The analysis of these models allowed to understand the involvement of other cellular pathways in the pathogenesis of LSDs. In particular, it was observed that alterations of autophagic pathway, together with alterations of the lysosomal degradative system, can take to the accumulation of misfolded proteins, which in turn activates the UPR (Unfolded Proteins Response) and, therefore, leads to endoplasmic reticulum stress (Maor et al., 2013; Suzuki et al., 2013; Braunstein et al., 2020).

These studies, performed during the last few years, highlighted the potential of the use of *Drosophila* as a model for LSDs, as they permitted to characterize cellular mechanisms involved in their pathogenesis, not known to be involved before.

The emerging roles of these mechanisms can permit the identification of new therapeutic targets, on which pharmacological studies could be carried out, also taking advantage of the possibility to conduct rapid drug screening procedures in *Drosophila*.

4. Autophagy in LSDs

Lysosomes play a central role in processing the clearance of cellular substrates within the endosomal-autophagic-lysosomal system. Autophagy is a highly conserved mechanism among different species, through which the cell degrades and recycles proteins, as well as ageing damaged organelles (Di Malta et al., 2019). Three different types of autophagy are known so far: microautophagy, chaperone-mediated autophagy and macroautophagy, the latter usually referred simply as autophagy.

During macroautophagy there is the formation of a double-membrane vesicle, the autophagosome, which encapsulates cytoplasmic cargo and fuses with lysosomes to generate autophagolysosomes, where substrates are degraded by lysosomal enzymes and recycled (Mizushima and Komatsu, 2011). In microautophagy, some portion of the cytoplasm are directly englobed in lysosomes, through the invagination of the lysosomal membrane (Sahu et al., 2011). Finally, chaperone-mediated autophagy does not involve membranes remodelling; instead, cytosolic proteins are transferred directly into the lysosomal lumen through some lysosomal membrane proteins, such as Lamp2 (Lysosome-associated membrane protein-2) (Orenstein and Cuervo, 2010).

The autophagic process, although constitutively active at a very low rate, is essential during pathologic conditions and other physiologic processes: autophagy is activated at a high rate in case of lack of nutrients, of some drug treatments, and of stress conditions; furthermore, during the developmental stages, when its role is fundamental for the correct remodelling of the tissues, the autophagic process is effectively activated (Mizushima et al., 2008).

Autophagy is a dynamic process, in which three main stages are recognized (initiation, elongation and fusion) with the involvement of different genes and proteins (Mizushima, 2007; Noda et al., 2009).

Autophagosome begins to generate at multiple sites throughout the cytoplasm (initiation); next, the membrane starts to expand, and a structure called phagophore is formed (elongation). During the elongation phase, the phagophore completely surrounds the cargo and its membrane fuses, building a double-membraned autophagosome. Once the autophagosome is completed, it delivers the cargo to the lysosome, with which it fuses through its outer membrane, forming the autolysosome. Into the autolysosome, the autophagosome inner membrane is degraded and the autophagic cargo is exposed to the acidic pH and to the lysosomal hydrolases, which degrade the content of the autophagosome, while the component parts are exported back into the cytoplasm

to be used by the cell in biosynthetic processes or to produce energy (**Figure III**) (Parzych and Klionsky, 2014).

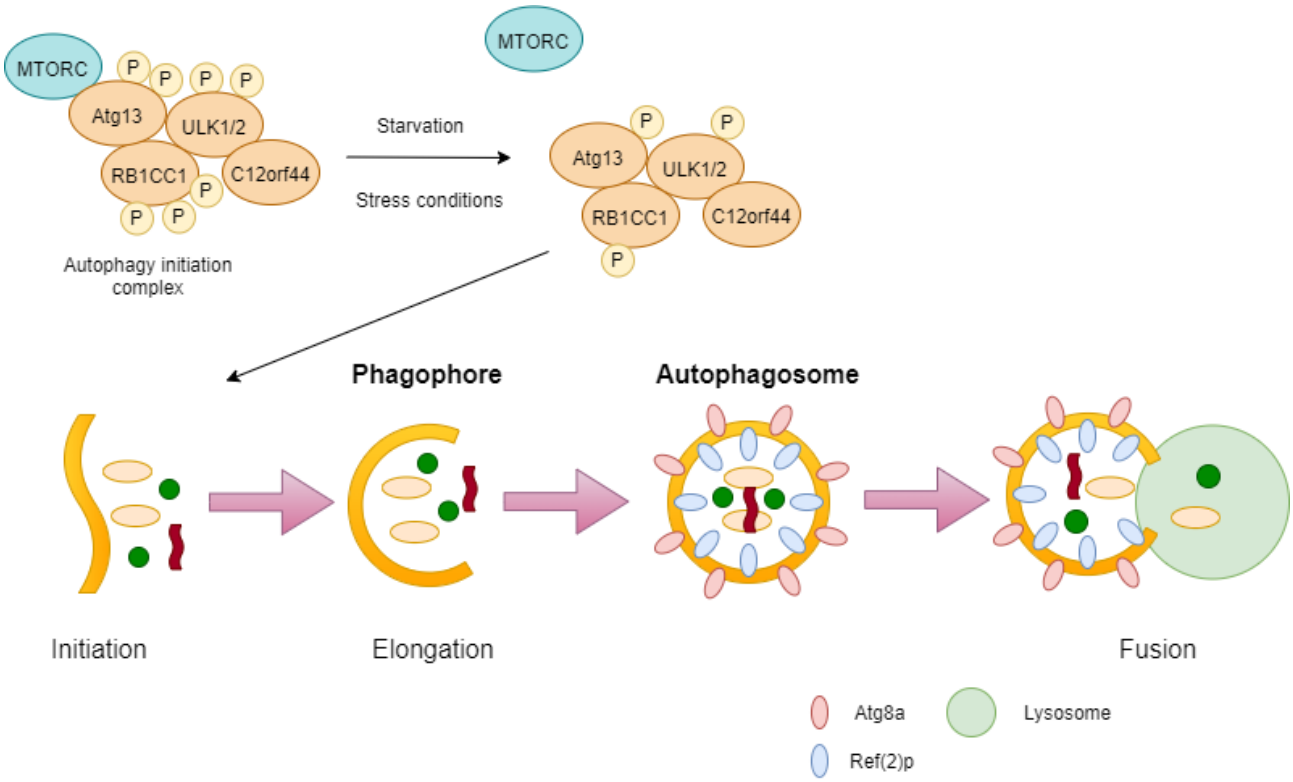

Figure III. Schematic representation of the autophagic process.

During the autophagic process, different proteins of the Atg-related group and of the Rab group take part in every step. However, the start of the process is regulated by the association of the mechanistic target of rapamycin complex 1 (MTORC) to the initiation complex. MTORC is nutrient-dependent, thus it associates with the autophagic initiation complex when the cell is in nutrient-rich conditions, while it dissociates from the complex in absence of nutrients, activating the autophagic process. MTORC is responsible of the phosphorylation of the Atg proteins of the initiation complex, which remains inactive when it is phosphorylated. When MTORC dissociates from the initiation complex, Atg proteins are dephosphorylated and, therefore, the complex activates the autophagic process (Hosokawa et al., 2009).

In the last few years, dysregulation of autophagy was observed to be involved in the pathogenesis of some LSDs (Lieberman et al., 2012). In particular, it was found that there is an accumulation and a defective degradation of autophagic vesicles in Pompe and Danon disease, in MPS IIIA and VI, in

Niemann-Pick disease type 1 and 2, in Fabry disease and in mucolipidosis type IV (Lieberman et al., 2012).

Drosophila melanogaster is particularly suitable for studies on the autophagic process, since in recent years many reporter lines have been developed by the scientific community and made available through public stock centres. In particular, UAS-fluorescent lines have been developed for the easy *in vivo* detection of proteins involved in the autophagic process (such as Atg and Rab proteins), as well as for the detection of the number and structure of lysosomes (especially using lysosomal-associated membrane proteins, such as Lamp1). In fact, GFP and/or mCherry-tagged Atg8a are used to detect the autophagic structures (autophagosomes); reporter lines expressing other tagged-Atg proteins (Atg5 and Atg12) allow the detection of phagophores; GFP and/or mCherry-tagged Lamp lines identify lysosomes and autolysosomes. Moreover, the combination of GFP-Lamp1 with mCherry- Atg8a allows to distinguish autophagosomes from autolysosomes; tagged-Rab proteins (i.e., Rab5, Rab7, Rab11) allow to follow the endocytic pathway and the maturation of endosomes. Furthermore, taking advantage of the different resistance of the GFP and the mcherry proteins to the lysosomal hydrolases, it is possible to use lines with a double reporter (GFP-mcherry tandem construct) and to detect the whole autophagic process, in relation to the acidification of lysosomes. All these lines, crossed with proper enhancer-GAL4 lines, allow to analyse very easily the endolysosomal and autophagic pathways in a cell- and tissue-specific manner (Lőrincz et al., 2017). In addition, a lot of UAS lines are available for the autophagic proteins, both for the downregulation and the overexpression of the autophagic genes, and the combination of these lines together with the model of interest can be useful to conduct rescue experiments, as well as to evaluate the main autophagic genes involved in the pathogenic process.

5. Altered Metabolism in LSDs

Although long recognized as metabolic disorders, still little is known about the metabolic changes associated to lysosomal storage disorders.

It is known that the autophagic pathway is essential for maintaining cellular metabolic homeostasis, and the diminished efflux of monomeric products from autolysosomes can lead to a metabolic insufficiency, where key catabolic products are unavailable to enter a variety of metabolic recycling pathways (Platt et al., 2018).

In addition, autophagy directly regulates lipid metabolism, including fatty acids oxidation, lipolysis, lipogenesis, ketogenesis, and cholesterol efflux, and the suppression of autophagy leads to

defective β-oxidation and ketogenesis (Saito et al., 2019). In particular, autophagy is involved in the lipolysis process, which consists of the breakdown of triacylglycerols and esters by cytosolic lipases, through the modulation of lipoprotein trafficking, and through the supply of lipid droplets (LDs) (Zhang et al., 2018). Moreover, lipid storage can be broken down via lipophagy, a specific selective autophagy that targets LDs and catabolizes their components into free fatty acids and glycerol (Kounakis et al., 2019).

Mitochondria are known to be the main regulators of the cell metabolism and, when damaged, they need to be removed via mitophagy, the autophagic process designated to their selective degradation (Onishi et al., 2021). When autophagy is impaired, no degradation of disrupted mitochondria takes place and this leads to oxidative stress, due to accumulation of reactive oxygen species (ROS), consequence of impaired oxidative phosphorylation, and to an imbalance in lipid and glucose metabolism (Cabrera-Reyes et al., 2021). Still little is known about the involvement of mitochondria in LSDs; however, some studies observed an accumulation of enlarged disrupted mitochondria, presenting an altered oxidation activity and an inefficient production of energy for the cell; instead they were producing ROS, which can lead to cell damage and death.

Mitochondria with altered morphology and altered expression of respiratory chain enzymes were observed for example in Pompe disease muscle cells and mouse model (Lim et al., 2015; Sato et al., 2017), in the MPS IIIC mouse model (Martins et al., 2015), in MPS VI fibroblasts (Tessitore et al., 2009) and in mucolipidosis type IV fibroblasts (Jennings et al., 2006).

In the last years, more evidence is emerging about the essential role of lysosomes in the cellular homeostasis and their involvement in the regulation of cellular metabolism, as well as in the regulation of the autophagic pathway. The lysosome is the endpoint of many catabolic pathways, therefore it can serve as a nutrient reservoir and it can buffer variations in nutrient availability, by modifying the composition and abundance of the cytoplasmic metabolite pool. Consequently, the lysosome can actively affect the rate of metabolic reactions of the cell and communicate the metabolic state to other cellular compartments (Lim and Zoncu, 2016). In fact, it was recently demonstrated that lysosomes are essential for maintaining the cellular homeostasis, because of their capacity to sense the nutrient status of the cell and accordingly adapting the metabolic reactions, through modulation of starvation. Upon lysosomal stress, TFEB translocates to the nucleus and induces lysosomal biogenesis, as well as transcription control of lipid catabolism and lipophagy (Settembre et al., 2012, 2013). Moreover, lysosomes interface physically and

functionally with other organelles, as changes in lipid composition caused by disruption of lysosomal function can lead to changes in mitochondria membrane composition, which therefore can impair mitochondrial function. In fact, it was seen that induction of lysosomal stress leads to a reduction of mitochondrial cardiolipin content (one of the main component of the mitochondrial inner membrane), induces fissions and disrupts mitochondrial function, thus leading to cell apoptosis (Bartel et al., 2019).

Being lysosomes functionality, autophagy and mitochondria deeply interconnected and involved in the metabolic balance of the cell, and being all of them impaired in LSDs, it could be of great interest to examine the possible alterations of these metabolic pathways. This would allow to better characterize the molecular pathogenesis of these diseases and to identify new therapeutic approaches, to re-establish the energetic balance of the cell, which is fundamental to restore its physiological functions.

MATERIALS AND METHODS

1. Fly strains and husbandry

Fly stocks were raised in standard medium (yeast 27 g/l, agar 10 g/l, cornmeal 22 g/l, molasses 66 ml/l, nipagin 2.5 g/l, 12.5 ml/l ethanol 96%) and in standard conditions, at 25°C and 12:12 h light:dark cycles. UAS/Gal4 crosses were performed at 28°C. Fly strains used in this project are reported in **Table 1**. As a control, the strain w^{1118} was used, crossed with the GAL4 drivers.

Table 1. *Drosophila* strains used in the project.

Strain	Source	Code
w^{1118}	Bloomington Drosophila Stock Center	BL 5905
Tubulin-Gal4	Bloomington Drosophila Stock Center	BL 5138
Actin-Gal4	Bloomington Drosophila Stock Center	BL 4414
Mef2-Gal4	Bloomington Drosophila Stock Center	BL 27390
Elav-Gal4	Bloomington Drosophila Stock Center	BL 458
Repo-Gal4	Bloomington Drosophila Stock Center	BL 7415
UAS-GFP-mcherryAtg8a	Bloomington Drosophila Stock Center	BL 37749
UAS-GFP-Lamp1	Kindly provided by Helmut Krämer (Department of Neuroscience, University of Texas, Dallas, TX)	
UAS-$Idua^{RNAi1}$	Vienna Drosophila Resource Center	13244/GD
UAS-$Idua^{RNAi2}$	Vienna Drosophila Resource Center	103771/KK
UAS-$Idua^{RNAi3}$	Vienna Drosophila Resource Center	13245/GD
MHC-Gal4	Bloomington Drosophila Stock Center	BL-55132
Hand-Gal4	Bloomington Drosophila Stock Center	BL-48396
Clk-Gal4	Bloomington Drosophila Stock Center	BL-36316
UAS-mitoGFP	Bloomington Drosophila Stock Center	BL-8442
Mex-Gal4	Bloomington Drosophila Stock Center	BL-91368
fkh-XB30-Gal4	Kindly provided by Reinhard Bauer (LIMES Institute, University of Bonn, Bonn, DE)	

Cad-Gal4	Bloomington Drosophila Stock Center	BL-3042
Tsp42Ec-Gal4	Bloomington Drosophila Stock Center	BL-25620
XSa14-3-Gal4	Kindly provided by Reinhard Bauer (LIMES Institute, University of Bonn, Bonn, DE)	
How-Gal4	Bloomington Drosophila Stock Center	BL-1767
C179-Gal4	Bloomington Drosophila Stock Center	BL-6450
Twi-Gal4	Bloomington Drosophila Stock Center	BL-914
UAS-Dcr; Twi-Gal4	Bloomington Drosophila Stock Center	BL-25707
Pnr-Gal4	Bloomington Drosophila Stock Center	BL-67077

2. RNA extraction and quantitative RT-PCR (qRT-PCR)

Total RNA was isolated from 6-7 third instar larvae using the GRS FullSample Purification Kit (GK26.0050 GriSP, Lda, Porto, Portugal), according to the manufacturer's instructions. The concentration and purity of RNA samples were determined using a NanoDrop 2000c spectrophotometer (Thermo Fisher Scientific, Waltham, MA, United States). Real-time PCR (qRT-PCR) was performed on Eco Real-Time PCR System (Illumina Inc, San Diego, CA, United States), using One-Step SYBR® Prime Script TM RT-PCR Kit II (Takara-Clontech, Kusatsu, Japan). Relative mRNA expression levels were calculated using the Eco Real-Time PCR software. qRT-PCR conditions are reported in **Table 2**. Data represented are the result of three independent biological replicates, analysed in double, and each sample was loaded in triplicate. The housekeeping gene *Rp49* was used as internal control. Primers of the genes analysed are reported in **Table 3**.

Table 2. qRT-PCR conditions.

Step	Temperature	Time
Reverse Transcription	50°C	15 min
Polymerase activation	95°C	2 min
Elongation (x40)	95°C	15 s
	60°C	1 min
Melting curve	95°C	15 s
	55°C	15 s
	95°C	15 s

Table 3. *Drosophila* primer pairs used for the qRT- PCR analysis.

Gene	Primer sequence
Idua	Fw: 5'-GCCCTTCGACTTAATCTTCGCC-3'
	Rv: 5'-GATTGCCCATCCACTCCAGAAC-3'
Rp49	Fw: 5'-AGGCCCAAGATCGTGAAGAA-3'
	Rv: 5'-TCGATACCCTTGGGCTTGC-3'
Tpi	Fw: 5'-GACTGGAAGAACGTGGTGGT-3'
	Rv: 5'-CGTTGATGATGTCCACGAAC-3'
Pfk	Fw: 5'-CTGCAGCAGGATGTCTACCA-3'
	Rv: 5'-GTCGATGTTCGCCTTGATCT
Ldh	Fw: 5'-GTGTGACATCCGTGGTCAAG-3'
	Rv: 5'-CTACGATCCGTGGCATCTTT-3'
Acc	Fw: 5'-TAACAACGGAGTCACCCACA-3'
	Rv: 5'-CAGGTCACAACCGATGTACG-3'
Fasn	Fw: 5'-CGTACGACCCCTCTGTTGAT-3'
	Rv: 5'-AGTGCAAGTTACCGGGAATG-3'
Acly	Fw: 5'-TCCGGCAAGGACATCCTGA-3'
	Rv: 5'-GGAATTTACTGTGGAAAAACGGC-3'
Schlank	Fw: 5'-CGGCAAATGTTCCTATTCTG-3'
	Rv: 5'-CTCGCTATATCCGTCTG-3'
Bmm	Fw: 5'-AGATCTACGAAGGCTCTGTC-3'
	Rv: 5'-GGCATTACTTGTACTGATTCG-3'

3. IDUA enzyme activity

20 third instar larvae were homogenised in 0.9% NaCl plus protease inhibitors (Roche, 05892791001). Following centrifugation, supernatant was recovered, and protein concentration determined (Bradford Reagent, # 39222.03, Serva, Heidelberg, Germany). IDUA activity was measured as previously described (Piller Puicher et al., 2012). Briefly, 100 µg of proteins were incubated with the substrate 4-methylumbelliferyl α-L-iduronide (4MU-iduronide) (Glycosynth #44076, Warrington, UK) and the fluorescence was read at the spectrofluorometer at 365nm excitation/446nm emission wavelengths (Wallac Victor^{2}$_{TM}$, 1420 Multilabel Counter). Final IDUA

activity is given as nanomoles of substrate hydrolysed in 1 h per mg of protein. Three independent extracts were analysed in double, loaded in duplicate.

4. GAG quantification

10 third instar larvae were lyophilized, homogenized in 0.9% NaCl + 0.2% Triton X-100 (PanReac AppliChem GmbH, Darmstadt, Germany) by using a Polytron®PT1200E Disperser (Kinematica AG, Luzern, Switzerland), left under stirring overnight at 4°C, centrifuged at 1000 g for 5 min and, finally, the supernatant was recovered. Protein concentration was determined, and GAG content measured using the Björnsson's protocol (Bjornsson, 1993) with modifications, as previously described (Friso et al., 2010). Three independent extracts were analysed in double, loaded in duplicate.

5. Eclosion rate

Virgin female and male flies were placed in a tube in a 10:5 ratio and allowed to lay eggs for 48h. Then, adults were discarded, and larvae allowed to develop until pupal stage. Eclosed adults were counted every day and the number of adults eclosed/number of pupae was scored as percentage of eclosion.

6. Climbing assay

20 to 30 new eclosed flies were collected and placed in a vial and allowed to recover from anaesthesia for 24h. For the assay, flies were gently tapped down and the flies above the 2cm line from the bottom in 20s were recorded as flies able to climb. Flies were tested three times every 3-4 days.

7. Lifespan assay

New eclosed flies were placed in a vial at low density (<20 flies/vial) and kept at food and temperature standard conditions. They were moved every 3 days in a new vial with fresh food, counted, and dead flies were recorded. Lifespan plots were generated by calculating the percentage of survivorship and plotting viability as a function of time.

8. Starvation assay

For starvation assay, third instar larvae were placed for 4h in a Petri dish with a solution of 20% sucrose in PBS 1X.

9. Western blot

For protein analysis, third instar larvae were homogenized and purified using the GRS FullSample Purification Kit (GriSP, Lda, Porto, Portugal), according to the manufacturer's instructions. Proteins were quantified using the Bradford method (Serva, Heidelberg, Germany). For western blot analysis, 20 µg of extracted proteins were mixed with the LDS sample buffer 4x (Invitrogen, Waltham, MA, USA) and the reducing agent 10x (Invitrogen, Waltham, MA, USA), then boiled for 10 min at 75 °C. Next, they were loaded and electrophoresed in Bolt 4–12% gradient gel (Invitrogen,Waltham, MA, USA) and transferred onto PVDF membranes. The membranes were blocked in blocking buffer (Thermo Fisher Scientific,Waltham, MA, USA). Immunodetections were performed using the following antibodies: rabbit anti-Ref(2)p (1:1000, ab178440, Abcam plc, Cambridge, UK), rabbit anti-LC3 (1:2000, ABC974, Sigma-Aldrich, MO, USA), and mouse anti-actin (1:5000, A5441, Sigma-Aldrich, MO, USA) as loading control. The secondary antibody anti-rabbit HRP was used at a concentration of 1:5000 (A16110, Invitrogen, MA, USA) and anti-mouse HRP (A4416, Sigma-Aldrich, MO, USA) was used at a concentration of 1:20,000. The signals were detected using the Western blotting luminol reagent by Santa Cruz Biotechnology, Inc. (Dallas, TX, USA). The protein bands were detected using the iBright FL1500 Imaging System (Thermo Fisher Scientific, Waltham, MA, USA) and densitometry measurements of the western blot images were performed using Fiji software. Three independent biological replicates were analyzed in double.

10. Immunohistochemistry

Third instar larvae raised at 28°C were harvested, dissected in HL3 (Haemolymph-like) solution and fixed 10 min in 4% PFA. After washing with PBT 0.3% (0.3% Triton-x100 in PBS1X), three times for 5min each, larvae were incubated in primary antibody O/N +4°C. After three further washing in PBT 0.3%, larvae were incubated 1h at RT with secondary antibody. After three final washing in PBT 0.3%, larvae were mounted on glass slides with Mowiol 40-88 mounting medium and covered with a cover glass. Primary antibodies used were: rabbit anti-Ref(2)p (1:200, ab178440, Abcam plc, Cambridge, UK), mouse anti-Elav (1:100, 9F8A9, DSHB, Douglas Huston), mouse anti-Repo (1:100, 8D12, DSHB, Douglas Huston) and mouse anti-FasII (1:100, DSHB, Douglas Huston). Secondary

antibody used were: anti-Rabbit CyTM5 (1:500, Cat# 111-175-144) or anti-Mouse CyTM3 (1:500, Cat# 115-165-003) (Jackson ImmunoResearch Europe Ltd, Cambridge, UK). Phalloidin (1:1000, ThermoFisher Scientific) was incubated 1h at RT, together with the secondary antibody.

11. Lysotracker staining

For Lysotracker staining, third instar larvae were dissected in HL3, incubated 10 minutes in LysoTracker® (1:2000, L7528, Life Technologies) with 20 µM glutamate solution, covered with a glass slide and immediately photographed under a Confocal Microscope.

12. TMRE staining

TMRE (T669, ThermoFisher Scientific) 1:1000 stock solution and, starting from this one, a 1:200 working solution were prepared, in PBS 1X. Third instar larvae were dissected in PBS 1X, incubated 10 minutes in TMRE working solution, rapidly rinsed with PBS 1X, covered with a glass slide, and immediately photographed, all at the same conditions of laser intensity and gain.

13. Brain volume

Third instar larvae were dissected in cold PBS 1X and brains transferred in wells with PBS and washed for 15 min three times. After washing, brains were transferred on glass slides prepared as in **Fig. a** with Flouromount + DAPI and recorded within 3-4 days.

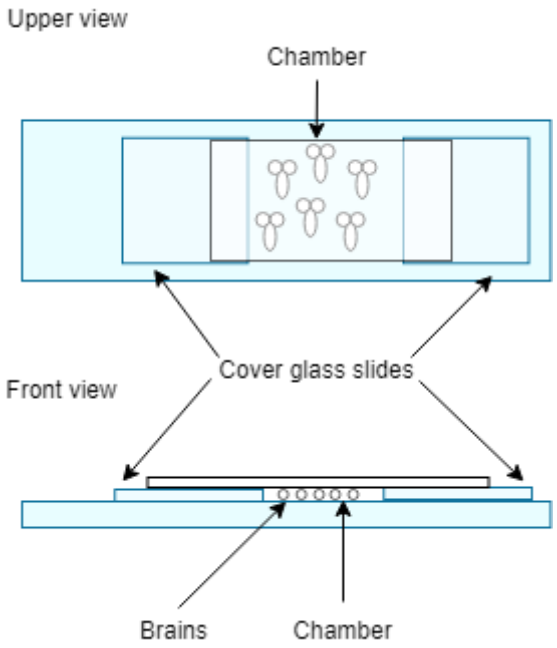

Figure a. Schematic view of glass slides prepared for brain volume measurement.

14. Microscopy imaging

Lysotracker images were acquired by a confocal microscope (Nikon D-ECLIPSE C1), equipped with a Nikon 60x/1.40 oil Plan Apochromat objective, by using the Nikon EZ-C1 acquisition software. All other images were acquired using a confocal microscope ZEISS LSM 800 Confocal Laser Scanning Microscope (Carl Zeiss, Jena, Germany), equipped with a Zeiss 63x/1.4– Plan Apochromat oil objective, by using the ZEN Blue acquisition software. Muscles and brains were recorded with a step size respectively of 0.5 µm and 1 µm and the whole stack of every tissue was acquired. Images for brain volumes were recorded with a Zeiss 10x Plan Apochromat water objective: a complete stack of the brain was recorded by positioning the first and the last planes 15µm before and after the first/last DAPI signal detectable, with a step size of 3 µm. Images of muscles stained with FasII antibody were recorded with a 20x Plan Apochromat water objective. Muscles and ventral nerve cord of ten third instar larvae per group were quantified and analysed with ImageJ Fiji 1.52 software (Schindelin et al., 2012).

15. Microscopy analysis

15.1. Lysosomes and autophagy markers

ImageJ was used to produce a maximum intensity projection of the stack. Threshold of the GFP, mcherry and Cy5 signals was produced with the automatic threshold function. This allowed the elimination of background signal, and the number of particles, as well as their area, were calculated using the 'particle analysis' tool. For quantification of co-localized particles, ImageJ was used to threshold the red and green channels and count the GFP and mcherry dots. Channels co-localization was calculated using co-localization function of ImageJ. For each sample, two muscles and three Regions of Interest (ROI) per muscle, with a range of about 300-500 μm^2, were analysed. The percentage of autolysosomes was calculated as follows:

$$\frac{\text{yellow puncta (autolysosomes)}}{\text{red puncta (autophagosomes)}} \times 100$$

The percentage of mature autophagosomes was calculated as follows:

$$\frac{\text{red puncta (autophagosomes + mature autophagosomes)} - \text{green puncta (autophagosomes)}}{\text{red puncta}} \times 100$$

15.2. Mitochondria analysis in the brain

ImageJ was used to produce a maximum intensity projection of the central slices of the stack. In brain, single cells were selected, and automatic threshold was performed. Using the 'analyse particles' tool, number and average size of mitochondria/cell, of five cells/each brain were quantified.

15.3. Mitochondria oxidation

Analysis of mitochondria oxidation was performed measuring both the fluorescence intensity of TMRE and the percentage of oxidised mitochondria in muscles.

For fluorescence intensity, a ROI of 225 μm^2 was selected and the mean grey value was quantified. Three ROIs per muscle and two muscles per larva were analysed.

Percentage of oxidised mitochondria was measured by first producing a maximum intensity projection of the central slices of the stack. After adjusting the brightness, the tool 'Analyze co-localization threshold' was used to record the co-localized particles between the red (TMRE) and the green (mitoGFP) channel. The green channel was used to count the total number of mitochondria, as already described above in 15.1.

The percentage of oxidised mitochondria was calculated as follows:

$$\frac{\text{number of colocalized particles}}{\text{total number of mitochondria}} \times 100$$

Three ROIs of 225 μm^2/each muscle and two muscles/each larva were analysed.

15.4. Brain volume

Images for brain volume measurement were processed using ImageJ Fiji Software. Firstly, brain images were prepared by carefully removing every tissue not belonging to the brain. Then, the brain volume was measured using the macro in **Fig. b** and setting the parameters 'Gaussian blur X&Y' and 'Empty intensity threshold' to obtain a complete middle slice of the brain as in **Fig. c**. For each group, 50 brains were analysed.

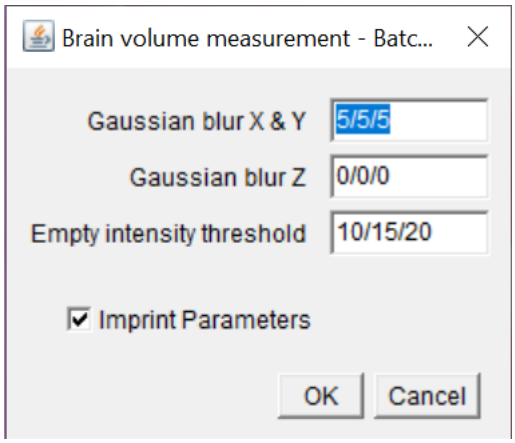

Figure b. Brain volume macro

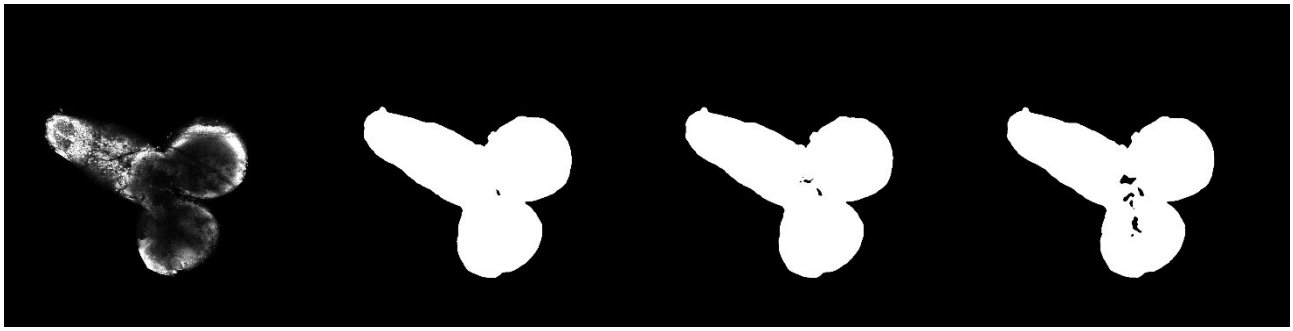

Figure c. Example of brain volume measurement. From left to right: the image acquired at the confocal microscope; the correct blur and threshold settings for brain measurement; incorrect blur and threshold settings with two and more holes in the middle slice of the brain (third and fourth brains).

16. Statistical analysis

Statistical analysis was conducted using GraphPad Prism Software. Student's t-test, one-way ANOVA or two-way ANOVA with Tukey´s *post hoc* tests were applied. Error bars represent standard errors of the means. $p<0.05$ was taken as threshold for the statistical significance.

RESULTS AND DISCUSSION

1. Identification of the *Drosophila melanogaster* homologue of the human *Idua* gene

The first step for the generation of the *Drosophila melanogaster* model of MPS I was the identification of the fly homologue of the human *Idua* gene. A BLAST of the human *Idua* was performed and the *Drosophila* homologue was identified as *CG6201*. *CG6201* encodes for a protein, which displays 30% identity and 47% similarity with the human and the murine IDUA protein (**Figure 1**). As shown in **Figure 1**, the aminoacidic residues of the active sites are conserved between the three species, therefore we tested whether the CG6201 protein has a conserved specific activity as well.

To this aim, I measured the capability of CG6201 to catabolise the IDUA substrate 4MU-Iduronide in wild-type third instar larvae and adult flies, where I found a conserved protein activity of 4.69 and 3.57 nmol/1 h/mg respectively.

With these results I could conclude that *CG6201* encodes for a protein, which is conserved both in the structure and in the enzymatic activity with the human IDUA, therefore CG6201 can be considered an active orthologue of IDUA. In this work, *CG6201* will be thoroughly indicated as *D-idua*, short name for *Drosophila-idua*.

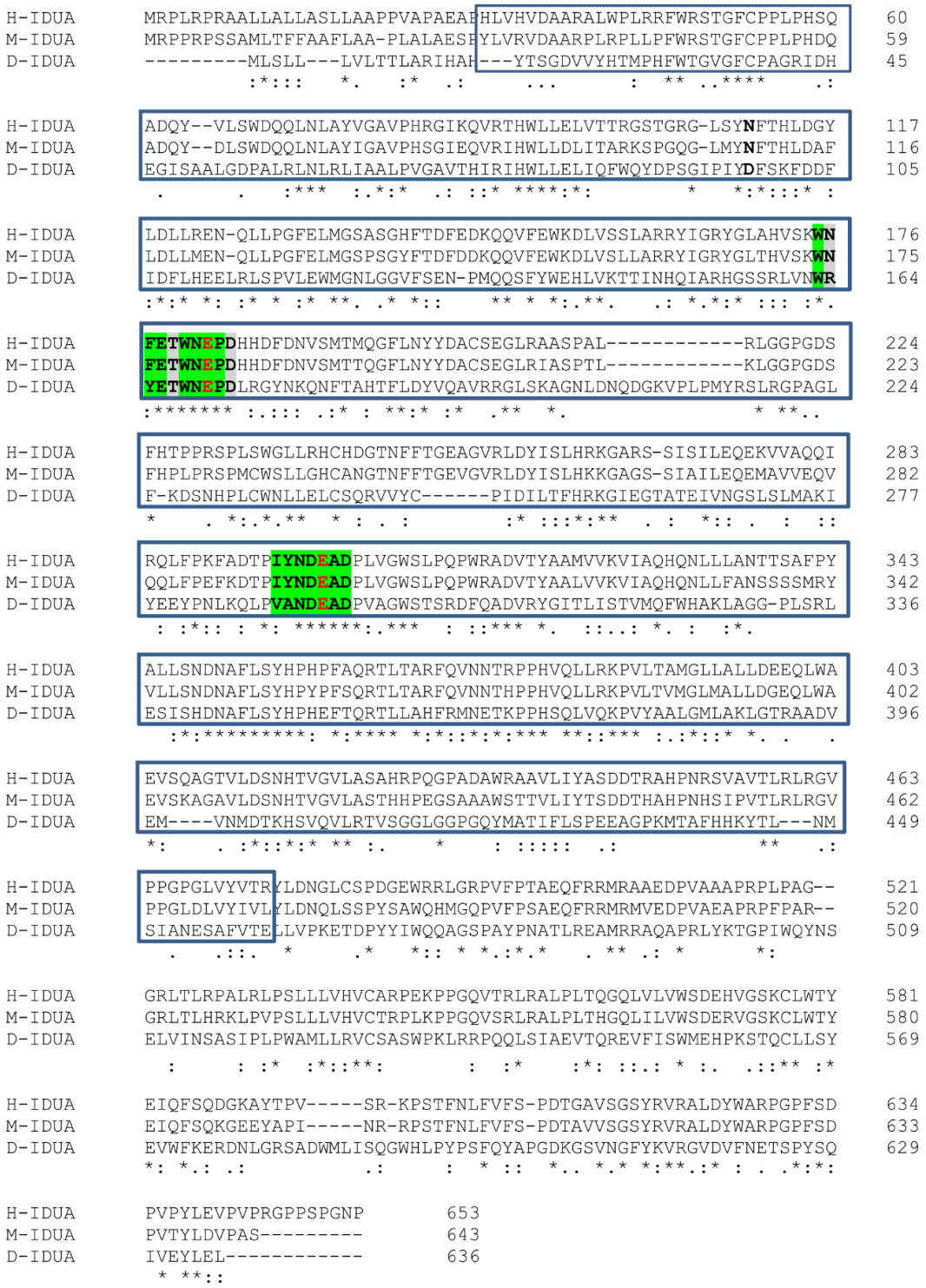

Figure 1. Human, mouse, and *Drosophila* IDUA protein alignment. Sequence alignments of human (H-IDUA), mouse (M-IDUA), and *Drosophila* (D-IDUA) IDUA proteins. The glycosyl hydrolase domain is boxed in blue, highlighted in green are the regions flanking the predicted nucleophiles and acid/base catalysts, and the acid/base residue and nucleophile are marked in red. Asterisk indicates positions which have a single, fully conserved residue. Colon indicates conservation between groups of aminoacids with strongly similar properties. Period indicates conservation between groups of aminoacids with weakly similar properties (from De Filippis et al. 2022).

2. Evaluation of *D-idua* biological functions

The *Drosophila* model of MPS I was generated through the RNA interference (RNAi) approach and taking advantage of the use of the UAS-Gal4 system available in *Drosophila melanogaster*. As shown in **Figure 2**, the crossing between a UAS RNAi line with a tissue-specific or ubiquitous Gal4 driver line, permits the selective downregulation of the gene of interest, through the expression of shRNA related to that gene and the formation of dsRNA, which in turn is degraded by the defence mechanisms of the cell (Duffy, 2002). This system permits to easily and rapidly study the phenotypes associated to the diminished expression of the target gene.

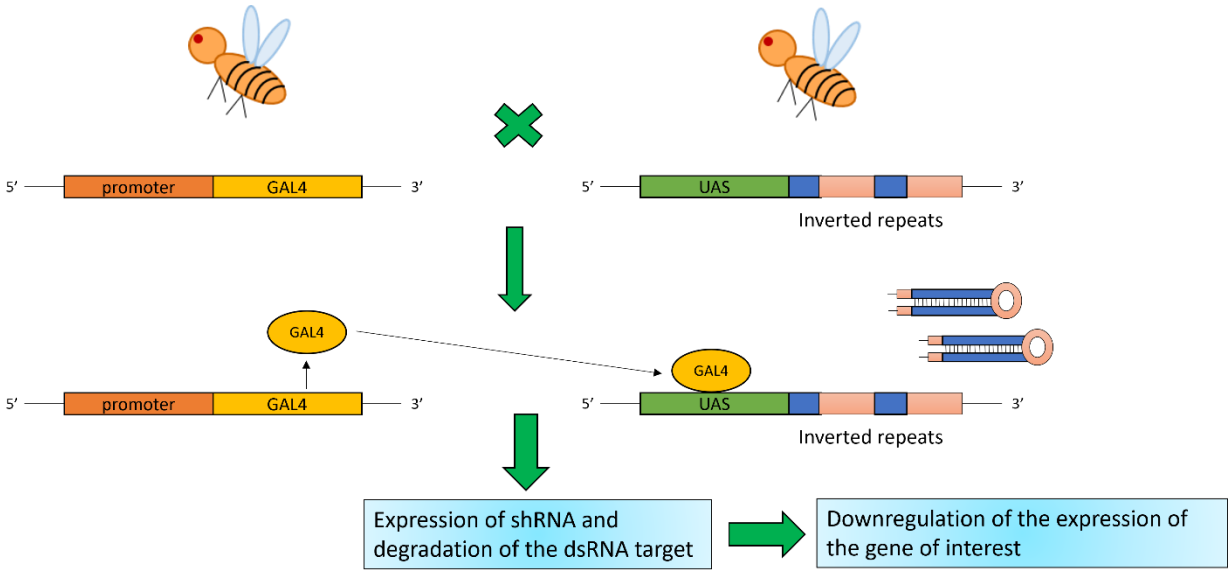

Figure 2. Scheme of the UAS-Gal4 crossings in *Drosophila melanogaster*.

In the public facility Vienna *Drosophila* Resource Center (VDRC) three different UAS RNAi lines were available for *CG6201*: 13244/GD hereafter referred to as D-idua^{RNAi1}, 103771/KK (referred as D-idua^{RNAi2}), and 13245/GD (referred as D-idua^{RNAi3}). The three lines were initially tested to investigate at which level the downregulation was efficient. To this aim, the three UAS RNAi lines were crossed with the ubiquitous strong driver Tubulin-Gal4, which led to a reduction of the *D-idua* expression by 39% in D-idua^{RNAi1}, 53% in D-idua^{RNAi2} and 61% in D-idua^{RNAi3} (**Figure 3A**). The reduction of *D-idua* expression well correlated with the resultant D-idua enzyme activity, where no reduction was observed in the D-idua^{RNAi1}, a reduction to a half in the D-idua^{RNAi2} and a reduction to one third in the D-idua^{RNAi3} lines (**Figure 3B**). Because of the different enzyme activities, different effects on the lethality were observed in the three lines: D-idua^{RNAi1} showed no lethality at pupal stage; D-idua^{RNAi2} showed a partial lethality at pupal stage, with about 70% of escapers

reaching the adult stage; D-idua^{RNAi3} showed complete lethality at pupal stage, with none of the flies able to reach the adult stage (**Figure 3C**). Since D-idua^{RNAi3} showed to be most effective in the downregulation of the gene and showed the strongest *in vivo* phenotype, it was selected for the following analyses, and it will be named D-idua from now on.

The main biomarker used in MPSs is the GAG level measurement. A measurement of GAG levels was performed to see whether the downregulation of *D-idua* leads to GAG accumulation, as already seen in the human pathology, in the mouse model and in some *Drosophila* MPS models (Piller Puicher et al., 2012; Webber et al., 2018; Bar et al., 2018). As shown in **Figure 3D**, a slight increase of GAG levels, although not significant, was observed in third instar larvae, where *D-idua* was ubiquitously downregulated. The hypothesis is that the residual enzyme activity present in the knockdown model may be enough to maintain GAGs degradation; alternatively, this could be due to the early time of analysis in the larval stage, where GAG deposits may not be significantly established yet; in fact, in the MPS IIIB *Drosophila* model, recently described, a very slightly significant increase in GAG levels was observed only starting from the day 1 of adult life (Webber et al., 2018), which could not be analysed in the present model, because of the lethality at pupal stage.

These results suggest that *D-idua* is a vital gene in *Drosophila melanogaster* and that an enzyme threshold is required for the correct development of this organism.

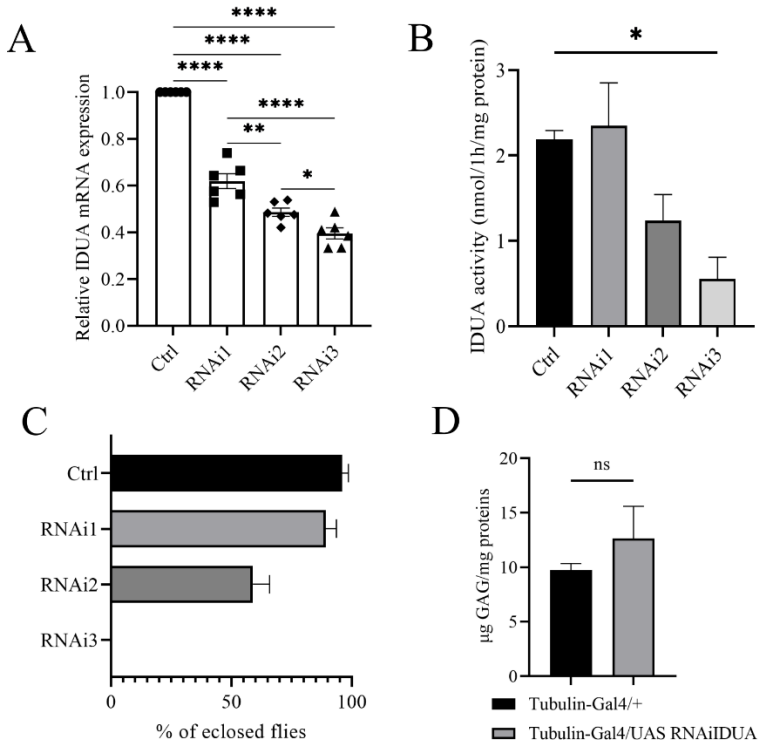

Figure 3. Characterization of the D-idua RNAi lines. (A) qRT-PCR on third instar larvae downregulated for the *D-idua* gene with the driver Tubulin-Gal4 (one-way ANOVA with Tukey's *post hoc* test. * $p < 0.05$; ** $p < 0.01$; **** $p < 0.0001$). (B) D-idua activity in third instar larvae when *D-idua* was ubiquitously downregulated with the driver Tubulin-Gal4. (two-tailed Student's t-test * $p < 0.05$) (C) % of eclosed flies when *D-idua* was downregulated with the driver Tubulin-Gal4 in the three different UAS IDUA strains. (D) GAG analysis in third instar larvae when *D-idua* was ubiquitously downregulated with the driver Tubulin-Gal4. (two-tailed Student's t-test). n = 5-6 larvae/extract. Results are the mean of three different extracts analysed in double. All data are expressed as means ± SEM. Asterisks indicate a statistically significant difference (from De Filippis et al. 2022).

3. Lethality and behavioural phenotypes associated to tissue-specific downregulation of *D-idua*

An important advantage of the use of *Drosophila* as a model organism is the possibility to selectively downregulate the gene or the genes of interest in specific cell types or tissues and to study the changes that this can produce.

As shown in **Figure 4A**, the downregulation of *D-idua* in neurons, using the driver Elav-Gal4 caused no lethality at pupal stage, whereas the downregulation of *D-idua* in glial cells using the driver Repo-Gal4 caused partial lethality at pupal stage, with about 70% of flies reaching adult stage. The downregulation of *D-idua* with the driver Actin-Gal4, a ubiquitous driver, but with a weaker expression compared to the driver Tubulin-Gal4 (Chintapalli et al., 2015), led to a partial lethality at pupal stage, though, surprisingly, the 20% of flies reaching the adult stage were all females

(**Figure 4B**), and this could be due to the higher *D-idua* expression in females compared to males (data from RNA-seq on flybase.org). This could strengthen the hypothesis that *Drosophila* needs a D-idua threshold for the correct development.

In contrast, downregulation of *D-idua* in muscles, obtained using the driver Mef2-Gal4, caused a complete lethality at pupal stage (**Figure 4A**). This unexpected result will be discussed on the base of other findings, shown in the next paragraph 8 of this section.

The negative geotaxis assay, commonly known as climbing assay, is a behavioural test generally used in *Drosophila* to assess the climbing activity. Impairment of climbing ability is often associated to neurological dysfunctions, as well as to locomotion deficits (Ali et al., 2011).

As shown in **Figure 4C-D**, the selective downregulation of *D-idua* in glial cells and neurons led to a mild progressive climbing impairment, starting from day 1 and day 5 of age, respectively. The climbing dysfunction was more prominent when *D-idua* was downregulated in glial cells rather than in neurons, suggesting that D-idua activity is essential in glial cells and, at a lower extent, in neurons, for the correct functionality of the nervous system. Among the LSD *Drosophila* models to date available, still little is known about the effect of the selective downregulation of the genes of interest on climbing. The only *Drosophila* model where the climbing ability was assessed after a tissue-specific downregulation was the MPS IIIA fly model, where the flies presented a significantly decreased climbing activity when the gene *Sgsh* (*N-sulfoglucosamine sulfohydrolase*) was downregulated in neurons (Webber et al., 2018). For all the other models, the climbing abilities were tested in case of a ubiquitous downregulation or gene knock-out. In some of these models, impaired climbing abilities were found, suggesting the decline of climbing activity as a common phenotype of LSD *Drosophila* models; this could be possibly associated to some aspects of the neurological pathology in the MPS I patients (Venkatachalam et al., 2008; Phillips et al., 2008; Maor et al., 2013; Kawasaki et al., 2017; Bar et al., 2018; Lee et al., 2019).

Despite the climbing impairment, the flies where *D-idua* was downregulated in glial cells and neurons showed an increased lifespan (**Figure 4E-F**). In fact, we observed that 50% of adult flies where *D-idua* was downregulated in glial cells were still alive after 40 days, compared to 50% of alive flies after 25 days in controls (**Figure 4G**). The same results were obtained in adult flies where *D-idua* was downregulated in neurons, where 50% of flies were still alive after 35 days, compared to 50% of alive flies after 25 days in controls (**Figure 4H**).

These results were unexpected, since in other *Drosophila* models of LSDs a great reduction in the average lifespan of mutated or ubiquitously downregulated flies was always observed, whereas no

data are available so far about the viability of flies after a tissue-specific downregulation of some genes (Rigon et al., 2021).

Some hypotheses about this phenotype can be based on the currently available literature.

In yeast, it was shown that lifespan can be regulated through the activity of MTORC. It was seen that decreased activity of MTORC is associated with increased lifespan. In addition, the use of rapamycin, a pharmacological inhibitor of MTORC, greatly extended yeast lifespan, probably thanks to the upregulation of the expression of some genes involved in the response of the cell to stress conditions, as of enzymes capable of detoxifying free radicals, degrading damaged proteins through autophagy, and protecting other vital cellular functions (Powers et al., 2006).

Similar mechanisms of lifespan modulation were found in studies conducted in *D. melanogaster*, where it was shown that the insulin signalling, as well as changes in the expression of some genes involved in some metabolic pathways, as lipogenesis and glycolysis, are associated with the extension of lifespan (Hwangbo et al., 2004; Peleg et al., 2016; Parkhitko et al., 2020).

Therefore, deep analyses of these pathways can be conducted to understand the basis of the observed increased lifespan. In this context, one of the advantages of *Drosophila* is the availability of fly lines expressing tagged genes, which, in this particular case, can be used to sort neurons and glial cells (using for example GFP and/or HA tagged neuronal/glial proteins), and extensive metabolic analyses can be conducted on the single cell type.

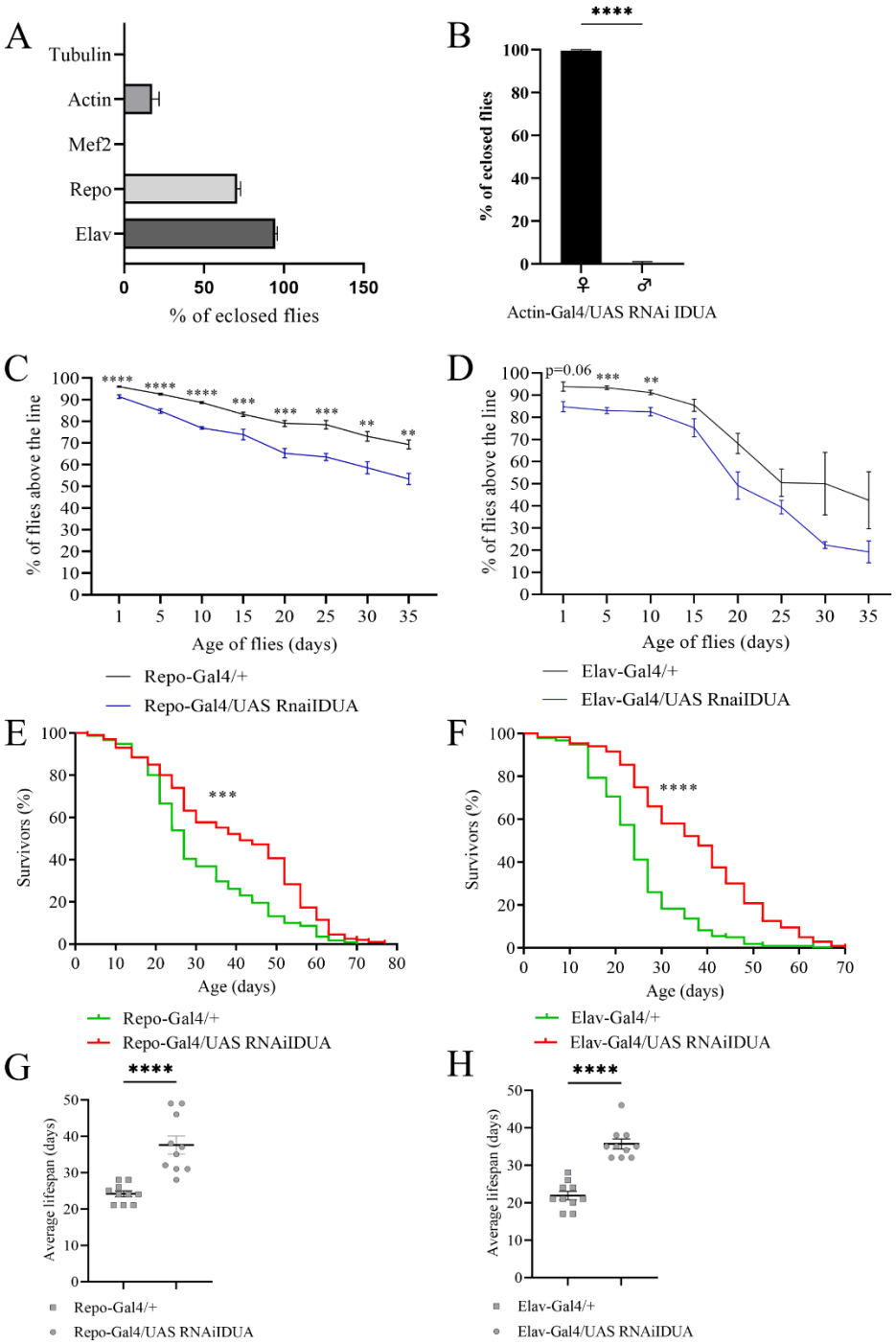

Figure 4. Effects of tissue-specific downregulation of *D-idua*. (A) % of eclosed flies when *D-idua* was downregulated with different ubiquitous and tissue-specific drivers. (B) % of female and male flies eclosed when *D-idua* was downregulated with the ubiquitous driver Actin-Gal4 (two-tailed Student's t-test **** $p < 0.0001$). Climbing activity of adult flies when *D-idua* was downregulated in (C) glial cells and (D) neurons (multiple unpaired t-tests ** $p < 0.01$; *** $p < 0.001$; **** $p<0.0001$). n = 250–300 flies/group. The lifespan of adult flies when *D-idua* was downregulated in (E) glial cells and (F) neurons (Long-rank (Mantel–Cox) test *** $p<0.001$; **** $p < 0.0001$). n = 200–250 flies/group. The average lifespan of adult flies when *D-idua* was down-regulated in (G) glial cells and (H) neurons (two-tailed Student's t-test **** $p < 0.0001$) (from De Filippis et al. 2022).

4. Lysosomal phenotype associated to *D-idua* downregulation

Being MPS I a lysosomal storage disorder, the number and size of lysosomes were also analysed in this model.

To this aim, we used the UAS-GFP-Lamp1 fly line, which has the lysosomal protein Lamp1 fused with the GFP (Green Fluorescent Protein), therefore it allows to directly visualize lysosomes *in vivo*. The crossings performed for these experiments are reported in **Figure 5**.

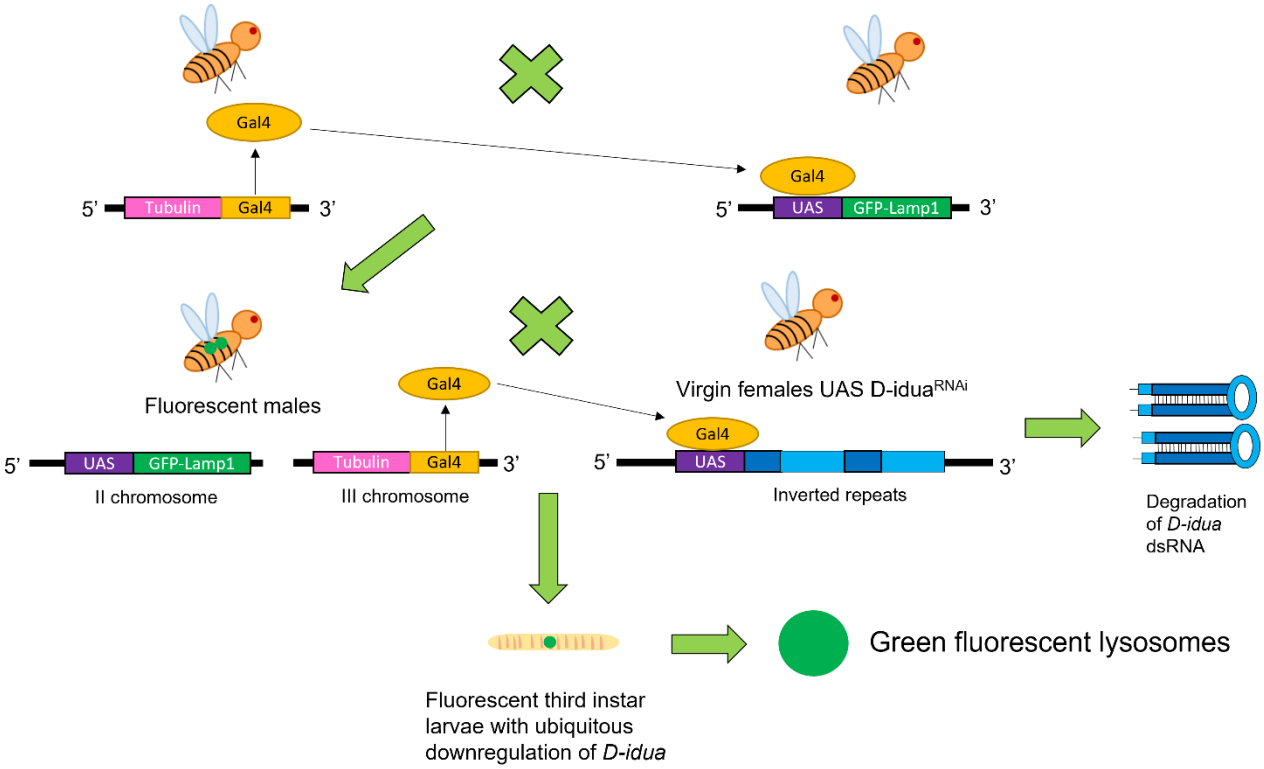

Figure 5. Scheme of the crossings performed for the *in vivo* study of lysosomal phenotype using the UAS-GFP-Lamp1 flies.

As reported in **Figure 6**, central nerve cords of third instar larvae where *D-idua* was ubiquitously downregulated present an increased number and size of lysosomes (**Figure 6C-D**).

The same phenotype was observed in muscles of third instar larvae, where lysosomes number and size were found to be increased to the same extent of the central nervous system (**Figure 7D-E**).

This phenotype is in line with what already observed in the mouse model of MPS I (Ohmi et al., 2003; Wilkinson et al., 2012), confirming that the *Drosophila* model of MPS I mimics some pathological features already observed in other models of the disease.

Lysotracker is a vital dye that easily permeates through the muscle membrane, whereas it has more difficulties in permeating the brain barrier. Therefore, live image tracing of the lysotracker

signal was performed in muscle tissue to quantify the acidification of organelles. As reported in **Figure 7C-F**, muscles of third instar larvae where *D-idua* was ubiquitously downregulated present a significantly decreased percentage of acidified lysosomes compared to controls, with only the 20% of acidified lysosomes, compared to the 40% of controls, leading to the hypothesis that lysosomes may have an impaired functionality, as already observed in the mouse model of MPS I (Pereira et al., 2010).

In some other models of LSDs, lysosomes present an increased percentage of acidified lysosomes, although the mechanisms leading to an altered acidification of lysosomes are not clear yet. What is emerging from LSD studies is that the correct acidification of lysosomes is fundamental to maintain their homeostasis and for their correct functionality.

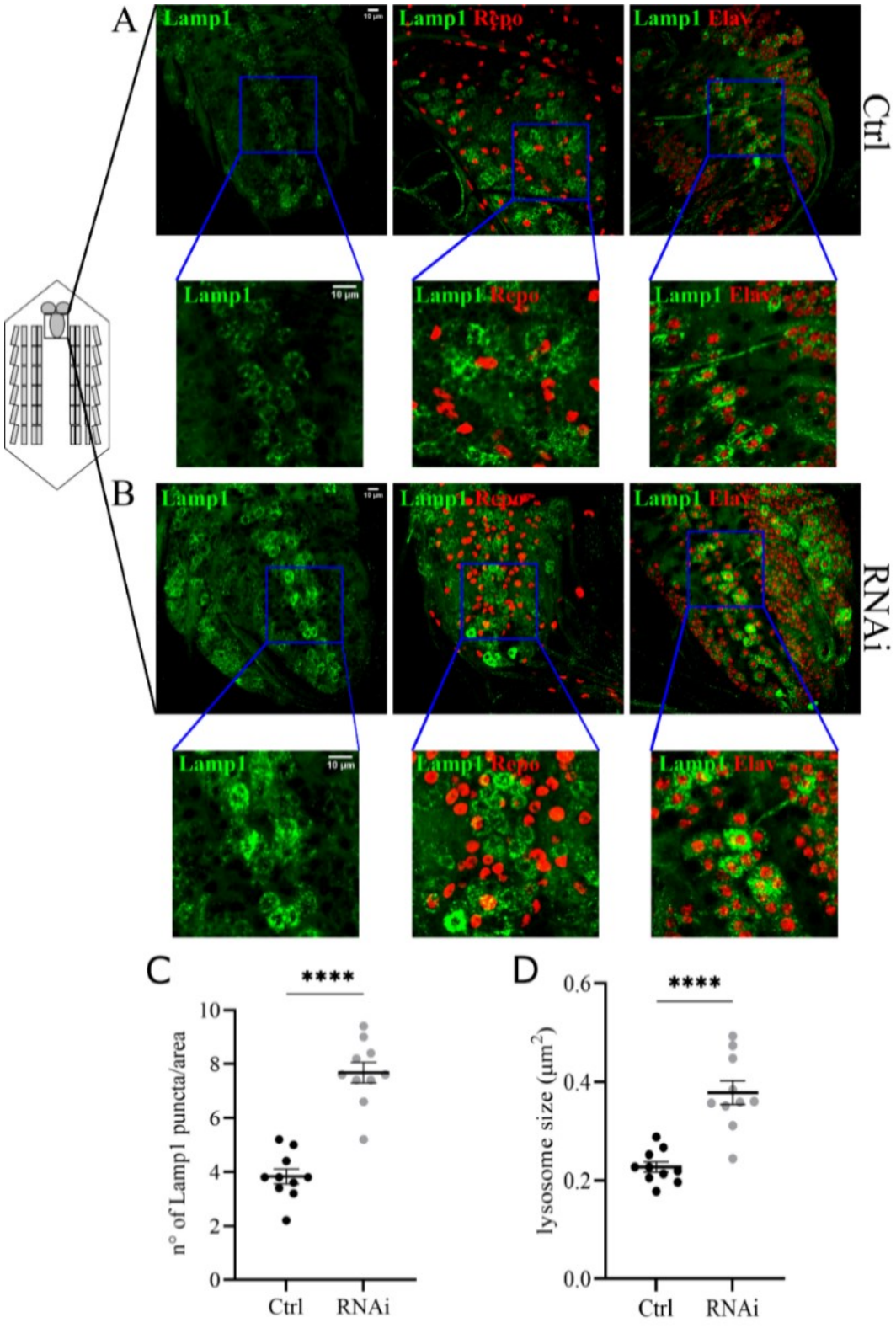

Figure 6. Downregulation of *D-idua* leads to the accumulation of enlarged lysosomes in the central nerve cord. Representative confocal images of central nerve cords expressing the marker GFP-Lamp1 in (A) control and (B) RNAi third instar larvae and the relative quantification of the (C) number and (D) size of lysosomes. n = 10 larvae/group. All data are expressed as means ± SEM. Asterisks indicate a statistically significant difference with respect to control (two-tailed Student's t-test **** $p < 0.0001$). Area = 150 µm^2. Genotypes of samples: Ctrl = Tubulin-Gal4; UAS GFP-Lamp1/+; RNAi = Tubulin-Gal4; UAS GFPLamp1/UAS D-idua^{RNAi} (from De Filippis et al. 2022).

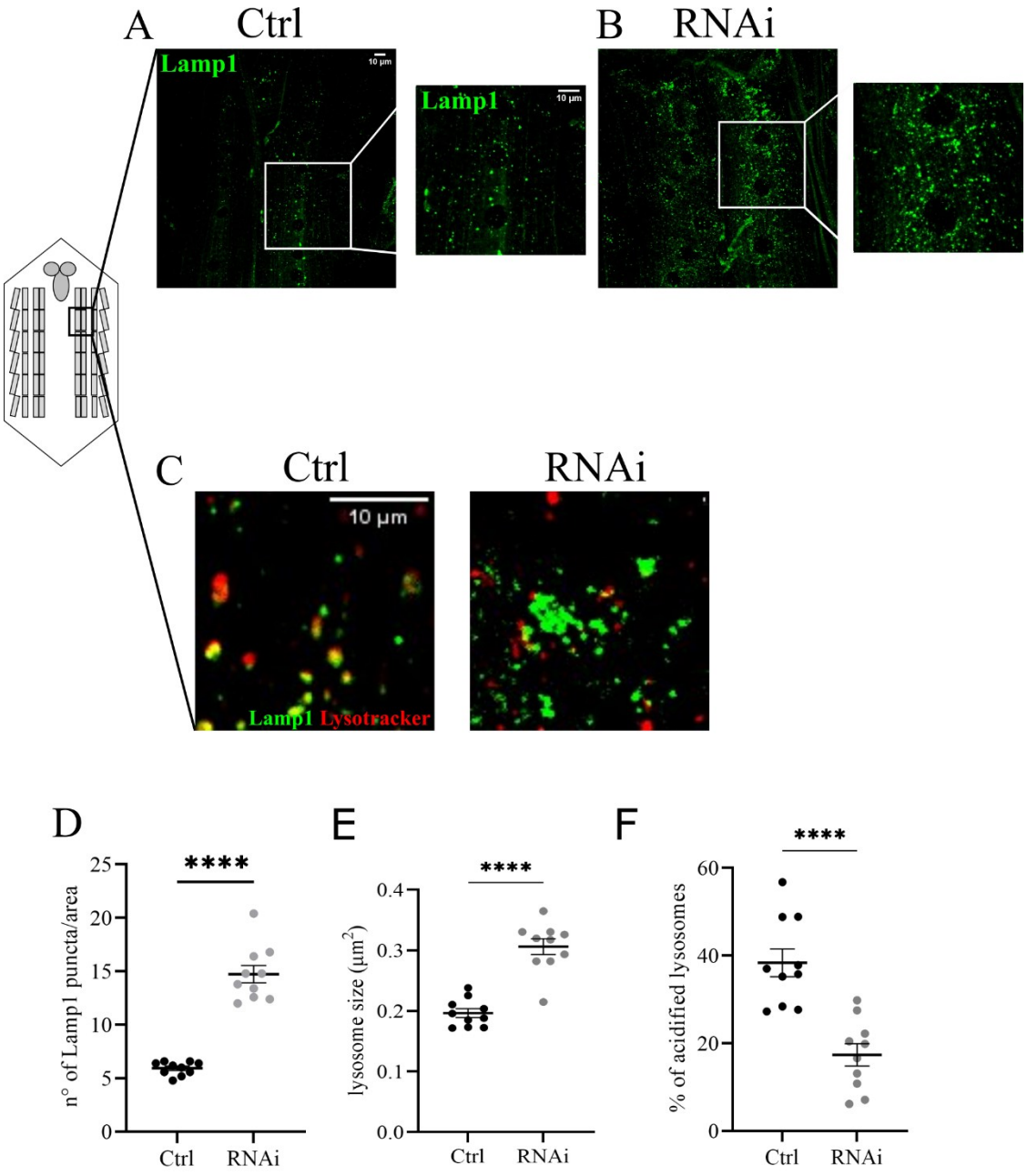

Figure 7. Lysosomal defects associated with a reduction of *D-idua* in muscles. Representative confocal images of muscles expressing the marker GFP-Lamp1 in (A) control and (B) RNAi third instar larvae and the relative quantification of the (D) number and (E) size of lysosomes. (C) Representative confocal images of third instar larvae muscles expressing the marker GFP-Lamp1 and stained with the probe Lysotracker red. (F) Quantification of correctly acidified lysosomes in the muscles of third instar larvae. n = 10 larvae/group. All data are expressed as means ± SEM. Asterisks indicate a statistically significant difference from the control (two-tailed Student's t-test **** $p < 0.0001$). Area = 350 µm^2. Genotypes of samples: Ctrl = Tubulin-Gal4; UAS GFP-Lamp1/+; RNAi = Tubulin-Gal4; UAS GFP-Lamp1/UAS D-idua^{RNAi} (from De Filippis et al. 2022).

5. Autophagy impairment is associated to D-idua reduction and autophagic flux is ameliorated in starvation conditions

The abnormal lysosomal function, as well as an inefficient degradative capability of the lysosomes, have a negative impact on the autophagic flux and autophagy alterations have already been found in many LSDs (Lieberman et al., 2012; Myerowitz et al., 2021).

The role of D-idua in this process was here investigated together with the capability of autophagosomes to fuse with lysosomes, as well as the autophagic flux. These experiments were conducted in standard food conditions and in starvation condition, which is known to be one of the main activators of autophagy.

Autophagosomes-lysosomes fusion was analysed by expressing the fluorescent autophagosomal marker mcherry-Atg8a, together with the fluorescent lysosomal marker GFP-Lamp1 using the ubiquitous driver Tubulin-Gal4, as shown in **Figure 8**.

The use of these lines permits to see autolysosome, marked in yellow (mCherry-Atg8a positive and GFP-Lamp1 positive) and autophagosome vesicles, marked in red (mCherry-Atg8a positive and GFP-Lamp1 negative), and the ratio between autolysosomes and autophagosomes represents a measure of the dynamic autophagosome-lysosome fusion events (DeVorkin and Gorski, 2014). In addition, third instar larvae were stained with the antibody Ref(2)p, the human orthologue of p62, which is another autophagosomal marker and is degraded after the fusion with the lysosomes by the lysosomal hydrolases (Mizushima et al., 2010).

As shown in **Figure 9A-B**, muscles of third instar larvae where *D-idua* was ubiquitously downregulated presented an increased number of lysosomes (GFP-Lamp1 positive particles), as already seen, and an increased number of autophagosomes (mcherry-Atg8a and Ref(2)p positive particles), compared to controls. Despite the increased number of lysosomes and autophagosomes, a block of the autophagosomes-lysosomes fusion was observed, since only about 30% of autophagosomes were fused with lysosomes in the *D-idua* larvae compared with the about 50% of fused particles in the controls (**Figure 9C**). Moreover, the increased number of Ref(2)p particles may suggest a deficit in the delivery of the autophagosomal cargo to the lysosomes, as this protein is not correctly degraded in the lysosomal compartment.

Starvation is known to increase the number of both autophagosomes and lysosomes (Lőrincz et al., 2017). Indeed, in control larvae, starvation induced an increase of lysosomes and autophagosomes number, without changes in the autophagosome-lysosome fusion ratio, as well

as without increasing the number of Ref(2)p particles, both signs of a correctly working autophagic flux (**Figure 9B-C**).

In third instar larvae where *D-idua* was ubiquitously downregulated, starvation greatly ameliorated the autophagic flux: as shown in **Figure 9 B**, lysosome and autophagosome numbers are comparable with those of control larvae in the same conditions, and there is a significant increase of autophagosome-lysosome fusion rate up to the 50%, the same observed in control larvae (**Figure 9C**). The significant decrease of Ref(2)p-positive particles (**Figure 9B**) also indicates a correct delivery of the autophagosomal cargo to the lysosomes, where it will be degraded.

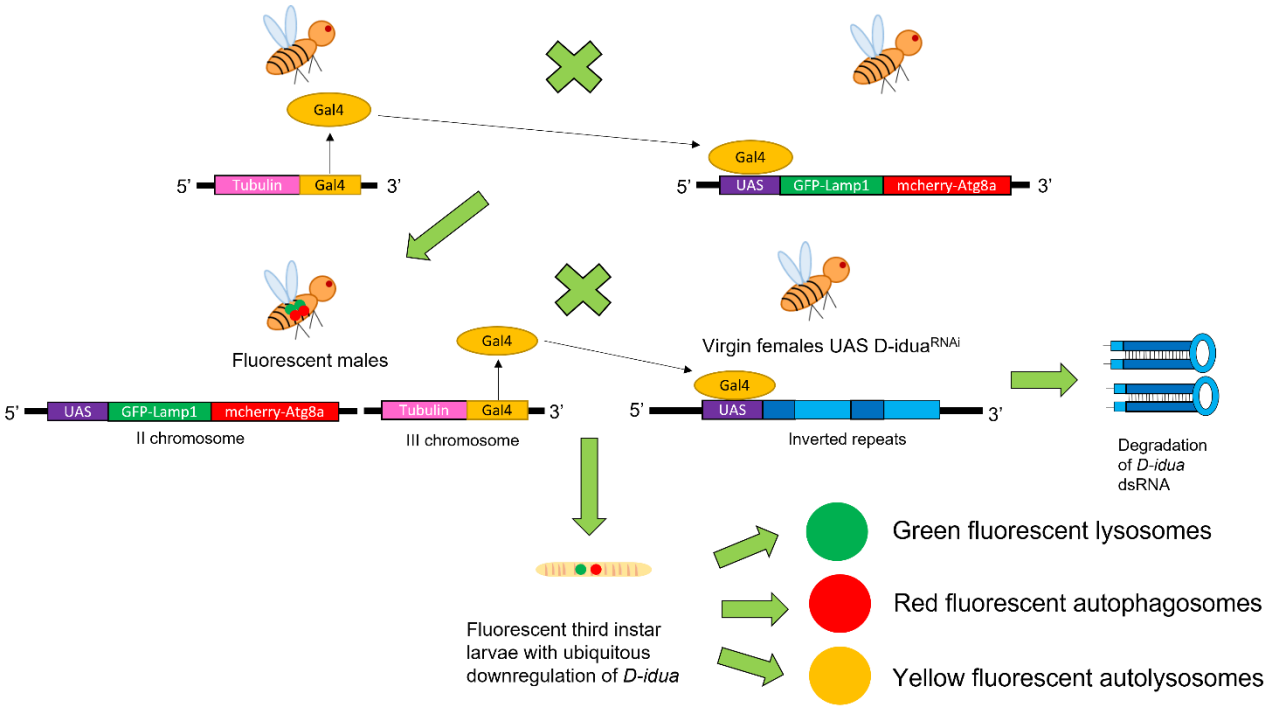

Figure 8. Scheme of the crossings performed to analyse the lysosome-autophagosome fusion using the UAS-GFP-Lamp1 and UAS-mcherry-Atg8a flies.

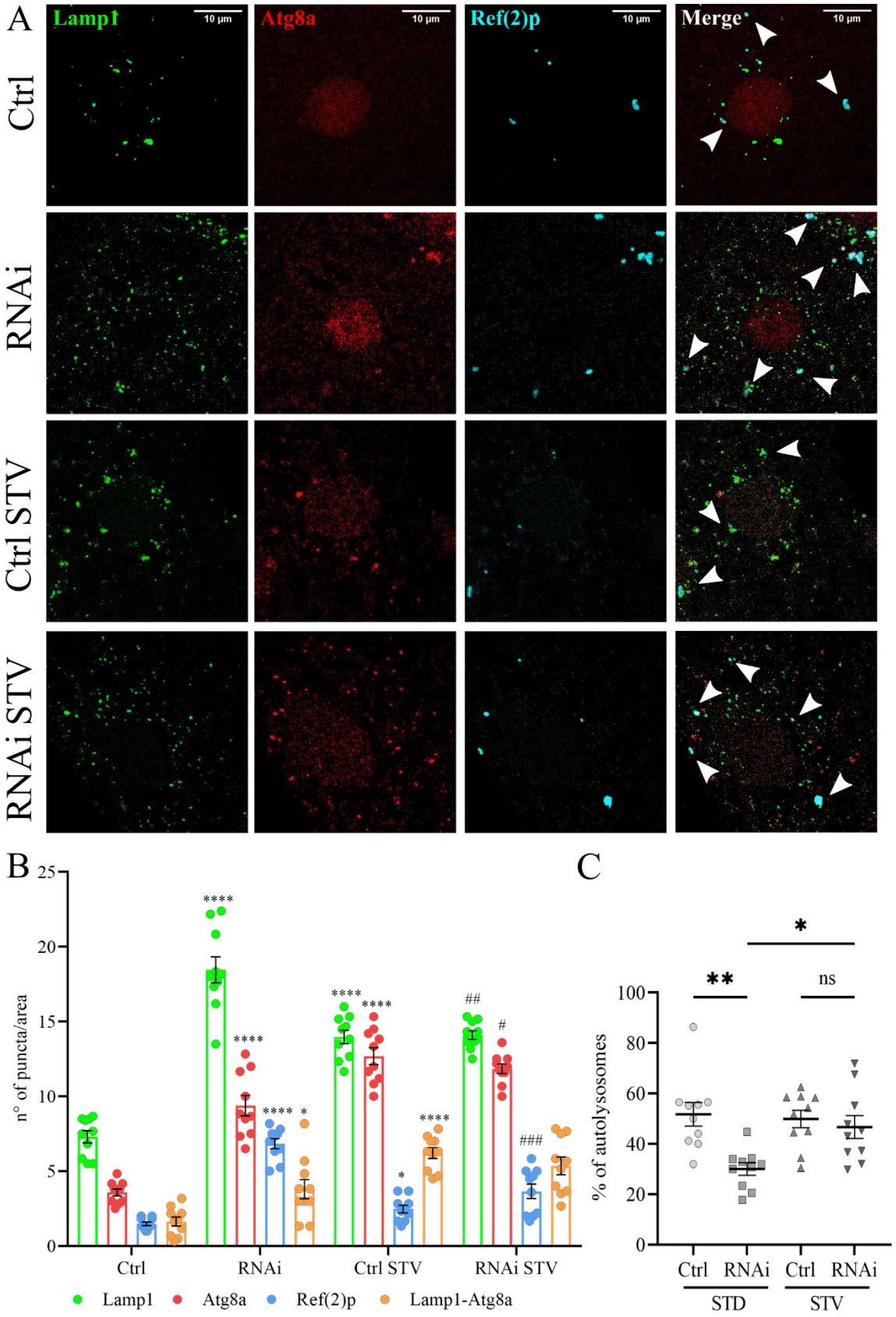

Figure 9. Reduction of D-idua induces defective autophagosome fusion. (A) Representative confocal images of third instar larvae muscles expressing the markers GFP-Lamp1, mcherry-Atg8a, and Ref(2)p. (B) Number of lysosomes, autophagosomes, and Ref(2)p puncta in third instar larvae muscles. Asterisks indicate a statistically significant

difference vs. Ctrl and hash marks indicate a statistically significant difference vs. RNAi (two-way ANOVA with Tukey's *post hoc* test. * $p < 0.05$; **** $p < 0.0001$; # $p < 0.05$; ## $p < 0.01$; ### $p < 0.001$). (C) % of autolysosomes in third instar larvae muscles. Asterisks indicate a statistically significant difference (one-way ANOVA with Tukey's *post hoc* test. * $p < 0.05$; ** $p < 0.01$); n = 10 larvae/group. All data are expressed as means ± SEM. Area = 250 μm^2. Genotypes of samples: Ctrl = Tubulin-Gal4; UAS GFP-Lamp1, mcherry-Atg8a/+; RNAi = Tubulin-Gal4/UAS GFP-Lamp1, mcherry-Atg8a/UAS D-idua^{RNAi3}. STD indicates standard conditions; STV indicates a starvation of 4 h. Arrows indicate autophagosomes (from De Filippis et al. 2022).

The experiment was then repeated by using the tandem construct GFP-mcherry-Atg8a. As shown in **Figure 10**, this construct permits to follow the autophagic flux taking advantage of the different resistance of GFP and mcherry to lysosomal hydrolases: in this context, the autophagosomes marked in yellow (GFP and mcherry positive), after the fusion with lysosomes, are only marked in red, since the GFP signal quenches after the degradation in the acidic pH present in the lysosomes. In the *D-idua* larvae under standard food conditions, we observed an increased number of autophagosomes (increased number of GFP, mcherry and Ref(2)p positive particles) compared to controls (**Figure 11A-B**) and a block of the autophagic flux, as only the 30% of the autophagosomes are mature compared to the 70% in control larvae (**Figure 11C**). Starvation ameliorates the autophagic flux in the *D-idua* larvae, where a decreased number of autophagosomes, as well as an increased percentage of mature autophagosomes were observed: after starvation about 70% of mature autophagosomes were detected in the *D-idua* larvae, a percentage comparable with the about 80% of mature autophagosomes in controls, in the same conditions (**Figure 11B-C**). In addition, the reduction of Ref(2)p particles observed in starvation in the *D-idua* larvae also suggests a correct delivery of autophagosomes cargo and its degradation inside lysosomes (**Figure 11B**). No significant changes were observed in control larvae between standard food conditions and starvation, this meaning a well-working autophagic flux.

Western blot analysis further confirmed immunostaining results. Protein quantification in whole larvae homogenates showed increased levels of Ref(2)p in *D-idua* third instar larvae, returning at control levels after starvation. No significant changes in control larvae were observed in both nutrient conditions (**Figure 11D**).

Atg8a is synthesized as a precursor form and is cleaved at its C-ter, resulting in the cytosolic isoform Atg8a-I. Atg8a-I is then conjugated to phosphatidylethanolamine (PE) to form Atg8a-II. During the elongation phase of autophagy, Atg8a-II is specifically targeted to the autophagosome membrane and remains on completed autophagosomes until fusion with the lysosomes, where

Atg8a-II is delipidated and recycled. Atg8a processing is considered a good marker to assess the status of the autophagic pathway (Ravikumar et al., 2010; Rodríguez-Arribas et al., 2017). Western blot analysis showed an increased Atg8a-I and Atg8a-II protein levels in the *D-idua* third instar larvae, compared to controls. The increase of Atg8a-II levels suggests an increased number of autophagosomes; however, the simultaneous increase of Atg8a-I could also indicate a block in the autophagic flux (Mizushima and Yoshimori, 2007). In addition, the increase of the Atg8a-II/Atg8a-I ratio indicates both autophagosomes formation and an autophagy block in the *D-idua* third instar larvae (**Figure 11E**). All these markers are restored to normal levels under starvation conditions, further confirming immunofluorescence assay data here obtained.

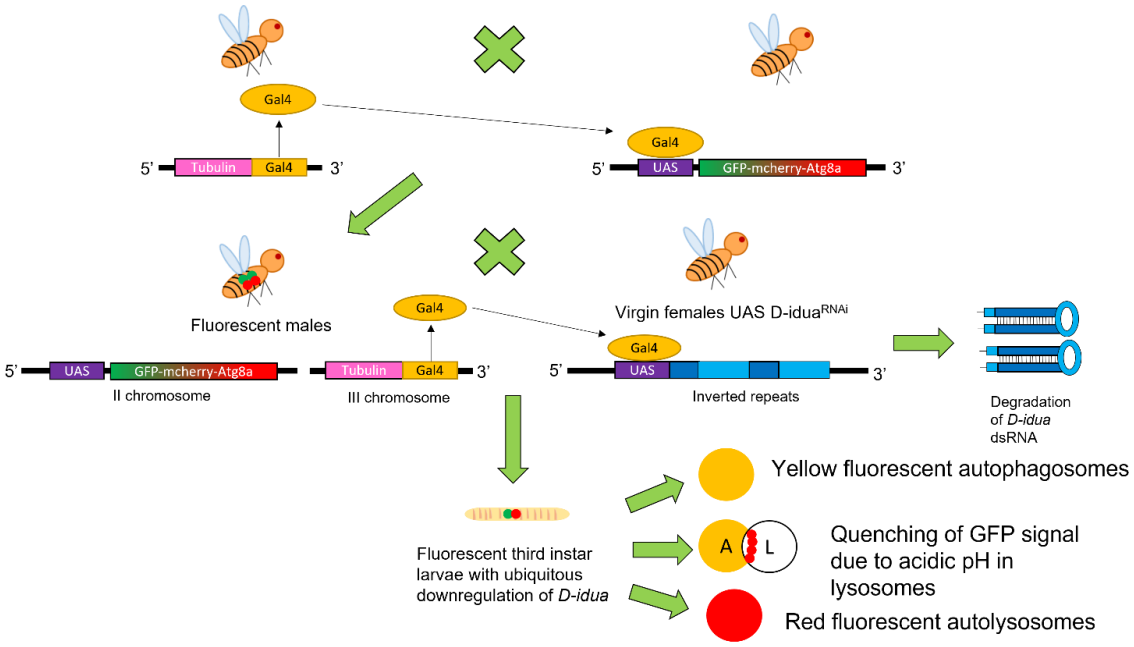

Figure 10. Scheme of the crossings performed for the analysis of autophagic flux, using the UAS-GFP-mcherry-Atg8a flies.

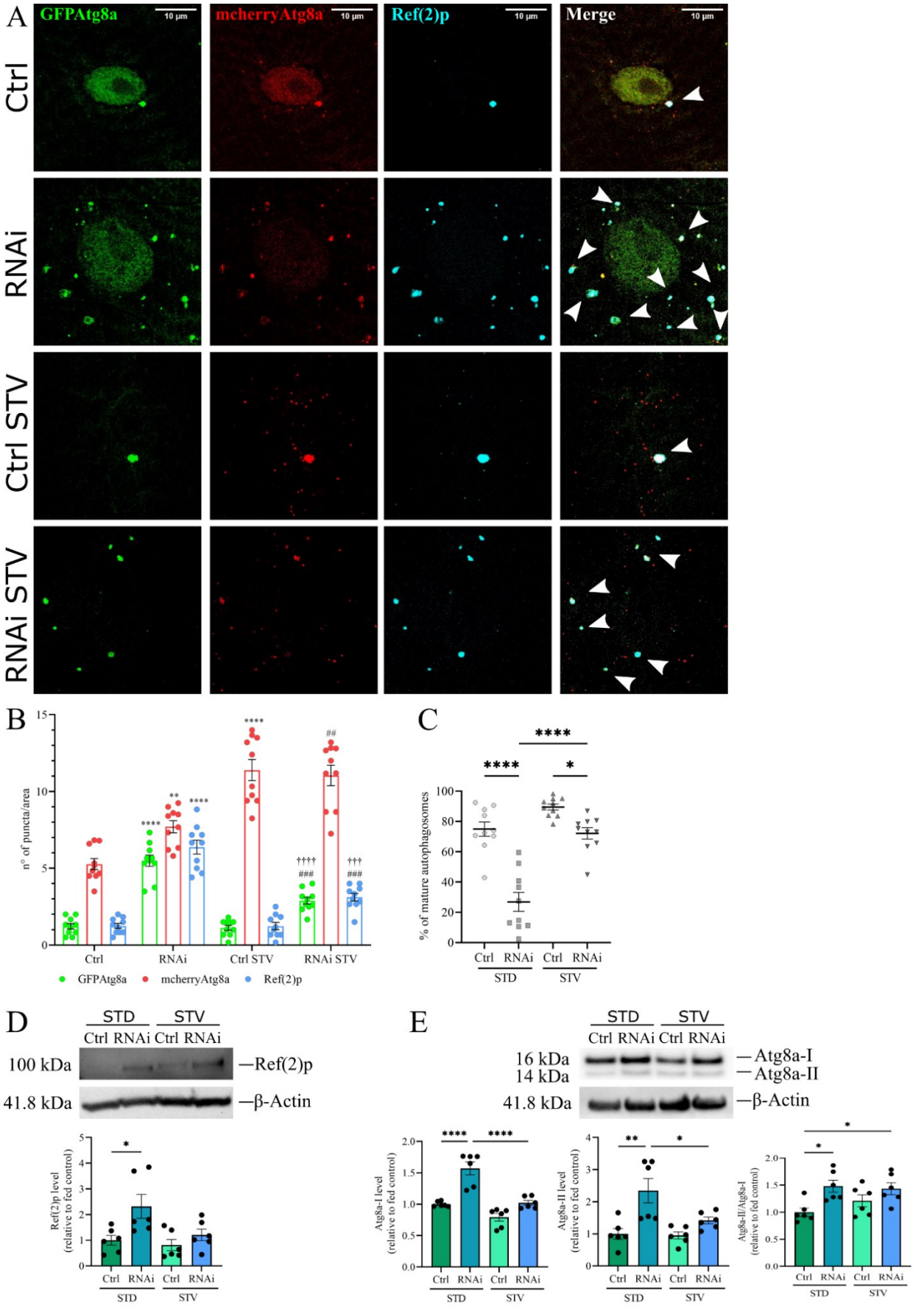

Figure 11. Reduction of D-idua leads to the accumulation of defective autophagic structures. (A) Representative confocal images of third instar larvae muscles expressing the markers GFP-mcherry-Atg8a and Ref(2)p. (B) Number of

autophagosomes, mature autophagosomes, and Ref(2)p puncta in third instar larvae muscles. Asterisks indicate a statistically significant difference vs. Ctrl, hash marks indicate a statistically significant difference vs. RNAi, and crosses indicate a statistically significant difference from Ctrl STV (two-way ANOVA with Tukey's *post hoc* test. ** $p < 0.01$; **** $p < 0.0001$; ## $p < 0.01$; ### $p < 0.001$; ††† $p < 0.001$; †††† $p < 0.0001$). (C) % of mature autophagosomes in third instar larvae muscles. Asterisks indicate a statistically significant difference (one-way ANOVA with Tukey's *post hoc* test. * $p < 0.05$; **** $p < 0.0001$); n = 10 larvae/group. Area = 250 μm^2. Genotypes of samples: Ctrl = Tubulin-Gal4; UAS GFP-mcherry-Atg8a/+; RNAi = Tubulin-Gal4/UAS GFP-mcherry-Atg8a/UAS D-idua^{RNAi}. (D) Western blot of Ref(2)p and the relative quantification (one-way ANOVA with Tukey's *post hoc* test. * $p < 0.05$). n = 5-6 larvae/each extract. Results are the mean of three different extracts analysed in double. (E) Western blot of Atg8a and the relative quantification (one-way ANOVA with Tukey's *post hoc* test. * $p < 0.05$; ** $p < 0.01$; **** $p < 0.0001$). n = 5-6 larvae/each extract. Results are the mean of three different extracts analysed in double. Genotypes of samples: Ctrl = Tubulin- Gal4;/+; RNAi = Tubulin-Gal4/UAS D-idua^{RNAi}. All data are expressed as means ± SEM. STD indicates standard conditions; STV indicates a starvation of 4 h. Arrows indicate autophagosomes (from De Filippis et al. 2022).

Autophagy is a process well-known to be involved in several LSDs; however, the mechanisms leading to autophagic flux alterations are still not well-understood (Myerowitz et al., 2021; Rigon et al., 2021). What it is known so far is that alterations of lysosomes acidification can cause the block of the autophagic flux and, in particular, it was observed that the decreased acidification of lysosomes inhibits the autophagosomes-autolysosomes fusion (Séité et al., 2019; Fedele and Proud, 2020), which is consistent with the phenotype observed in the MPS I *Drosophila* model, here described. It was also demonstrated that lysosomal function is fundamental for the regulation of MTORC and that, when lysosomes present a reduced function, MTORC is downregulated and autophagy is activated (Li et al., 2013). This mechanism was proposed by the authors as a feedback mechanism, through which the cell responses to a reduced molecules degradation in lysosomes; this can help to sustain nutrients need of the cell and to provide for the reduction of molecules caused by the impairment of lysosomal function. On the other hand, in absence of an appropriate degradation system, autophagosomes can accumulate, leading to autophagic stress that contributes to disease progression (Li et al., 2013).
At the same time, starvation is a positive stimulus inducing autophagy and, via mTOR inactivation, induces TFEB (Transcription Factor EB) translocation into the cell nucleus, thus activating the transcription of different genes involved in lysosomal function, and consequently modulating cellular homeostasis (Martina et al., 2012). The same mechanism could be possibly involved in the comprehension of the rescue phenotype observed in the MPS I *Drosophila* model under starvation condition.

Thus, some factors of the autophagic pathway could represent a new therapeutic target for MPS I, as already seen in the MPS IIIB mouse model, where the use of trehalose, a well-known autophagy stimulator, was shown to greatly ameliorate the pathological phenotype (Lotfi et al., 2018).

6. Metabolic shifts are associated to D-idua reduction

Defective autophagy and lysosomal dysfunction lead to changes in the cellular metabolism (Sur et al., 2019; Bosc et al., 2020; Lin et al., 2021). In this project, the levels of expression of some genes involved in the glycolysis and in the lipidogenesis were analysed, to evaluate whether and how lysosomal alterations may affect the metabolic pathways in MPS I (**Figure 12A**).

Concerning the glycolysis, expression levels of 3 different genes were analysed and next described. The first one was *Tpi*, a gene encoding for the enzyme Triose phosphate isomerase, that catalyzes the reversible interconversion of the triose phosphate isomers dihydroxyacetone phosphate and D-glyceraldehyde 3-phosphate and is a key enzyme of the glycolysis for the efficient ATP production. The second one was *Pfk*, a gene encoding for the enzyme phosphofructokinase, that catalyzes the conversion of fructose 6-phosphate and ATP to fructose 1, 6-bisphosphate, and adenosine diphosphate (ADP) and it is the most rate-limiting enzyme of glycolysis. The last gene analysed was *Ldh*, encoding for the enzyme lactate dehydrogenase, that catalyzes the interconversion of pyruvate and lactate (Li et al., 2015).

As reported in **Figure 12B**, the expression of these three genes is significantly upregulated in third instar larvae where *D-idua* was ubiquitously downregulated compared to controls. After starvation, control larvae show a significant reduction of expression of these gene, result that reflects what is already known about the decrease of glycolysis rate under starvation conditions (Lowery et al., 1987; Torres et al., 1988). Interestingly, levels of gene expression of the *D-idua* third instar larvae in starvation are similar to those observed in the control larvae in the same condition (**Figure 12B**).

As for lipidogenesis, expression levels of 3 genes were analysed also in this case. The first one was *Acc*, encoding for the enzyme Acetyl-coenzyme A carboxylase, that catalyzes the carboxylation of acetyl-CoA to produce malonyl-CoA and has a crucial role in the metabolism of fatty acids. The second was *Fasn*, encoding for the enzyme fatty acid synthase, one of the main enzymes involved in the fatty acids production. The last gene analysed was *Acly*, encoding for the enzyme ATP citrate synthase, one of the enzyme responsible for the production of cytosolic Acetyl-CoA, which is

essential for *de novo* synthesis of fatty acids (Tong, 2005; Bueno et al., 2019; Dominguez et al., 2021).

As shown in **Figure 12C**, we found a significantly increased expression only for the gene *Acc* in *D-idua* third instar larvae compared to controls. Starvation significantly reduces *Acc* expression levels in the *D-idua* larvae, lowering them to levels similar to those detected in the control larvae in standard food conditions.

Such data show that the induction of glycolysis in the *D-idua* larvae is accompanied by an increased *de novo* lipogenesis, resulting in coordinated changes of metabolic gene expression. Similar metabolic shifts have been previously observed in an MPS I mouse model, whose liver was deficient in simple sugars, nucleotides, and lipids (Woloszynek et al., 2009). Previously, it was demonstrated that the recycling of GAG metabolites into the lysosomes is fundamental for the *de novo* GAGs synthesis, as well as for the production of raw material which can be reused by the cell to produce energy (Rome and Hill, 1986). Woloszynek and colleagues hypothesized that in MPSs the interrupted GAGs recycling, due to lysosomal dysfunction, would lead to increased utilization of carbohydrates for normal GAGs synthesis and increased lipid use for membrane synthesis, leading therefore to an upregulation of both glycolysis and lipidogenesis. In addition, they found elevated levels of several lipid metabolites, such as cholesterol, sphingosine, and glycerolipids, which are involved in membrane synthesis, and this is consistent with the increased number and size of lysosomes in cells affected by LSDs. In fact, more lysosomal membranes are required to accommodate the accumulation of undegraded substrates, this leading to an increased lipids demand of the cells. These data support the hypothesis that impaired recycling coupled with the homeostatic synthesis of GAGs result in metabolite deficiencies and that cells may undergo a metabolic reprogramming in order to compensate for the metabolite deficiencies (Woloszynek et al., 2007, 2009).

Thus, our findings suggest that the upregulation of glycolysis and *de novo* lipid synthesis may be a response of the cell to deregulated sugar and lipid homeostasis, which may be consequences of the defective degradative system of lysosomes.

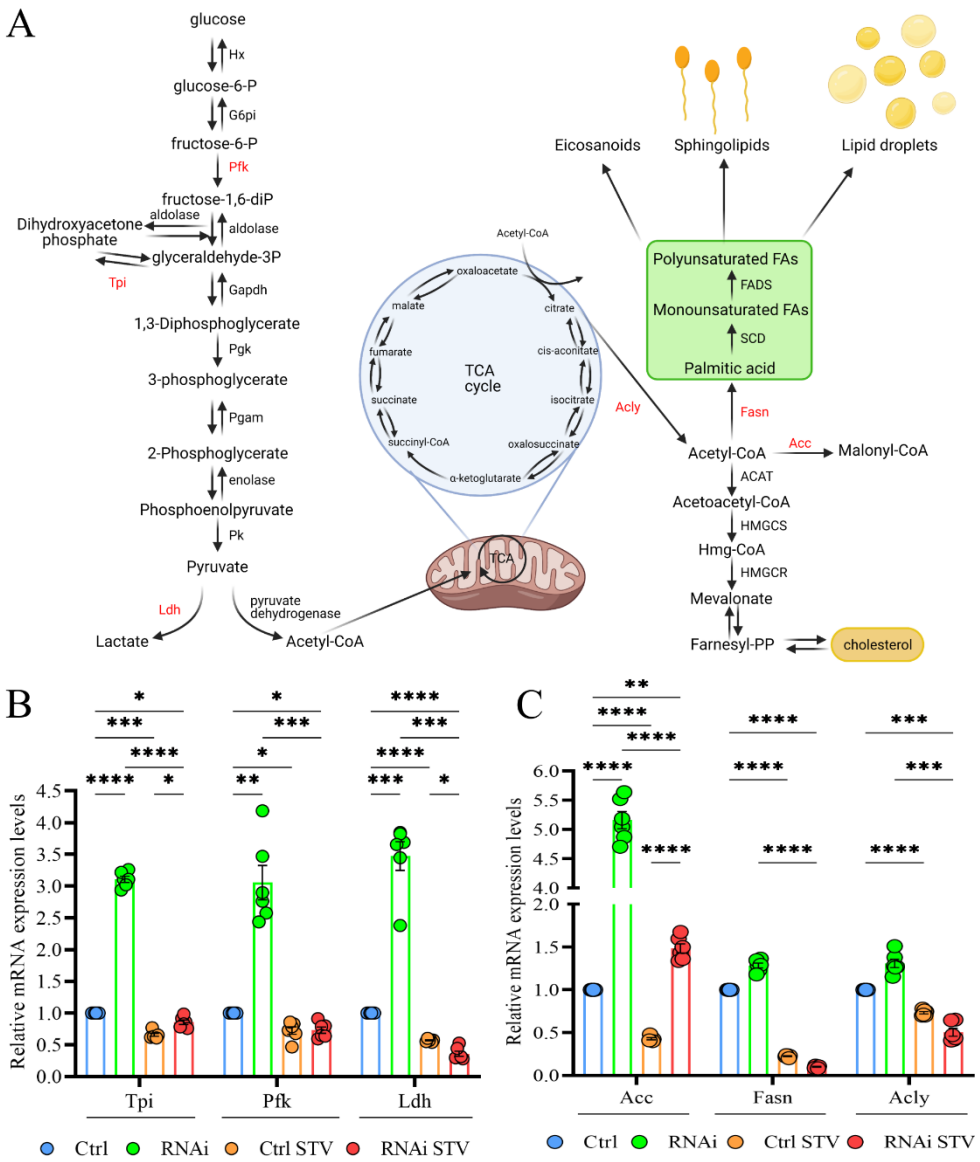

Figure 12. Downregulation of D-idua results in dysregulated glycolysis and lipogenesis. (A) Schematic representation of the crosstalk between glycolysis (on the left) and lipogenesis (on the right). The genes considered in our analyses are marked in red (Created with BioRender). (B) Relative mRNA expression levels of genes involved in glycolysis. (C) Relative mRNA expression levels of genes involved in lipogenesis. Data are the results of three different third instar larvae extracts, each of them analysed twice, in triplicate. All data are presented as means ± SEM. Asterisks indicate a statistically significant difference (two-way ANOVA with Tukey's *post hoc* test. * $p < 0.05$; ** $p < 0.01$; *** $p < 0.001$; **** $p < 0.0001$). Genotypes of samples: Ctrl = Tubulin-Gal4/+; RNAi = Tubulin-Gal4/UAS D-idua^{RNAi}. STV indicates a starvation of 4 h (from De Filippis et al. 2022).

Sphingolipids are abundant species on neural cellular membranes and are involved in the regulation of brain homeostasis. Ceramide (Cer), the precursor of all complex sphingolipids, is a signalling molecule that mediates key events of cellular pathophysiology. Intracellular Cer levels are precisely regulated, as alterations of the sphingolipid-ceramide profile contribute to the

development of neurological and neuroinflammatory diseases. Ceramide Synthase (CerS) is the enzyme involved in the acylation of sphinganine to dihydroceramide, which is subsequently reduced to Cer. CerS isoforms play a role in diverse biological processes such as proliferation, differentiation, apoptosis, stress response, cancer, and neurodegeneration (Mencarelli and Martinez–Martinez, 2013). Unlike mammals, *Drosophila* has only one isoform of CerS, called Schlank.

Brummer (Bmm) is a lipid storage droplet-associated triacylglycerol (TAG) lipase, whose activity is fundamental for the energy homeostatis in *Drosophila melanogaster.* Food deprivation or chronic *bmm* overexpression cause the depletion of fat storage, whereas loss of bmm activity causes obesity in flies (Grönke et al., 2005).

Schlank gene expression is significantly reduced in *D-idua* third instar larvae compared to controls, and it returns to controls levels in starvation conditions (**Figure 13**). Similarly, *Bmm* expression is significantly reduced in *D-idua* third instar larvae compared to controls, whereas it returns at control levels after starvation (**Figure 13**).

It has been demonstrated that *Schlank* has a fundamental role for the central nervous system development, through the *de novo* sphingolipids synthesis pathway, and when *Schlank* is downregulated, this leads to altered sphingolipids metabolism (Mullen et al., 2011; Voelzmann and Bauer, 2011). Thus, the alterations of *Schlank* expression observed in the MPS I *Drosophila* model can lead to dysfunctions of central nervous system development, and further analyses would help to better characterize this pathway and to possibly identify a correlation between the MPS I pathology in *Drosophila* and the neurological involvement often present in MPS I patients. In addition, it was demonstrated that downregulation of *CerS2*, one of the mammalian isoforms of CerS leads to autophagy activation and to the upregulation of unfolded protein response (Spassieva et al., 2009). This aspect could be in agreement with our findings, where the reduced expression of *Schlank*, may contribute to the activation of autophagy, observed in this MPS I model.

The mutant mouse model for the gene *Atgl*, the mammals homologue of *Bmm*, showed accumulation of TAG in heart, and cardiac steatosis, which lead to cardiac dysfunction (Schoiswohl et al., 2010; Kienesberger et al., 2013). Similarly, in the MPS I *Drosophila* model generated in the present project, the reduced expression of the *Bmm* gene can cause cardiac dysfunction, which can be analysed in the future and possibly correlated with the cardiac pathology observed in the MPS I patients, whose cardiac failure is one of the most common causes of death.

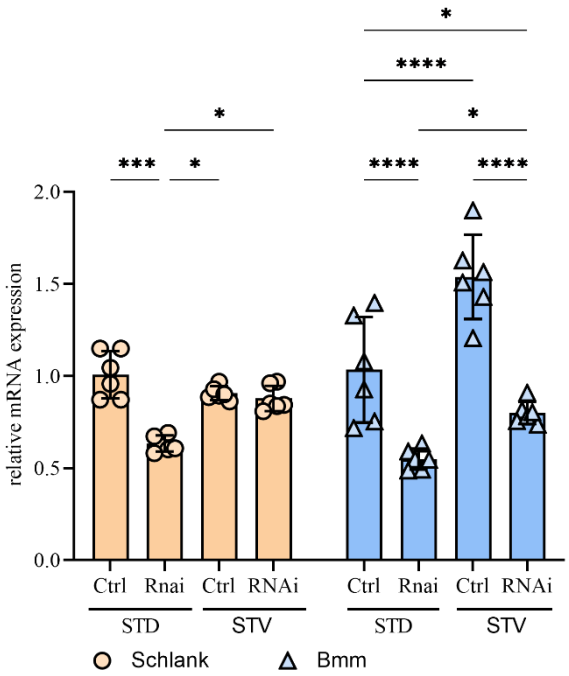

Figure 13. qRT-PCR of *Schlank* and *Bmm* genes in third instar larvae where *D-idua* was ubiquitously down-regulated. Data are the result of three independent biological replicates analysed in double and are presented as mean ± SEM. Asterisks indicate a statistically significant difference (two-way ANOVA with Tukey's *post hoc* test. * p<0.05; *** p<0.001; **** p<0.0001). Genotypes of samples are the following: Ctrl = Tubulin-Gal4/+; RNAi = Tubulin-Gal4/UAS D-idua^{RNAi}. STD indicates standard food conditions. STV indicates a starvation of 4h.

7. D-idua reduction causes alterations in mitochondria morphology and functionality

In the last few years, the role of mitochondria in LSDs is emerging and alterations of mitochondria morphology and functionality were found in several diseases (Jennings et al., 2006; Lim et al., 2015; Martins et al., 2015).

Mitochondria alterations have never been investigated in MPS I and the *D-idua* model offers the opportunity to easily analyse and characterize these mitochondria-associated phenotype thanks to the availability of the UAS GFP-mito line, which permits to directly see mitochondria marked with the GFP *in vivo*.

Crossings performed for mitochondria analysis are the same of those presented in **Figure 5**, using the UAS GFP-mito flies instead of the UAS GFP-Lamp1 flies.

In **Figure 14A** the alteration in the structure of mitochondria can be clearly seen: in control larvae muscles, mitochondria are well interconnected, forming a continuous network; on the contrary, in the *D-idua* larvae, mitochondria present with fragmentation and a disrupted network. This

phenotype was already observed in human MPS II fibroblasts, where mitochondria chains present a decreased elongation (Zalfa et al., 2016).

In CNS cells, an increased number and size of mitochondria was observed (**Figure 14B-D**), this well correlating with some findings in MPS VI cells, where an increased number of enlarged mitochondria was observed (Tessitore et al., 2009).

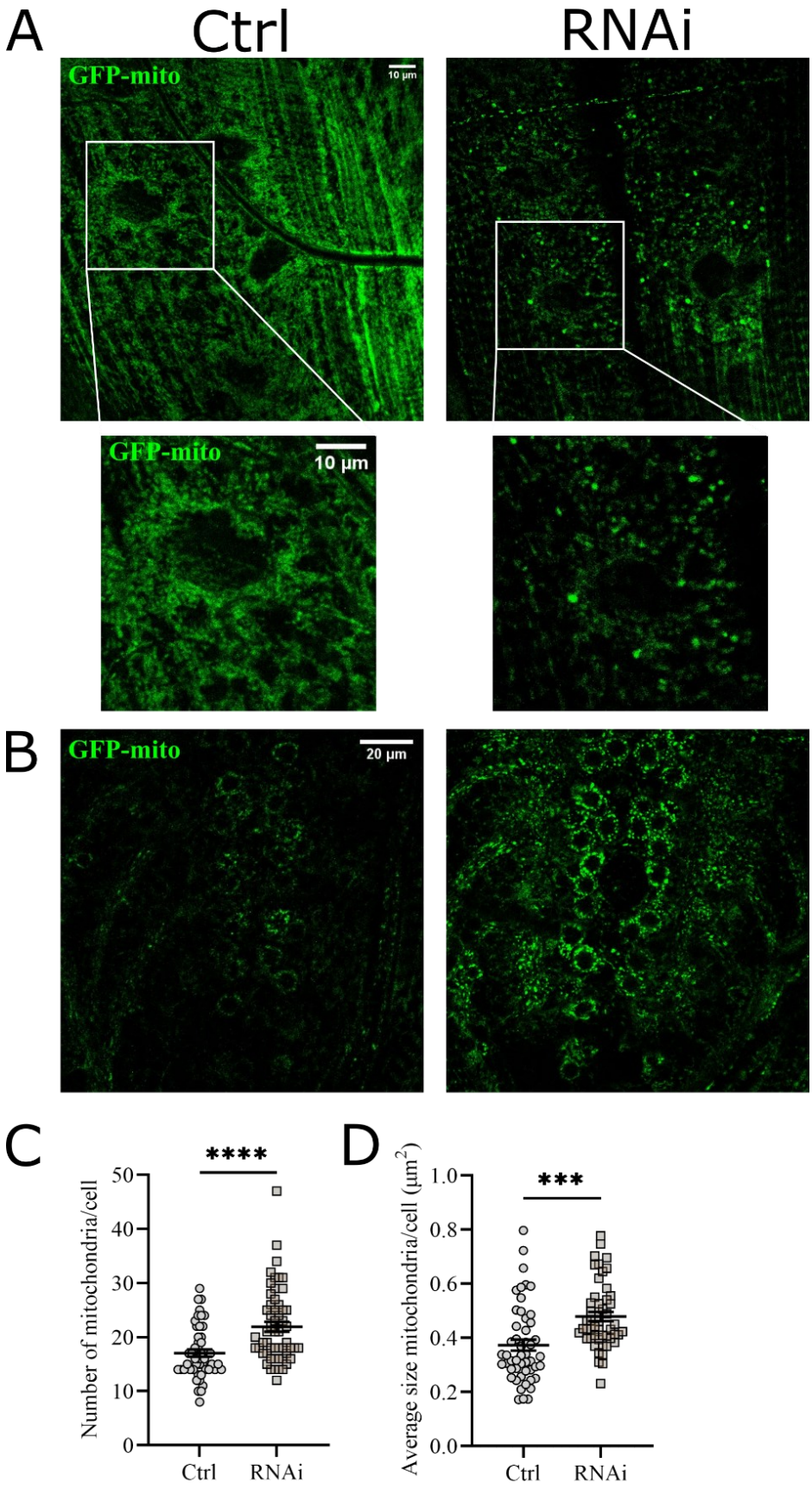

Figure 14. Mitochondria analysis in third instar larvae. (A) Representative confocal images of third instar larvae muscles. (B) Representative confocal images of third instar larvae central nerve cords and relative quantification of (C) number and (D) size of mitochondria in neuronal cells. 10 brains per group and 5 cells per each brain were analysed

(n= 50 cells/group). Asterisks represent a statistically significant difference. (unpaired two-tailed Student's t-test. *** p<0.001; **** p<0.0001). Data presented as mean ± SEM. Genotypes of samples are the following: Ctrl = Tubulin-Gal4/UAS-GFP-mito; RNAi = Tubulin-Gal4/UAS-GFP-mito; UAS D-idua^{RNAi}.

The analysis of mitochondria functionality was conducted using the well-known vital dye TMRE (tetramethylrhodamine, ethyl ester), which is sensitive to mitochondrial potential and, therefore, selectively marks polarized mitochondria (Perry et al., 2011). The analysis was conducted in muscles, where TMRE can easily permeate the cellular membrane.

As shown in **Figure 15A-B**, *D-idua* third instar larvae present a significant decrease of the percentage of polarized mitochondria compared to control larvae, as only the 65% of mitochondria are polarized compared to almost 90% in control larvae.

However, TMRE fluorescence intensity was significantly increased in the *D-idua* third instar larvae, meaning that, despite the decreased number of polarized mitochondria, the ones that are polarized present an alteration of the membrane potential (**Figure 15C-D**).

Fragmentation of mitochondrial network and alterations of mitochondria oxidation have already been reported in MPS VI, Gaucher disease, Krabbe disease and Multiple Sulphatase Deficiency (Tessitore et al., 2009; de Pablo-Latorre et al., 2012; Osellame et al., 2013; Voccoli et al., 2014).

It has been demonstrated that increased mitochondria potential leads to production of reactive oxygen species and activates cellular apoptosis (Banki et al., 1999; Li et al., 1999). Therefore, further investigations need to be conducted in the MPS I *Drosophila* model to see whether the altered mitochondrial phenotype can lead to cellular death via apoptosis as well, and to disrupted tissue structures with altered functionality.

Furthermore, mitophagy defects have been observed in several LSD models, leading to accumulation of aberrant mitochondria, that present impaired activity inducing an increased lactate production, decreased fatty acid β-oxidation, and activation of the catabolism of branched-chain amino acids to provide acetyl-CoA for the *de novo* lipid synthesis (Houten et al., 2016; Sánchez-González et al., 2020; Stepien et al., 2020). The observed increased glycolysis coupled to the increased lipogenesis seen in the *D-idua* model here described (**Figure 12**) suggest that cells may undergo a metabolic reprogramming, providing an alternative way to maintain an energetic balance, which may not be guaranteed by the activity of mitochondria.

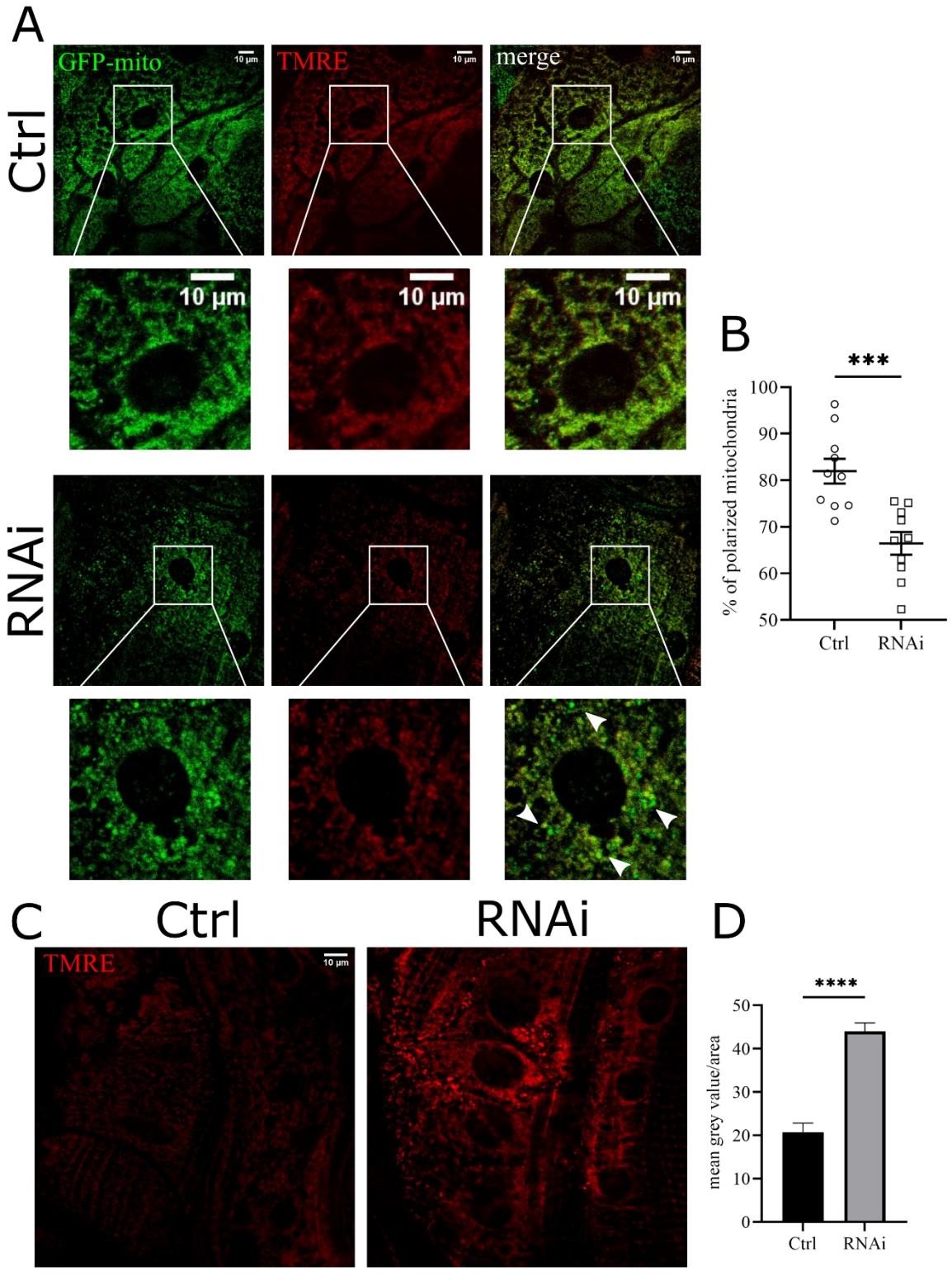

Figure 15. Analysis of polarized mitochondria. (A) Representative confocal live images of third instar larvae muscles expressing the fluorescent marker GFP-mito and stained with the vital dye TMRE. (B) Quantification of percentage of polarized mitochondria in third instar larvae muscles. Genotypes of samples are the following: Ctrl = Tubulin-Gal4/UAS GFP-mito; RNAi = Tubulin-Gal4/UAS GFP-mito; UAS D-idua^{RNAi}. (C) Representative confocal live images of third instar

larvae muscles stained with the vital dye TMRE and (D) relative quantification of TMRE fluorescence intensity. Area = 225 μm^2. Genotypes of samples are the following: Ctrl = Tubulin-Gal4/+; RNAi = Tubulin-Gal4/UAS D-idua^{RNAi}. n=10 larvae/group. Data are presented as mean ± SEM. Asterisks indicate a statistically significant difference (unpaired two-tailed Student's t-test. *** p<0.001; **** p<0.0001).

8. D-idua reduction leads to altered brain morphology and to altered motor axons-muscles connection

MPS I patients often present neurological involvement, not only in terms of developmental delay, but also in terms of accumulation of cerebrospinal fluid, which leads to ventricular space enlargement (Gabrielli et al., 2004).

As shown in **Figure 16**, third instar larvae of the *D-idua* model have a significantly increased brain volume as compared to control larvae.

Still little is known about the morphological changes associated to *Drosophila* brain, but in some *Drosophila* models an increased brain volume, caused by hyperproliferation of neural cells, was described (Wang et al., 2006; Unhavaithaya and Orr-Weaver, 2012). However, the mechanisms underlying the increased brain volume of *D-idua* need to be clarified. It can be caused either by hyperproliferation, as already seen in the *Drosophila* models depicted above, or by the accumulation of fluids, similar to the cerebrospinal fluid, that can lead to the enlargement of the brain itself, or again to alterations of the neural structure, according to what is known for MPS I patients.

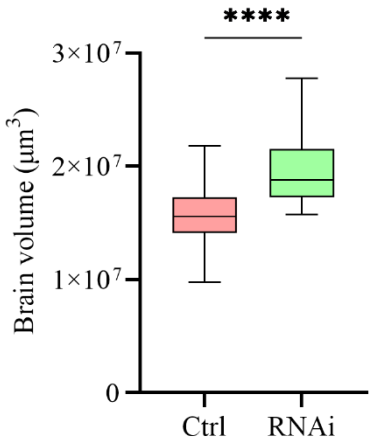

Figure 16. Brain volume measurement in third instar larvae. Data are the result of the measurement of 50 brains per each group. Asterisks indicate a statistically significant difference (unpaired two-tail Student's t-test. **** p<0.0001). Genotypes of samples are the following: Ctrl = Tubulin-Gal4/+; RNAi = Tubulin-Gal4/ UAS D-idua^{RNAi}.

One of the most unexpected results in this work was the lethality at pupal stage using the muscle-specific driver Mef2-Gal4 (**Figure 4A**). Even if commonly used as a muscular-specific driver, in literature it is reported that Mef2 is expressed in different tissues as muscles, heart, some portions of the gut, salivary glands, mushroom bodies, and it starts to be expressed during early stages of development in the mesoderm (data from RNAseq available on flybase.org). Therefore, *D-idua* was selectively downregulated in these different tissues, to assess where the gene is essential for the correct development.

The selective downregulation of *D-idua* gene was performed in:

- Heart (driver Hand-Gal4)
- Muscles (driver MHC-Gal4)
- Mushroom bodies (driver Clk-Gal4)
- Gut (drivers Fkh-XB30-Gal4, Tsp42Ec-Gal4, Mex-Gal4, Cad-Gal4, XSa14-3-Gal4)
- Salivary glands (driver pnr-Gal4)
- Mesoderm (drivers C179-Gal4, Twi-Gal4, How-Gal4, UAS Dcr;Twi-Gal4)

The only drivers where a phenotype was observed were How-Gal4 and UAS Dcr;Twi-Gal4. In particular, the How-Gal4 driver led to a complete lethality at pupal stage, while the UAS Dcr;Twi-Gal4 led to a partial lethality at pupal stage (**Figure 17A**); in addition, changes in the morphology of the pupae, which resulted smaller compared to controls, were observed (**Figure 17B**).

The phenotype observed using the driver UAS Dcr;Twi-Gal4 was particularly interesting. It is known that the *Twist* gene regulates the expression of all the genes involved in the development of the different tissues where Mef2-Gal4 is expressed (**Figure 17C**) (Furlong et al., 2001).

A recent paper reported that in *Drosophila*, *Twist* is expressed starting from the embryonal stage in adult muscle precursor cells (AMP), which are essential for the development of muscles, as well as for the branching of the segmental nerves and the correct innervation of muscles (Lavergne et al., 2020).

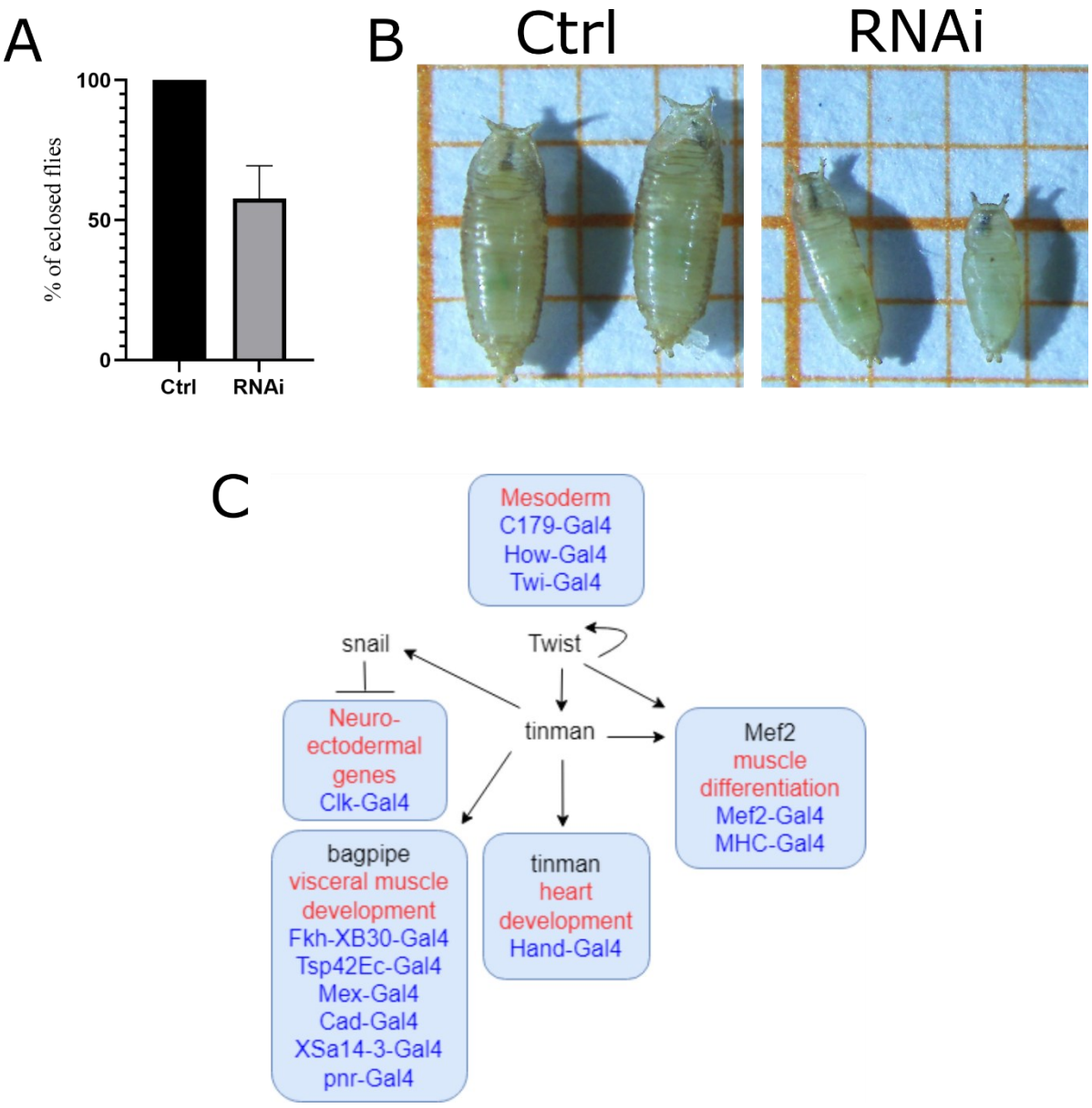

Figure 17. D-idua is essential in *Twist* expressing cells. (A) Eclosion rate using the driver UAS-Dcr;Twi-Gal4**.** Percentage of eclosion was calculated on 200 pupae/group. (B) Representative images of pupae. Genotypes of samples are: Ctrl = UAS Dcr;Twi-Gal4/+; RNAi = UAS Dcr;Twi-Gal4/UAS D-idua^{RNAi}. (C) Twist downstream regulation pathway.

To assess if the downregulation of *D-idua* could possibly cause alterations in motor axons development, third instar larvae were stained with the antibody FasII, which is specific for these cell types (**Figure 18**). As shown in **Figure 18**, terminations of motor axons are morphologically very different in *D-idua* third instar larvae, compared to controls. In particular, in control larvae motor axons ends appear to be elongated and well connected with muscles, whereas in the *D-idua* larvae they appear shortened and damaged.

Therefore, this can bring to the hypothesis that *D-idua* is essential in *Twi* expressing cells for the correct development of motor axons, as well as for their connection with muscles.
A recent study showed that AMP cells interact with both the insulin and the MTORC pathways. In particular, it was observed that insulin and MTORC pathways are essential for AMP cells proliferation (Aradhya et al., 2015). It is also known that the insulin pathway finely regulates glycolysis and the expression of genes involved in the glycolytic pathway (Tixier et al., 2013). Starting from the evidence that in this MPS I *Drosophila* model glycolysis and autophagy (of which MTORC is one of the main regulators) are drastically affected, the deep analysis of the interconnections of these pathways may result extremely interesting. This, together with the characterization of structural changes of the nervous system, can help to understand the neural pathogenesis associated to the MPS I disease, and possibly to understand whether and how the nervous system development is affected.

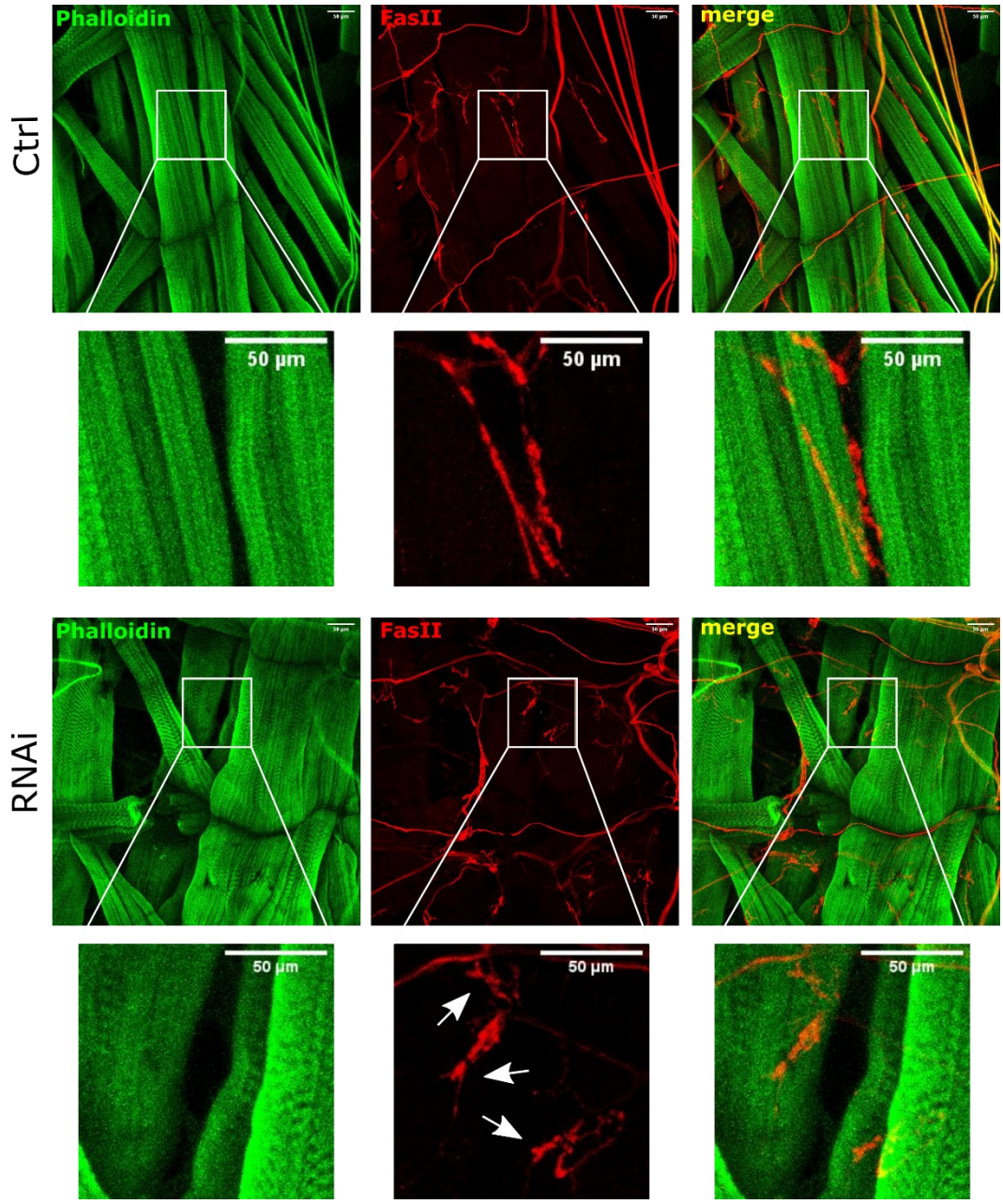

Figure 18. FasII staining of third instar larvae muscles. Representative confocal images of third instar larvae muscles were *D-idua* was ubiquitously down-regulated. Phalloidin (Green) selectively marks actin filaments in muscles. FasII (Red) marks motor axons. Genotypes of samples are the following: Ctrl=Tubulin-Gal4/+; RNAi=Tubulin-Gal4/UAS D-idua^{RNAi}. Arrows indicates damaged terminals of motor axons.

CONCLUSIONS

Mucopolysaccharidosis type I is a disorder whose enzymatic deficit is well-known since several decades; however, molecular alterations involved in its pathogenesis remain poorly understood. In this work a *Drosophila* model for MPS I, obtained through an RNAi approach, was generated and characterized. While unable to fully and faithfully represent, for evolutionary reasons, signs and symptoms of the human pathology, the analysis of the fly model has clearly highlighted some aspects of the disease in districts with analogue functions to the human ones.

Drosophila as a model of disease is extremely useful for its simplicity and ease of handling, for its reduced costs of maintenance and for the fewer ethical problems with respect to the use of other animal models. The evaluation of endocellular or tissue pathogenic processes can be conducted reliably and accurately in *Drosophila*, and in short times, as well as pharmacological screening studies. The analysis of the model here presented allowed to highlight significant alterations of districts, as the muscle and the neurological one, which represent in a reproducible way those affecting the analogue human districts. The identification of *D-idua* as a vital gene for *Drosophila*, the increased number and size of lysosomes due to its reduced expression, as happens in this model, the reduced acidification inside lysosomes, have shown since the beginning the possibility to employ *Drosophila* as a model for MPS I. The model thus represents a useful instrument to obtain further information on these aspects, as well as on others related to the alteration of the autophagosome-lysosome fusion, the metabolic changes associated to the enzyme activity reduction and the conditioning of the starvation on these processes. The extensive study on mitochondria alterations may lead to the evaluation of other cell compartments not yet characterized, and the integration of all these impaired pathways, which are strictly interconnected, may help to assemble the complex picture of the MPS I pathogenesis.

The analysis of the neurological compartment, together with further behavioral studies to be conducted, and with other structural studies in this district, may help a possible comprehension of the neurological molecular alterations progressively taking to the CNS impairment in the severe forms of MPS I, the so-called CNS pathogenesis. This *Drosophila* model will allow a first identification of the molecular actors included in this scenario, providing suggestions on the main pathways and molecules involved. Some of these molecules, selected from this first screening may be next evaluated or confirmed in other animal models, closer to the human beings in the evolutionary scale, as the mouse model. Also, the consequent pharmacological screening through

the testing of therapeutic molecules, easily evaluable through experiments of phenotype rescuing, will be much faster performed in the fly model.

In conclusion, the data here shown only represent the basic characterization of the model, asserting its representativeness, and highlighting alterations of important cellular and lysosomal processes, already known for the human disease, hence the interest of the model for the conduction of significant future studies on MPS I pathogenesis and treatment.

REFERENCES

Aldenhoven, M., Wynn, R.F., Orchard, P.J., O'Meara, A., Veys, P., Fischer, A., Valayannopoulos, V., Neven, B., Rovelli, A., Prasad, V.K., Tolar, J., Allewelt, H., Jones, S.A., Parini, R., Renard, M., Bordon, V., Wulffraat, N.M., de Koning, T.J., Shapiro, E.G., Kurtzberg, J., Boelens, J.J., 2015. Long-term outcome of Hurler syndrome patients after hematopoietic cell transplantation: an international multicenter study. Blood 125, 2164–2172. https://doi.org/10.1182/blood-2014-11-608075

Ali, Y.O., Escala, W., Ruan, K., Zhai, R.G., 2011. Assaying Locomotor, Learning, and Memory Deficits in Drosophila Models of Neurodegeneration. JoVE J. Vis. Exp. e2504. https://doi.org/10.3791/2504

Aradhya, R., Zmojdzian, M., Da Ponte, J.P., Jagla, K., 2015. Muscle niche-driven Insulin-Notch-Myc cascade reactivates dormant Adult Muscle Precursors in Drosophila. eLife 4, e08497. https://doi.org/10.7554/eLife.08497

Baldo, G., Mayer, F.Q., Martinelli, B., Dilda, A., Meyer, F., Ponder, K.P., Giugliani, R., Matte, U., 2012. Evidence of a progressive motor dysfunction in Mucopolysaccharidosis type I mice. Behav. Brain Res. 233, 169–175. https://doi.org/10.1016/j.bbr.2012.04.051

Baldo, G., Tavares, A.M.V., Gonzalez, E., Poletto, E., Mayer, F.Q., Matte, U. da S., Giugliani, R., 2017. Progressive heart disease in mucopolysaccharidosis type I mice may be mediated by increased cathepsin B activity. Cardiovasc. Pathol. 27, 45–50. https://doi.org/10.1016/j.carpath.2017.01.001

Banki, K., Hutter, E., Gonchoroff, N.J., Perl, A., 1999. Elevation of Mitochondrial Transmembrane Potential and Reactive Oxygen Intermediate Levels Are Early Events and Occur Independently from Activation of Caspases in Fas Signaling. J. Immunol. 162, 1466–1479.

Bar, S., Prasad, M., Datta, R., 2018. Neuromuscular degeneration and locomotor deficit in a Drosophila model of mucopolysaccharidosis VII is attenuated by treatment with resveratrol. Dis. Model. Mech. 11, dmm036954. https://doi.org/10.1242/dmm.036954

Bartel, K., Pein, H., Popper, B., Schmitt, S., Janaki-Raman, S., Schulze, A., Lengauer, F., Koeberle, A., Werz, O., Zischka, H., Müller, R., Vollmar, A.M., von Schwarzenberg, K., 2019. Connecting lysosomes and mitochondria – a novel role for lipid metabolism in cancer cell death. Cell Commun. Signal. 17, 87. https://doi.org/10.1186/s12964-019-0399-2

Bjornsson, S., 1993. Simultaneous Preparation and Quantitation of Proteoglycans by Precipitation with Alcian Blue. Anal. Biochem. 210, 282–291. https://doi.org/10.1006/abio.1993.1197

Bosc, C., Broin, N., Fanjul, M., Saland, E., Farge, T., Courdy, C., Batut, A., Masoud, R., Larrue, C., Skuli, S., Espagnolle, N., Pagès, J.-C., Carrier, A., Bost, F., Bertrand-Michel, J., Tamburini, J., Récher, C., Bertoli, S., Mansat-De Mas, V., Manenti, S., Sarry, J.-E., Joffre, C., 2020. Autophagy regulates fatty acid availability for oxidative phosphorylation through mitochondria-endoplasmic reticulum contact sites. Nat. Commun. 11, 4056. https://doi.org/10.1038/s41467-020-17882-2

Braunlin, E., Mackey-Bojack, S., Panoskaltsis-Mortari, A., Berry, J.M., McElmurry, R.T., Riddle, M., Sun, L.-Y., Clarke, L.A., Tolar, J., Blazar, B.R., 2006. Cardiac Functional and Histopathologic Findings in Humans and Mice with Mucopolysaccharidosis Type I: Implications for Assessment of Therapeutic Interventions in Hurler Syndrome. Pediatr. Res. 59, 27–32. https://doi.org/10.1203/01.pdr.0000190579.24054.39

Braunstein, H., Papazian, M., Maor, G., Lukas, J., Rolfs, A., Horowitz, M., 2020. Misfolding of Lysosomal α-Galactosidase a in a Fly Model and Its Alleviation by the Pharmacological Chaperone Migalastat. Int. J. Mol. Sci. 21, 7397. https://doi.org/10.3390/ijms21197397

Bravo, H., Neto, E.C., Schulte, J., Pereira, J., Filho, C.S., Bittencourt, F., Sebastião, F., Bender, F., de Magalhães, A.P.S., Guidobono, R., Trapp, F.B., Michelin-Tirelli, K., Souza, C.F.M., Rojas Málaga, D., Pasqualim, G., Brusius-Facchin, A.C., Giugliani, R., 2017. Investigation of newborns with abnormal results in a newborn screening program for four lysosomal storage diseases in Brazil. Mol. Genet. Metab. Rep. 12, 92–97. https://doi.org/10.1016/j.ymgmr.2017.06.006

Bueno, M.J., Jimenez-Renard, V., Samino, S., Capellades, J., Junza, A., López-Rodríguez, M.L., Garcia-Carceles, J., Lopez-Fabuel, I., Bolaños, J.P., Chandel, N.S., Yanes, O., Colomer, R., Quintela-Fandino,

M., 2019. Essentiality of fatty acid synthase in the 2D to anchorage-independent growth transition in transforming cells. Nat. Commun. 10, 5011. https://doi.org/10.1038/s41467-019-13028-1
Burlina, A.B., Polo, G., Salviati, L., Duro, G., Zizzo, C., Dardis, A., Bembi, B., Cazzorla, C., Rubert, L., Zordan, R., Desnick, R.J., Burlina, A.P., 2018. Newborn screening for lysosomal storage disorders by tandem mass spectrometry in North East Italy. J. Inherit. Metab. Dis. 41, 209–219. https://doi.org/10.1007/s10545-017-0098-3
Cabrera-Reyes, F., Parra-Ruiz, C., Yuseff, M.I., Zanlungo, S., 2021. Alterations in Lysosome Homeostasis in Lipid-Related Disorders: Impact on Metabolic Tissues and Immune Cells. Front. Cell Dev. Biol. 9, 3502. https://doi.org/10.3389/fcell.2021.790568
Celik, B., Tomatsu, S.C., Tomatsu, S., Khan, S.A., 2021. Epidemiology of Mucopolysaccharidoses Update. Diagnostics 11, 273. https://doi.org/10.3390/diagnostics11020273
Chan, M.-J., Liao, H.-C., Gelb, M.H., Chuang, C.-K., Liu, M.-Y., Chen, H.-J., Kao, S.-M., Lin, H.-Y., Huang, Y.-H., Kumar, A.B., Chennamaneni, N.K., Pendem, N., Lin, S.-P., Chiang, C.-C., 2019. Taiwan National Newborn Screening Program by Tandem Mass Spectrometry for Mucopolysaccharidoses Types I, II, and VI. J. Pediatr. 205, 176–182. https://doi.org/10.1016/j.jpeds.2018.09.063
Chintapalli, V.R., Kato, A., Henderson, L., Hirata, T., Woods, D.J., Overend, G., Davies, S.A., Romero, M.F., Dow, J.A.T., 2015. Transport proteins NHA1 and NHA2 are essential for survival, but have distinct transport modalities. Proc. Natl. Acad. Sci. 112, 11720–11725. https://doi.org/10.1073/pnas.1508031112
Clarke, L.A., 1993. Mucopolysaccharidosis Type I, in: Adam, M.P., Ardinger, H.H., Pagon, R.A., Wallace, S.E., Bean, L.J., Gripp, K.W., Mirzaa, G.M., Amemiya, A. (Eds.), GeneReviews®. University of Washington, Seattle, Seattle (WA).
Clarke, L.A., Russell, C.S., Pownall, S., Warrington, C.L., Borowski, A., Dimmick, J.E., Toone, J., Jirik, F.R., 1997. Murine Mucopolysaccharidosis Type I: Targeted Disruption of the Murine α-l-Iduronidase Gene. Hum. Mol. Genet. 6, 503–511. https://doi.org/10.1093/hmg/6.4.503
Clarke, L.A., Wraith, J.E., Beck, M., Kolodny, E.H., Pastores, G.M., Muenzer, J., Rapoport, D.M., Berger, K.I., Sidman, M., Kakkis, E.D., Cox, G.F., 2009. Long-term Efficacy and Safety of Laronidase in the Treatment of Mucopolysaccharidosis I. Pediatrics 123, 229–240. https://doi.org/10.1542/peds.2007-3847
Conrad, G.W., Sherman, D., Dorfman, A., 1972. An Ultrastructural Comparison of Normal and Hurler Syndrome Dermal Fibroblasts. Pediatr. Res. 6, 563–575. https://doi.org/10.1203/00006450-197206000-00005
Constantopoulos, G., Scott, J.A., Shull, R.M., 1989. Corneal opacity in canine MPS I. Changes after bone marrow transplantation. Invest. Ophthalmol. Vis. Sci. 30, 1802–1807.
Cox-Brinkman, J., Smeulders, M.J.C., Hollak, C.E.M., Wijburg, F.A., 2007. Restricted upper extremity range of motion in mucopolysaccharidosis type I: no response to one year of enzyme replacement therapy. J. Inherit. Metab. Dis. 30, 47–50. https://doi.org/10.1007/s10545-006-0490-x
De Filippis, C., Napoli, B., Rigon, L., Guarato, G., Bauer, R., Tomanin, R., Orso, G., 2022. Drosophila D-idua Reduction Mimics Mucopolysaccharidosis Type I Disease-Related Phenotypes. Cells 11, 129. https://doi.org/10.3390/cells11010129
de Pablo-Latorre, R., Saide, A., Polishhuck, E.V., Nusco, E., Fraldi, A., Ballabio, A., 2012. Impaired parkin-mediated mitochondrial targeting to autophagosomes differentially contributes to tissue pathology in lysosomal storage diseases. Hum. Mol. Genet. 21, 1770–1781. https://doi.org/10.1093/hmg/ddr610
de Ru, M.H., Boelens, J.J., Das, A.M., Jones, S.A., van der Lee, J.H., Mahlaoui, N., Mengel, E., Offringa, M., O'Meara, A., Parini, R., Rovelli, A., Sykora, K.-W., Valayannopoulos, V., Vellodi, A., Wynn, R.F., Wijburg, F.A., 2011. Enzyme replacement therapy and/or hematopoietic stem cell transplantation at diagnosis in patients with mucopolysaccharidosis type I: results of a European consensus procedure. Orphanet J. Rare Dis. 6, 55. https://doi.org/10.1186/1750-1172-6-55
de Ru, M.H., van der Tol, L., van Vlies, N., Bigger, B.W., Hollak, C.E.M., IJlst, L., Kulik, W., van Lenthe, H., Saif, M.A., Wagemans, T., van der Wal, W.M., Wanders, R.J., Wijburg, F.A., 2013. Plasma and urinary levels of dermatan sulfate and heparan sulfate derived disaccharides after long-term enzyme

replacement therapy (ERT) in MPS I: correlation with the timing of ERT and with total urinary excretion of glycosaminoglycans. J. Inherit. Metab. Dis. 36, 247–255. https://doi.org/10.1007/s10545-012-9538-2
Derrick-Roberts, A.L.K., Jackson, M.R., Pyragius, C.E., Byers, S., 2017. Substrate Deprivation Therapy to Reduce Glycosaminoglycan Synthesis Improves Aspects of Neurological and Skeletal Pathology in MPS I Mice. Diseases 5, 5. https://doi.org/10.3390/diseases5010005
DeVorkin, L., Gorski, S.M., 2014. Monitoring Autophagy in *Drosophila* Using Fluorescent Reporters in the UAS-GAL4 System. Cold Spring Harb. Protoc. 2014, pdb.prot080341. https://doi.org/10.1101/pdb.prot080341
Di Malta, C., Cinque, L., Settembre, C., 2019. Transcriptional Regulation of Autophagy: Mechanisms and Diseases. Front. Cell Dev. Biol. 7, 114. https://doi.org/10.3389/fcell.2019.00114
Dominguez, M., Brüne, B., Namgaladze, D., 2021. Exploring the Role of ATP-Citrate Lyase in the Immune System. Front. Immunol. 12, 14. https://doi.org/10.3389/fimmu.2021.632526
Duffy, J.B., 2002. GAL4 system in drosophila: A fly geneticist's swiss army knife. genesis 34, 1–15. https://doi.org/10.1002/gene.10150
Elliott, S., Buroker, N., Cournoyer, J.J., Potier, A.M., Trometer, J.D., Elbin, C., Schermer, M.J., Kantola, J., Boyce, A., Turecek, F., Gelb, M.H., Scott, C.R., 2016. Pilot study of newborn screening for six lysosomal storage diseases using Tandem Mass Spectrometry. Mol. Genet. Metab. 118, 304–309. https://doi.org/10.1016/j.ymgme.2016.05.015
Eyskens, F., Devos, S., 2019. Newborn Screening for Lysosomal Storage Disorders in Belgium The Importance of Sex- and Age-Dependent Reference Ranges. J. Inborn Errors Metab. Screen. 5. https://doi.org/10.1177/2326409817744231
Fedele, A.O., Proud, C.G., 2020. Chloroquine and bafilomycin A mimic lysosomal storage disorders and impair mTORC1 signalling. Biosci. Rep. 40, BSR20200905. https://doi.org/10.1042/BSR20200905
Filocamo, M., Tomanin, R., Bertola, F., Morrone, A., 2018. Biochemical and molecular analysis in mucopolysaccharidoses: what a paediatrician must know. Ital. J. Pediatr. 44, 129. https://doi.org/10.1186/s13052-018-0553-2
Friso, A., Tomanin, R., Salvalaio, M., Scarpa, M., 2010. Genistein reduces glycosaminoglycan levels in a mouse model of mucopolysaccharidosis type II. Br. J. Pharmacol. 159, 1082–1091. https://doi.org/10.1111/j.1476-5381.2009.00565.x
Furlong, E.E.M., Andersen, E.C., Null, B., White, K.P., Scott, M.P., 2001. Patterns of Gene Expression During Drosophila Mesoderm Development. Science. https://doi.org/10.1126/science.1062660
Gabrielli, O., Polonara, G., Regnicolo, L., Petroni, V., Scarabino, T., Coppa, G.V., Salvolini, U., 2004. Correlation between cerebral MRI abnormalities and mental retardation in patients with mucopolysaccharidoses. Am. J. Med. Genet. A. 125A, 224–231. https://doi.org/10.1002/ajmg.a.20515
Garcia-Rivera, M.F., Colvin-Wanshura, L.E., Nelson, M.S., Nan, Z., Khan, S.A., Rogers, T.B., Maitra, I., Low, W.C., Gupta, P., 2007. Characterization of an immunodeficient mouse model of mucopolysaccharidosis type I suitable for preclinical testing of human stem cell and gene therapy. Brain Res. Bull. 74, 429–438. https://doi.org/10.1016/j.brainresbull.2007.07.018
Gary-Bobo, M., Nirdé, P., Jeanjean, A., Morère, A., Garcia, M., 2007. Mannose 6-phosphate receptor targeting and its applications in human diseases. Curr. Med. Chem. 14, 2945–2953.
Gratz, S.J., Rubinstein, C.D., Harrison, M.M., Wildonger, J., O'Connor-Giles, K.M., 2015. CRISPR-Cas9 Genome Editing in Drosophila. Curr. Protoc. Mol. Biol. 111, 31.2.1-31.2.20. https://doi.org/10.1002/0471142727.mb3102s111
Grönke, S., Mildner, A., Fellert, S., Tennagels, N., Petry, S., Müller, G., Jäckle, H., Kühnlein, R.P., 2005. Brummer lipase is an evolutionary conserved fat storage regulator in Drosophila. Cell Metab. 1, 323–330. https://doi.org/10.1016/j.cmet.2005.04.003
Haskins, M.E., Aguirre, G.D., Jezyk, P.F., Desnick, R.J., Patterson, D.F., 1983. The pathology of the feline model of mucopolysaccharidosis I. Am. J. Pathol. 112, 27–36.

Haskins, M.E., Jezyk, P.F., Desnick, R.J., Mcdonough, S.K., Patterson, D.F., 1979. Alpha-L-iduronidase Deficiency in a Cat: A Model of Mucopolysaccharidosis I. Pediatr. Res. 13, 1294–1297. https://doi.org/10.1203/00006450-197911000-00018

Hinderer, C., Bell, P., Gurda, B.L., Wang, Q., Louboutin, J.-P., Zhu, Y., Bagel, J., O'Donnell, P., Sikora, T., Ruane, T., Wang, P., Haskins, M.E., Wilson, J.M., 2014. Liver-directed gene therapy corrects cardiovascular lesions in feline mucopolysaccharidosis type I. Proc. Natl. Acad. Sci. 111, 14894–14899. https://doi.org/10.1073/pnas.1413645111

Hobbs, J.R., Barrett, A.J., Chambers, D., James, D.C.O., Hugh-Jones, K., Byrom, N., Henry, K., Lucas, C.F., Rogers, T.R., Benson, P.F., Tansley, L.R., Patrick, A.D., Mossman, J., Young, E.P., 1981. REVERSAL OF CLINICAL FEATURES OF HURLER'S DISEASE AND BIOCHEMICAL IMPROVEMENT AFTER TREATMENT BY BONE-MARROW TRANSPLANTATION. The Lancet 318, 709–712. https://doi.org/10.1016/S0140-6736(81)91046-1

Hosokawa, N., Hara, T., Kaizuka, T., Kishi, C., Takamura, A., Miura, Y., Iemura, S., Natsume, T., Takehana, K., Yamada, N., Guan, J.-L., Oshiro, N., Mizushima, N., 2009. Nutrient-dependent mTORC1 Association with the ULK1–Atg13–FIP200 Complex Required for Autophagy. Mol. Biol. Cell 20, 1981–1991. https://doi.org/10.1091/mbc.e08-12-1248

Houten, S.M., Violante, S., Ventura, F.V., Wanders, R.J.A., 2016. The Biochemistry and Physiology of Mitochondrial Fatty Acid β-Oxidation and Its Genetic Disorders. Annu. Rev. Physiol. 78, 23–44. https://doi.org/10.1146/annurev-physiol-021115-105045

Hwangbo, D.S., Gersham, B., Tu, M.-P., Palmer, M., Tatar, M., 2004. Drosophila dFOXO controls lifespan and regulates insulin signalling in brain and fat body. Nature 429, 562–566. https://doi.org/10.1038/nature02549

Jennings, J.J., Zhu, J., Rbaibi, Y., Luo, X., Chu, C.T., Kiselyov, K., 2006. Mitochondrial Aberrations in Mucolipidosis Type IV *. J. Biol. Chem. 281, 39041–39050. https://doi.org/10.1074/jbc.M607982200

Jordan, M.C., Zheng, Y., Ryazantsev, S., Rozengurt, N., Roos, K.P., Neufeld, E.F., 2005. Cardiac manifestations in the mouse model of mucopolysaccharidosis I. Mol. Genet. Metab. 86, 233–243. https://doi.org/10.1016/j.ymgme.2005.05.003

Kakavanos, R., Turner, C.T., Hopwood, J.J., Kakkis, E.D., Brooks, D.A., 2003. Immune tolerance after long-term enzyme-replacement therapy among patients who have mucopolysaccharidosis I. The Lancet 361, 1608–1613. https://doi.org/10.1016/S0140-6736(03)13311-9

Kakkis, E.D., Muenzer, J., Tiller, G.E., Waber, L., Belmont, J., Passage, M., Izykowski, B., Phillips, J., Doroshow, R., Walot, I., Hoft, R., Yu, K.T., Okazaki, S., Lewis, D., Lachman, R., Thompson, J.N., Neufeld, E.F., 2009. Enzyme-Replacement Therapy in Mucopolysaccharidosis I [WWW Document]. http://dx.doi.org/10.1056/NEJM200101183440304. https://doi.org/10.1056/NEJM200101183440304

Kawasaki, H., Suzuki, T., Ito, K., Takahara, T., Goto-Inoue, N., Setou, M., Sakata, K., Ishida, N., 2017. Minos-insertion mutant of the Drosophila GBA gene homologue showed abnormal phenotypes of climbing ability, sleep and life span with accumulation of hydroxy-glucocerebroside. Gene 614, 49–55. https://doi.org/10.1016/j.gene.2017.03.004

Keeling, K.M., Brooks, D.A., Hopwood, J.J., Li, P., Thompson, J.N., Bedwell, D.M., 2001. Gentamicin-mediated suppression of Hurler syndrome stop mutations restores a low level of α-l-iduronidase activity and reduces lysosomal glycosaminoglycan accumulation. Hum. Mol. Genet. 10, 291–300. https://doi.org/10.1093/hmg/10.3.291

Khalid, O., Vera, M.U., Gordts, P.L., Ellinwood, N.M., Schwartz, P.H., Dickson, P.I., Esko, J.D., Wang, R.Y., 2016. Immune-Mediated Inflammation May Contribute to the Pathogenesis of Cardiovascular Disease in Mucopolysaccharidosis Type I. PLOS ONE 11, e0150850. https://doi.org/10.1371/journal.pone.0150850

Kienesberger, P.C., Pulinilkunnil, T., Nagendran, J., Young, M.E., Bogner-Strauss, J.G., Hackl, H., Khadour, R., Heydari, E., Haemmerle, G., Zechner, R., Kershaw, E.E., Dyck, J.R.B., 2013. Early structural and metabolic cardiac remodelling in response to inducible adipose triglyceride lipase ablation. Cardiovasc. Res. 99, 442–451. https://doi.org/10.1093/cvr/cvt124

Kim, C., Kwak, M.J., Cho, S.Y., Ko, A., Rheey, J., Kwon, J.-Y., Chung, Y., Jin, D.-K., 2015. Decreased performance in IDUA knockout mouse mimic limitations of joint function and locomotion in patients with Hurler syndrome. Orphanet J. Rare Dis. 10, 121. https://doi.org/10.1186/s13023-015-0337-3

Kinghorn, K.J., Grönke, S., Castillo-Quan, J.I., Woodling, N.S., Li, L., Sirka, E., Gegg, M., Mills, K., Hardy, J., Bjedov, I., Partridge, L., 2016. A Drosophila Model of Neuronopathic Gaucher Disease Demonstrates Lysosomal-Autophagic Defects and Altered mTOR Signalling and Is Functionally Rescued by Rapamycin. J. Neurosci. 36, 11654–11670. https://doi.org/10.1523/JNEUROSCI.4527-15.2016

Kounakis, K., Chaniotakis, M., Markaki, M., Tavernarakis, N., 2019. Emerging Roles of Lipophagy in Health and Disease. Front. Cell Dev. Biol. 7, 185. https://doi.org/10.3389/fcell.2019.00185

Kubaski, F., de Oliveira Poswar, F., Michelin-Tirelli, K., Burin, M.G., Rojas-Málaga, D., Brusius-Facchin, A.C., Leistner-Segal, S., Giugliani, R., 2020. Diagnosis of Mucopolysaccharidoses. Diagnostics 10, 172. https://doi.org/10.3390/diagnostics10030172

Laraway, S., Mercer, J., Jameson, E., Ashworth, J., Hensman, P., Jones, S.A., 2016. Outcomes of Long-Term Treatment with Laronidase in Patients with Mucopolysaccharidosis Type I. J. Pediatr. 178, 219-226.e1. https://doi.org/10.1016/j.jpeds.2016.08.033

Lavergne, G., Zmojdzian, M., Da Ponte, J.P., Junion, G., Jagla, K., 2020. Drosophila adult muscle precursor cells contribute to motor axon pathfinding and proper innervation of embryonic muscles. Development 147, dev183004. https://doi.org/10.1242/dev.183004

Lee, J.S., Kanai, K., Suzuki, M., Kim, W.S., Yoo, H.S., Fu, Y., Kim, D.-K., Jung, B.C., Choi, M., Oh, K.W., Li, Y., Nakatani, M., Nakazato, T., Sekimoto, S., Funayama, M., Yoshino, H., Kubo, S., Nishioka, K., Sakai, R., Ueyama, M., Mochizuki, H., Lee, H.-J., Sardi, S.P., Halliday, G.M., Nagai, Y., Lee, P.H., Hattori, N., Lee, S.-J., 2019. Arylsulfatase A, a genetic modifier of Parkinson's disease, is an α-synuclein chaperone. Brain 142, 2845–2859. https://doi.org/10.1093/brain/awz205

Li, M., Khambu, B., Zhang, H., Kang, J.-H., Chen, X., Chen, D., Vollmer, L., Liu, P.-Q., Vogt, A., Yin, X.-M., 2013. Suppression of Lysosome Function Induces Autophagy via a Feedback Down-regulation of MTOR Complex 1 (MTORC1) Activity *. J. Biol. Chem. 288, 35769–35780. https://doi.org/10.1074/jbc.M113.511212

Li, P.-F., Dietz, R., von Harsdorf, R., 1999. p53 regulates mitochondrial membrane potential through reactive oxygen species and induces cytochrome c-independent apoptosis blocked by Bcl-2. EMBO J. 18, 6027–6036. https://doi.org/10.1093/emboj/18.21.6027

Li, X., Gu, J., Zhou, Q., 2015. Review of aerobic glycolysis and its key enzymes – new targets for lung cancer therapy. Thorac. Cancer 6, 17–24. https://doi.org/10.1111/1759-7714.12148

Lieberman, A.P., Puertollano, R., Raben, N., Slaugenhaupt, S., Walkley, S.U., Ballabio, A., 2012. Autophagy in lysosomal storage disorders. Autophagy 8, 719–730. https://doi.org/10.4161/auto.19469

Lim, C.-Y., Zoncu, R., 2016. The lysosome as a command-and-control center for cellular metabolism. J. Cell Biol. 214, 653–664. https://doi.org/10.1083/jcb.201607005

Lim, J.-A., Li, L., Kakhlon, O., Myerowitz, R., Raben, N., 2015. Defects in calcium homeostasis and mitochondria can be reversed in Pompe disease. Autophagy 11, 385–402. https://doi.org/10.1080/15548627.2015.1009779

Lin, P.-W., Chu, M.-L., Liu, H.-S., 2021. Autophagy and metabolism. Kaohsiung J. Med. Sci. 37, 12–19. https://doi.org/10.1002/kjm2.12299

Lőrincz, P., Mauvezin, C., Juhász, G., 2017. Exploring Autophagy in Drosophila. Cells 6, 22. https://doi.org/10.3390/cells6030022

Lotfi, P., Tse, D.Y., Di Ronza, A., Seymour, M.L., Martano, G., Cooper, J.D., Pereira, F.A., Passafaro, M., Wu, S.M., Sardiello, M., 2018. Trehalose reduces retinal degeneration, neuroinflammation and storage burden caused by a lysosomal hydrolase deficiency. Autophagy 14, 1419–1434. https://doi.org/10.1080/15548627.2018.1474313

Lowery, M.S., Roberts, S.J., Somero, G.N., 1987. Effects of Starvation on the Activities and Localization of Glycolytic Enzymes in the White Muscle of the Barred Sand Bass Paralabrax nebulifer. Physiol. Zool. 60, 538–549.

Lyons, J.A., Dickson, P.I., Wall, J.S., Passage, M.B., Ellinwood, N.M., Kakkis, E.D., McEntee, M.F., 2011. Arterial pathology in canine mucopolysaccharidosis-I and response to therapy. Lab. Invest. 91, 665–674. https://doi.org/10.1038/labinvest.2011.7

Maor, G., Rencus-Lazar, S., Filocamo, M., Steller, H., Segal, D., Horowitz, M., 2013. Unfolded protein response in Gaucher disease: from human to Drosophila. Orphanet J. Rare Dis. 8, 140. https://doi.org/10.1186/1750-1172-8-140

Martina, J.A., Chen, Y., Gucek, M., Puertollano, R., 2012. MTORC1 functions as a transcriptional regulator of autophagy by preventing nuclear transport of TFEB. Autophagy 8, 903–914. https://doi.org/10.4161/auto.19653

Martins, C., Hůlková, H., Dridi, L., Dormoy-Raclet, V., Grigoryeva, L., Choi, Y., Langford-Smith, A., Wilkinson, F.L., Ohmi, K., DiCristo, G., Hamel, E., Ausseil, J., Cheillan, D., Moreau, A., Svobodová, E., Hájková, Z., Tesařová, M., Hansíková, H., Bigger, B.W., Hrebícek, M., Pshezhetsky, A.V., 2015. Neuroinflammation, mitochondrial defects and neurodegeneration in mucopolysaccharidosis III type C mouse model. Brain 138, 336–355. https://doi.org/10.1093/brain/awu355

Mencarelli, C., Martinez–Martinez, P., 2013. Ceramide function in the brain: when a slight tilt is enough. Cell. Mol. Life Sci. 70, 181–203. https://doi.org/10.1007/s00018-012-1038-x

Mendez, D.C., Stover, A.E., Rangel, A.D., Brick, D.J., Nethercott, H.E., Torres, M.A., Khalid, O., Wong, A.M., Cooper, J.D., Jester, J.V., Monuki, E.S., McGuire, C., Le, S.Q., Kan, S., Dickson, P.I., Schwartz, P.H., 2015. A novel, long-lived, and highly engraftable immunodeficient mouse model of mucopolysaccharidosis type I. Mol. Ther. - Methods Clin. Dev. 2. https://doi.org/10.1038/mtm.2014.68

Metz, T.F., Mechtler, T.P., Orsini, J.J., Martin, M., Shushan, B., Herman, J.L., Ratschmann, R., Item, C.B., Streubel, B., Herkner, K.R., Kasper, D.C., 2011. Simplified Newborn Screening Protocol for Lysosomal Storage Disorders. Clin. Chem. 57, 1286–1294. https://doi.org/10.1373/clinchem.2011.164640

Mizushima, N., 2007. Autophagy: process and function. Genes Dev. 21, 2861–2873. https://doi.org/10.1101/gad.1599207

Mizushima, N., Komatsu, M., 2011. Autophagy: Renovation of Cells and Tissues. Cell 147, 728–741. https://doi.org/10.1016/j.cell.2011.10.026

Mizushima, N., Levine, B., Cuervo, A.M., Klionsky, D.J., 2008. Autophagy fights disease through cellular self-digestion. Nature 451, 1069–1075. https://doi.org/10.1038/nature06639

Mizushima, N., Yoshimori, T., 2007. How to Interpret LC3 Immunoblotting. Autophagy 3, 542–545. https://doi.org/10.4161/auto.4600

Mizushima, N., Yoshimori, T., Levine, B., 2010. Methods in Mammalian Autophagy Research. Cell 140, 313–326. https://doi.org/10.1016/j.cell.2010.01.028

Mucopolysaccharidoses, n.d. . NORD Natl. Organ. Rare Disord. URL https://rarediseases.org/rare-diseases/mucopolysaccharidoses/ (accessed 12.1.21).

Muenzer, J., Wraith, J.E., Clarke, L.A., and the International Consensus Panel on the Management and Treatment of Mucopolysaccharidosis I, 2009. Mucopolysaccharidosis I: Management and Treatment Guidelines. Pediatrics 123, 19–29. https://doi.org/10.1542/peds.2008-0416

Mullen, T.D., Spassieva, S., Jenkins, R.W., Kitatani, K., Bielawski, J., Hannun, Y.A., Obeid, L.M., 2011. Selective knockdown of ceramide synthases reveals complex interregulation of sphingolipid metabolism. J. Lipid Res. 52, 68–77. https://doi.org/10.1194/jlr.M009142

Myerowitz, R., Puertollano, R., Raben, N., 2021. Impaired autophagy: The collateral damage of lysosomal storage disorders. EBioMedicine 63. https://doi.org/10.1016/j.ebiom.2020.103166

Navarrete-Martínez, J.I., Limón-Rojas, A.E., Gaytán-García, M. de J., Reyna-Figueroa, J., Wakida-Kusunoki, G., Delgado-Calvillo, Ma. del R., Cantú-Reyna, C., Cruz-Camino, H., Cervantes-Barragán, D.E., 2017. Newborn screening for six lysosomal storage disorders in a cohort of Mexican patients: Three-year findings from a screening program in a closed Mexican health system. Mol. Genet. Metab. 121, 16–21. https://doi.org/10.1016/j.ymgme.2017.03.001

Newkirk, K.M., Atkins, R.M., Dickson, P.I., Rohrbach, B.W., McEntee, M.F., 2011. Ocular Lesions in Canine Mucopolysaccharidosis I and Response to Enzyme Replacement Therapy. Invest. Ophthalmol. Vis. Sci. 52, 5130–5135. https://doi.org/10.1167/iovs.10-6751

Noda, T., Fujita, N., Yoshimori, T., 2009. The late stages of autophagy: how does the end begin? Cell Death Differ. 16, 984–990. https://doi.org/10.1038/cdd.2009.54

Oestreich, A.K., Garcia, M.R., Yao, X., Pfeiffer, F.M., Nobakhti, S., Shefelbine, S.J., Wang, Y., Brodeur, A.C., Phillips, C.L., 2015. Characterization of the MPS I-H knock-in mouse reveals increased femoral biomechanical integrity with compromised material strength and altered bone geometry. Mol. Genet. Metab. Rep. 5, 3–11. https://doi.org/10.1016/j.ymgmr.2015.08.004

Ohmi, K., Greenberg, D.S., Rajavel, K.S., Ryazantsev, S., Li, H.H., Neufeld, E.F., 2003. Activated microglia in cortex of mouse models of mucopolysaccharidoses I and IIIB. Proc. Natl. Acad. Sci. 100, 1902–1907. https://doi.org/10.1073/pnas.252784899

Onishi, M., Yamano, K., Sato, M., Matsuda, N., Okamoto, K., 2021. Molecular mechanisms and physiological functions of mitophagy. EMBO J. 40, e104705. https://doi.org/10.15252/embj.2020104705

Orenstein, S.J., Cuervo, A.M., 2010. Chaperone-mediated autophagy: Molecular mechanisms and physiological relevance. Semin. Cell Dev. Biol., The Molecular Machinery of Autophagy and its Role in Physiology and Disease and MicroRNAs in Animal Development 21, 719–726. https://doi.org/10.1016/j.semcdb.2010.02.005

Osellame, L.D., Rahim, A.A., Hargreaves, I.P., Gegg, M.E., Richard-Londt, A., Brandner, S., Waddington, S.N., Schapira, A.H.V., Duchen, M.R., 2013. Mitochondria and Quality Control Defects in a Mouse Model of Gaucher Disease—Links to Parkinson's Disease. Cell Metab. 17, 941–953. https://doi.org/10.1016/j.cmet.2013.04.014

Ou, L., Herzog, T.L., Wilmot, C.M., Whitley, C.B., 2014. Standardization of α-L-iduronidase enzyme assay with Michaelis–Menten kinetics. Mol. Genet. Metab. 111, 113–115. https://doi.org/10.1016/j.ymgme.2013.11.009

Pan, C., Nelson, M.S., Reyes, M., Koodie, L., Brazil, J.J., Stephenson, E.J., Zhao, R.C., Peters, C., Selleck, S.B., Stringer, S.E., Gupta, P., 2005. Functional abnormalities of heparan sulfate in mucopolysaccharidosis-I are associated with defective biologic activity of FGF-2 on human multipotent progenitor cells. Blood 106, 1956–1964. https://doi.org/10.1182/blood-2005-02-0657

Pan, D., Sciascia, A., Vorhees, C.V., Williams, M.T., 2008. Progression of multiple behavioral deficits with various ages of onset in a murine model of Hurler syndrome. Brain Res. 1188, 241–253. https://doi.org/10.1016/j.brainres.2007.10.036

Parini, R., Deodato, F., 2020. Intravenous Enzyme Replacement Therapy in Mucopolysaccharidoses: Clinical Effectiveness and Limitations. Int. J. Mol. Sci. 21, 2975. https://doi.org/10.3390/ijms21082975

Parini, R., Deodato, F., Di Rocco, M., Lanino, E., Locatelli, F., Messina, C., Rovelli, A., Scarpa, M., 2017. Open issues in Mucopolysaccharidosis type I-Hurler. Orphanet J. Rare Dis. 12, 112. https://doi.org/10.1186/s13023-017-0662-9

Parkhitko, A.A., Filine, E., Mohr, S.E., Moskalev, A., Perrimon, N., 2020. Targeting metabolic pathways for extension of lifespan and healthspan across multiple species. Ageing Res. Rev. 64, 101188. https://doi.org/10.1016/j.arr.2020.101188

Parzych, K.R., Klionsky, D.J., 2014. An Overview of Autophagy: Morphology, Mechanism, and Regulation. Antioxid. Redox Signal. 20, 460–473. https://doi.org/10.1089/ars.2013.5371

Peleg, S., Feller, C., Forne, I., Schiller, E., Sévin, D.C., Schauer, T., Regnard, C., Straub, T., Prestel, M., Klima, C., Schmitt Nogueira, M., Becker, L., Klopstock, T., Sauer, U., Bell, P., Imhof, A., Ladurner, A.G., 2016. Life span extension by targeting a link between metabolism and histone acetylation in Drosophila. EMBO Rep. 17, 455–469. https://doi.org/10.15252/embr.201541132

Pereira, V.G., Gazarini, M.L., Rodrigues, L.C., da Silva, F.H., Han, S.W., Martins, A.M., Tersariol, I.L.S., D'Almeida, V., 2010. Evidence of lysosomal membrane permeabilization in mucopolysaccharidosis type I: Rupture of calcium and proton homeostasis. J. Cell. Physiol. 223, 335–342. https://doi.org/10.1002/jcp.22039

Pereira, V.G., Martins, A.M., Micheletti, C., D'Almeida, V., 2008. Mutational and oxidative stress analysis in patients with mucopolysaccharidosis type I undergoing enzyme replacement therapy. Clin. Chim. Acta 387, 75–79. https://doi.org/10.1016/j.cca.2007.09.008

Perry, S.W., Norman, J.P., Barbieri, J., Brown, E.B., Gelbard, H.A., 2011. Mitochondrial membrane potential probes and the proton gradient: a practical usage guide. BioTechniques 50, 98–115. https://doi.org/10.2144/000113610

Phillips, S.E., Woodruff, E.A., Liang, P., Patten, M., Broadie, K., 2008. Neuronal Loss of Drosophila NPC1a Causes Cholesterol Aggregation and Age-Progressive Neurodegeneration. J. Neurosci. 28, 6569–6582. https://doi.org/10.1523/JNEUROSCI.5529-07.2008

Piller Puicher, E., Tomanin, R., Salvalaio, M., Friso, A., Hortelano, G., Marin, O., Scarpa, M., 2012. Encapsulated engineered myoblasts can cure Hurler syndrome: preclinical experiments in the mouse model. Gene Ther. 19, 355–364. https://doi.org/10.1038/gt.2011.94

Platt, F.M., d'Azzo, A., Davidson, B.L., Neufeld, E.F., Tifft, C.J., 2018. Lysosomal storage diseases. Nat. Rev. Dis. Primer 4, 1–25. https://doi.org/10.1038/s41572-018-0025-4

Poe, M.D., Chagnon, S.L., Escolar, M.L., 2014. Early treatment is associated with improved cognition in Hurler syndrome. Ann. Neurol. 76, 747–753. https://doi.org/10.1002/ana.24246

Powers, R.W., Kaeberlein, M., Caldwell, S.D., Kennedy, B.K., Fields, S., 2006. Extension of chronological life span in yeast by decreased TOR pathway signaling. Genes Dev. 20, 174–184. https://doi.org/10.1101/gad.1381406

Ravikumar, B., Sarkar, S., Davies, J.E., Futter, M., Garcia-Arencibia, M., Green-Thompson, Z.W., Jimenez-Sanchez, M., Korolchuk, V.I., Lichtenberg, M., Luo, S., Massey, D.C.O., Menzies, F.M., Moreau, K., Narayanan, U., Renna, M., Siddiqi, F.H., Underwood, B.R., Winslow, A.R., Rubinsztein, D.C., 2010. Regulation of Mammalian Autophagy in Physiology and Pathophysiology. Physiol. Rev. 90, 1383–1435. https://doi.org/10.1152/physrev.00030.2009

Reolon, G.K., Braga, L.M., Camassola, M., Luft, T., Henriques, J.A.P., Nardi, N.B., Roesler, R., 2006. Long-term memory for aversive training is impaired in Idua−/− mice, a genetic model of mucopolysaccharidosis type I. Brain Res. 1076, 225–230. https://doi.org/10.1016/j.brainres.2006.01.008

Reolon, G.K., Reinke, A., de Oliveira, M.R., Braga, L.M., Camassola, M., Andrades, M.É., Moreira, J.C.F., Nardi, N.B., Roesler, R., Dal-Pizzol, F., 2009. Alterations in Oxidative Markers in the Cerebellum and Peripheral Organs in MPS I Mice. Cell. Mol. Neurobiol. 29, 443–448. https://doi.org/10.1007/s10571-008-9335-5

Rigon, L., De Filippis, C., Napoli, B., Tomanin, R., Orso, G., 2021. Exploiting the Potential of Drosophila Models in Lysosomal Storage Disorders: Pathological Mechanisms and Drug Discovery. Biomedicines 9, 268. https://doi.org/10.3390/biomedicines9030268

Rodríguez-Arribas, M., Yakhine-Diop, S.M.S., González-Polo, R.A., Niso-Santano, M., Fuentes, J.M., 2017. Chapter Four - Turnover of Lipidated LC3 and Autophagic Cargoes in Mammalian Cells, in: Galluzzi, L., Bravo-San Pedro, J.M., Kroemer, G. (Eds.), Methods in Enzymology, Molecular Characterization of Autophagic Responses, Part A. Academic Press, pp. 55–70. https://doi.org/10.1016/bs.mie.2016.09.053

Rome, L.H., Hill, D.F., 1986. Lysosomal degradation of glycoproteins and glycosaminoglycans. Efflux and recycling of sulphate and N-acetylhexosamines. Biochem. J. 235, 707–713. https://doi.org/10.1042/bj2350707

Russell, C., Hendson, G., Jevon, G., Matlock, T., Yu, J., Aklujkar, M., Ng, K.-Y., Clarke, L.A., 1998. Murine MPS I: insights into the pathogenesis of Hurler syndrome. Clin. Genet. 53, 349–361. https://doi.org/10.1111/j.1399-0004.1998.tb02745.x

Ryder, E., Russell, S., 2003. Transposable elements as tools for genomics and genetics in Drosophila. Brief. Funct. Genomics 2, 57–71. https://doi.org/10.1093/bfgp/2.1.57

Sahu, R., Kaushik, S., Clement, C.C., Cannizzo, E.S., Scharf, B., Follenzi, A., Potolicchio, I., Nieves, E., Cuervo, A.M., Santambrogio, L., 2011. Microautophagy of cytosolic proteins by late endosomes. Dev. Cell 20, 131–139. https://doi.org/10.1016/j.devcel.2010.12.003

Saito, T., Kuma, A., Sugiura, Y., Ichimura, Y., Obata, M., Kitamura, H., Okuda, S., Lee, H.-C., Ikeda, K., Kanegae, Y., Saito, I., Auwerx, J., Motohashi, H., Suematsu, M., Soga, T., Yokomizo, T., Waguri, S., Mizushima, N., Komatsu, M., 2019. Autophagy regulates lipid metabolism through selective turnover of NCoR1. Nat. Commun. 10, 1567. https://doi.org/10.1038/s41467-019-08829-3

Sánchez-González, C., Nuevo-Tapioles, C., Cruz Herrero Martìn, J., Pereira, M.P., Serrano Sanz, S., Ramirez de Molina, A., Cuezva, J.M., Formentini, L., 2020. Dysfunctional oxidative phosphorylation shunts branched-chain amino acid catabolism onto lipogenesis in skeletal muscle. EMBO J. 39, e103812. https://doi.org/10.15252/embj.2019103812

Sato, Y., Kobayashi, H., Higuchi, T., Shimada, Y., Ida, H., Ohashi, T., 2017. Metabolomic Profiling of Pompe Disease-Induced Pluripotent Stem Cell-Derived Cardiomyocytes Reveals That Oxidative Stress Is Associated with Cardiac and Skeletal Muscle Pathology. Stem Cells Transl. Med. 6, 31–39. https://doi.org/10.5966/sctm.2015-0409

Schoiswohl, G., Schweiger, M., Schreiber, R., Gorkiewicz, G., Preiss-Landl, K., Taschler, U., Zierler, K.A., Radner, F.P.W., Eichmann, T.O., Kienesberger, P.C., Eder, S., Lass, A., Haemmerle, G., Alsted, T.J., Kiens, B., Hoefler, G., Zechner, R., Zimmermann, R., 2010. Adipose triglyceride lipase plays a key role in the supply of the working muscle with fatty acids. J. Lipid Res. 51, 490–499. https://doi.org/10.1194/jlr.M001073

Séité, S., Pioche, T., Ory, N., Plagnes-Juan, E., Panserat, S., Seiliez, I., 2019. The Autophagic Flux Inhibitor Bafilomycine A1 Affects the Expression of Intermediary Metabolism-Related Genes in Trout Hepatocytes. Front. Physiol. 10, 263. https://doi.org/10.3389/fphys.2019.00263

Settembre, C., De Cegli, R., Mansueto, G., Saha, P.K., Vetrini, F., Visvikis, O., Huynh, T., Carissimo, A., Palmer, D., Jürgen Klisch, T., Wollenberg, A.C., Di Bernardo, D., Chan, L., Irazoqui, J.E., Ballabio, A., 2013. TFEB controls cellular lipid metabolism through a starvation-induced autoregulatory loop. Nat. Cell Biol. 15, 647–658. https://doi.org/10.1038/ncb2718

Settembre, C., Zoncu, R., Medina, D.L., Vetrini, F., Erdin, Serkan, Erdin, SerpilUckac, Huynh, T., Ferron, M., Karsenty, G., Vellard, M., Facchinetti, V., Sabatini, D., Ballabio, A., 2012. A lysosome-to-nucleus signalling mechanism senses and regulates the lysosome via mTOR and TFEB. EMBO J. 31, 1095–1108. https://doi.org/10.1038/emboj.2012.32

Shull, R.M., Helman, R.G., Spellacy, E., Constantopoulos, G., Munger, R.J., Neufeld, E.F., 1984. Morphologic and biochemical studies of canine mucopolysaccharidosis I. Am. J. Pathol. 114, 487–495.

Shull, R.M., Munger, R.J., Spellacy, E., Hall, C.W., Constantopoulos, G., Neufeld, E.F., 1982. Canine alpha-L-iduronidase deficiency. A model of mucopolysaccharidosis I. Am. J. Pathol. 109, 244–248.

Simonaro, C.M., Tomatsu, S., Sikora, T., Kubaski, F., Frohbergh, M., Guevara, J.M., Wang, R.Y., Vera, M., Kang, J.L., Smith, L.J., Schuchman, E.H., Haskins, M.E., 2016. Pentosan Polysulfate: Oral Versus Subcutaneous Injection in Mucopolysaccharidosis Type I Dogs. PLOS ONE 11, e0153136. https://doi.org/10.1371/journal.pone.0153136

Sleeper, M.M., Kusiak, C.M., Shofer, F.S., O'Donnell, P., Bryan, C., Ponder, K.P., Haskins, M.E., 2008. Clinical characterization of cardiovascular abnormalities associated with feline mucopolysaccharidosis I and VI. J. Inherit. Metab. Dis. 31, 424–431. https://doi.org/10.1007/s10545-008-0821-1

Spassieva, S.D., Mullen, T.D., Townsend, D.M., Obeid, L.M., 2009. Disruption of ceramide synthesis by CerS2 down-regulation leads to autophagy and the unfolded protein response. Biochem. J. 424, 273–283. https://doi.org/10.1042/BJ20090699

Stepien, K.M., Roncaroli, F., Turton, N., Hendriksz, C.J., Roberts, M., Heaton, R.A., Hargreaves, I., 2020. Mechanisms of Mitochondrial Dysfunction in Lysosomal Storage Disorders: A Review. J. Clin. Med. 9, 2596. https://doi.org/10.3390/jcm9082596

Sur, S., Nakanishi, H., Flaveny, C., Ippolito, J.E., McHowat, J., Ford, D.A., Ray, R.B., 2019. Inhibition of the key metabolic pathways, glycolysis and lipogenesis, of oral cancer by bitter melon extract. Cell Commun. Signal. 17, 131. https://doi.org/10.1186/s12964-019-0447-y

Suzuki, T., Shimoda, M., Ito, K., Hanai, S., Aizawa, H., Kato, T., Kawasaki, K., Yamaguchi, T., Ryoo, H.D., Goto-Inoue, N., Setou, M., Tsuji, S., Ishida, N., 2013. Expression of Human Gaucher Disease Gene GBA Generates Neurodevelopmental Defects and ER Stress in Drosophila Eye. PLOS ONE 8, e69147. https://doi.org/10.1371/journal.pone.0069147

Tessitore, A., Pirozzi, M., Auricchio, A., 2009. Abnormal autophagy, ubiquitination, inflammation and apoptosis are dependent upon lysosomal storage and are useful biomarkers of mucopolysaccharidosis VI. PathoGenetics 2, 4. https://doi.org/10.1186/1755-8417-2-4
Tixier, V., Bataillé, L., Etard, C., Jagla, T., Weger, M., DaPonte, J.P., Strähle, U., Dickmeis, T., Jagla, K., 2013. Glycolysis supports embryonic muscle growth by promoting myoblast fusion. Proc. Natl. Acad. Sci. 110, 18982–18987. https://doi.org/10.1073/pnas.1301262110
Tong, L., 2005. Acetyl-coenzyme A carboxylase: crucial metabolic enzyme and attractive target for drug discovery. Cell. Mol. Life Sci. CMLS 62, 1784–1803. https://doi.org/10.1007/s00018-005-5121-4
Torres, N.V., Mateo, F., Meléndez-Hevia, E., 1988. Shift in rat liver glycolysis control from fed to starved conditions Flux control coefficients of glucokinase and phosphofructokinase. FEBS Lett. 233, 83–86. https://doi.org/10.1016/0014-5793(88)81360-7
Tylki-Szymanska, A., Marucha, J., Jurecka, A., Syczewska, M., Czartoryska, B., 2010. Efficacy of recombinant human α-L-iduronidase (laronidase) on restricted range of motion of upper extremities in mucopolysaccharidosis type I patients. J. Inherit. Metab. Dis. 33, 151–157. https://doi.org/10.1007/s10545-010-9059-9
Unhavaithaya, Y., Orr-Weaver, T.L., 2012. Polyploidization of glia in neural development links tissue growth to blood–brain barrier integrity. Genes Dev. 26, 31–36. https://doi.org/10.1101/gad.177436.111
Venkatachalam, K., Long, A.A., Elsaesser, R., Nikolaeva, D., Broadie, K., Montell, C., 2008. Motor Deficit in a Drosophila Model of Mucolipidosis Type IV due to Defective Clearance of Apoptotic Cells. Cell 135, 838–851. https://doi.org/10.1016/j.cell.2008.09.041
Viana, G.M., Buri, M.V., Paredes-Gamero, E.J., Martins, A.M., D'Almeida, V., 2016. Impaired Hematopoiesis and Disrupted Monocyte/Macrophage Homeostasis in Mucopolysaccharidosis Type I Mice. J. Cell. Physiol. 231, 698–707. https://doi.org/10.1002/jcp.25120
Viana, G.M., do Nascimento, C.C., Paredes-Gamero, E.J., D'Almeida, V., 2017. Altered Cellular Homeostasis in Murine MPS I Fibroblasts: Evidence of Cell-Specific Physiopathology. JIMD Rep. 36, 109–116. https://doi.org/10.1007/8904_2017_5
Voccoli, V., Tonazzini, I., Signore, G., Caleo, M., Cecchini, M., 2014. Role of extracellular calcium and mitochondrial oxygen species in psychosine-induced oligodendrocyte cell death. Cell Death Dis. 5, e1529–e1529. https://doi.org/10.1038/cddis.2014.483
Voelzmann, A., Bauer, R., 2011. Embryonic expression of Drosophila ceramide synthase schlank in developing gut, CNS and PNS. Gene Expr. Patterns 11, 501–510. https://doi.org/10.1016/j.gep.2011.08.006
Wang, D., Shukla, C., Liu, X., Schoeb, T.R., Clarke, L.A., Bedwell, D.M., Keeling, K.M., 2010. Characterization of an MPS I-H Knock-In Mouse that Carries a Nonsense Mutation Analogous to the Human IDUA-W402X Mutation. Mol. Genet. Metab. 99, 62–71. https://doi.org/10.1016/j.ymgme.2009.08.002
Wang, H., Somers, G.W., Bashirullah, A., Heberlein, U., Yu, F., Chia, W., 2006. Aurora-A acts as a tumor suppressor and regulates self-renewal of Drosophila neuroblasts. Genes Dev. 20, 3453–3463. https://doi.org/10.1101/gad.1487506
Webber, D.L., Choo, A., Hewson, L.J., Trim, P.J., Snel, M.F., Hopwood, J.J., Richards, R.I., Hemsley, K.M., O'Keefe, L.V., 2018. Neuronal-specific impairment of heparan sulfate degradation in Drosophila reveals pathogenic mechanisms for Mucopolysaccharidosis type IIIA. Exp. Neurol. 303, 38–47. https://doi.org/10.1016/j.expneurol.2018.01.020
Wilkinson, F.L., Holley, R.J., Langford-Smith, K.J., Badrinath, S., Liao, A., Langford-Smith, A., Cooper, J.D., Jones, S.A., Wraith, J.E., Wynn, R.F., Merry, C.L.R., Bigger, B.W., 2012. Neuropathology in Mouse Models of Mucopolysaccharidosis Type I, IIIA and IIIB. PLOS ONE 7, e35787. https://doi.org/10.1371/journal.pone.0035787
Woloszynek, J.C., Coleman, T., Semenkovich, C.F., Sands, M.S., 2007. Lysosomal Dysfunction Results in Altered Energy Balance *. J. Biol. Chem. 282, 35765–35771. https://doi.org/10.1074/jbc.M705124200
Woloszynek, J.C., Kovacs, A., Ohlemiller, K.K., Roberts, M., Sands, M.S., 2009. Metabolic Adaptations to Interrupted Glycosaminoglycan Recycling *. J. Biol. Chem. 284, 29684–29691. https://doi.org/10.1074/jbc.M109.020818

Wraith, J.E., Clarke, L.A., Beck, M., Kolodny, E.H., Pastores, G.M., Muenzer, J., Rapoport, D.M., Berger, K.I., Swiedler, S.J., Kakkis, E.D., Braakman, T., Chadbourne, E., Walton-Bowen, K., Cox, G.F., 2004. Enzyme replacement therapy for mucopolysaccharidosis I: a randomized, double-blinded, placebo-controlled, multinational study of recombinant human α-L-iduronidase (laronidase). J. Pediatr. 144, 581–588. https://doi.org/10.1016/j.jpeds.2004.01.046

Xue, Y., Richards, S.M., Mahmood, A., Cox, G.F., 2016. Effect of anti-laronidase antibodies on efficacy and safety of laronidase enzyme replacement therapy for MPS I: A comprehensive meta-analysis of pooled data from multiple studies. Mol. Genet. Metab. 117, 419–426. https://doi.org/10.1016/j.ymgme.2016.02.006

Zalfa, C., Verpelli, C., D'Avanzo, F., Tomanin, R., Vicidomini, C., Cajola, L., Manara, R., Sala, C., Scarpa, M., Vescovi, A.L., De Filippis, L., 2016. Glial degeneration with oxidative damage drives neuronal demise in MPSII disease. Cell Death Dis. 7, e2331. https://doi.org/10.1038/cddis.2016.231

Zhang, X., Evans, T.D., Jeong, S.-J., Razani, B., 2018. Classical and alternative roles for autophagy in lipid metabolism. Curr. Opin. Lipidol. 29, 203–211. https://doi.org/10.1097/MOL.0000000000000509

Zhou, J., Lin, J., Leung, W.T., Wang, L., 2020. A basic understanding of mucopolysaccharidosis: Incidence, clinical features, diagnosis, and management. Intractable Rare Dis. Res. 9, 1–9. https://doi.org/10.5582/irdr.2020.01011